Doctoral theses at NTNU, 2022:108

Danil Maksimov

Prediction and early detection of karsts for safer drilling in carbonates

Doctoral thesis

Danil Maksimov

ISBN 978-82-326-6827-4 (printed ver.)
ISBN 978-82-326-5465-9 (electronic ver.)
ISSN 1503-8181 (printed ver.)
ISSN 2703-8084 (online ver.)

NTNU
Norwegian University of Science and Technology

NTNU
Norwegian University of Science and Technology
Thesis for the Degree of
Philosophiae Doctor
Faculty of Engineering
Department of Geoscience and Petroleum

Doctoral theses at NTNU, 2022:108

NTNU

Prediction and early detection of karsts for safer drilling in carbonates

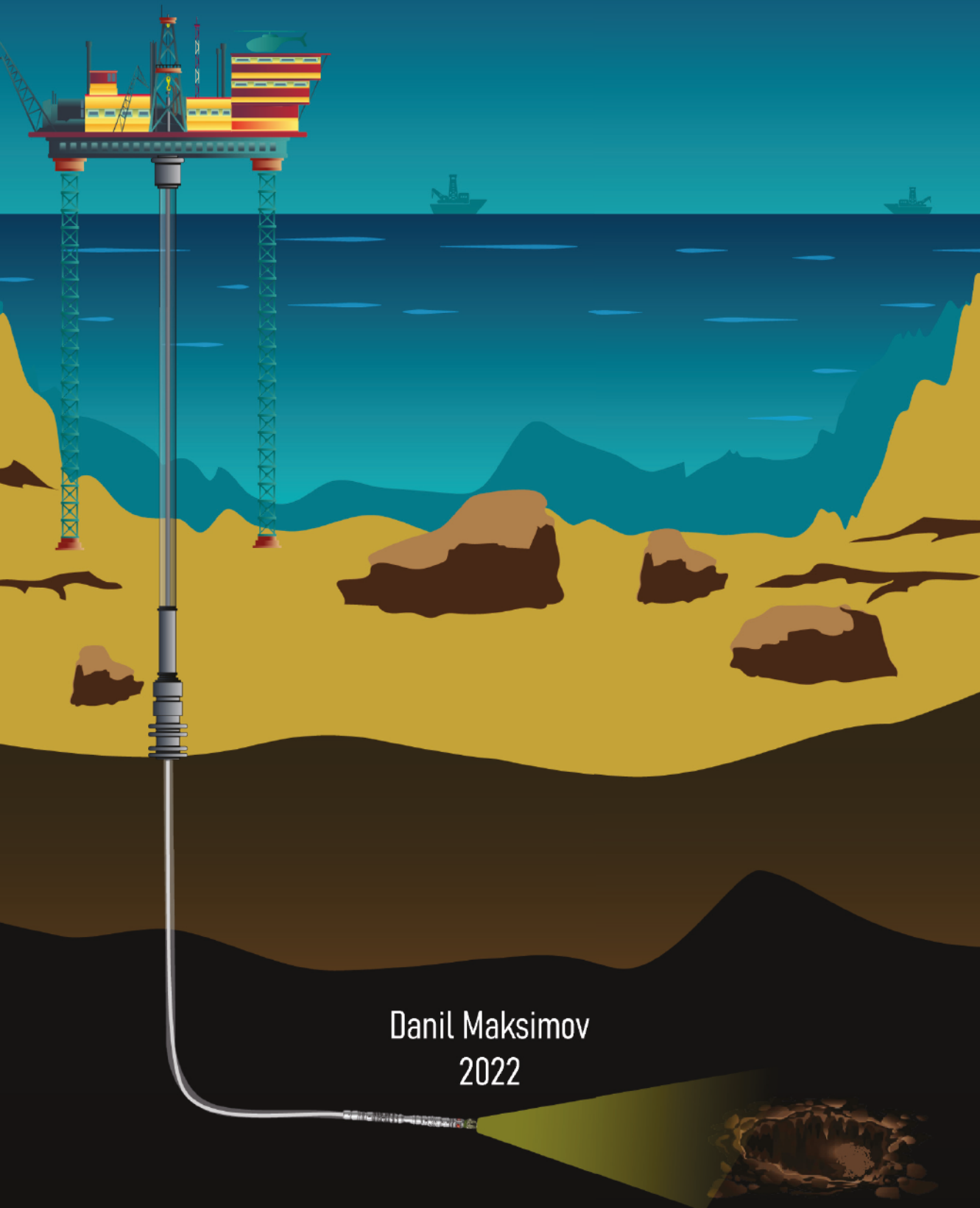

Danil Maksimov

2022

Danil Maksimov

Prediction and early detection of karsts for safer drilling in carbonates

Thesis for the Degree of Philosophiae Doctor

Trondheim, January 2022

Norwegian University of Science and Technology
Faculty of Engineering
Department of Geoscience and Petroleum

NTNU
Norwegian University of
Science and Technology

NTNU
Norwegian University of Science and Technology

Thesis for the Degree of Philosophiae Doctor

Faculty of Engineering
Department of Geoscience and Petroleum

ISBN 978-82-326-6827-4 (printed ver.)
ISBN 978-82-326-5465-9 (electronic ver.)
ISSN 1503-8181 (printed ver.)
ISSN 2703-8084 (online ver.)

Doctoral theses at NTNU, 2022:108

Printed by NTNU Grafisk senter

Abstract

Underestimation of drilling hazards in carbonates can lead to serious consequences to personnel and the environment. The history of drilling in carbonates has shown that the vast majority of drilling incidents are associated with drilling through unique carbonate features called karsts. Karsts come in a variety of sizes and shapes such as cavities, caves and underground channels. Accidents associated with drilling through karsts can result in the loss of well control with subsequent problems. This can lead not only to operational delays or damage to expensive drilling equipment, and also to possible personnel injuries, loss of life or environmental catastrophes. This thesis studies different strategies, methods and technologies for safer drilling in karstified carbonates.

It presents a general theoretical background of karstification phenomena and provides a description and classification of various karstification objects relevant for drilling. This classification enables the identification of important parameters of dangerous for drilling karsts. The obtained description and classification leads to a review of available technologies and methods that can be utilized for prediction or detection of dangerous for drilling karsts. This analysis reveals the gap in the available technologies for early detection of dangerous for drilling karsts. Based on in-depth analysis of an entire field in the Barents Sea, it is shown that karsts tend to appear in groups. This finding is utilized in a novel approach, where the not dangerous for drilling karst can be utilized as indicators of karstification zones. The analysis of the extensive set of field data, demonstrates that karstification objects can be detected from the analysis of certain patterns in real-time drilling data. These patterns serve as real-time indicators of karstification objects and zones. However these patterns often remain unforeseen during drilling. This work provides and tests a signal processing algorithm for automated karst-patterns detection. That can help engineers involved in real-time drilling data analysis to detect karst-related patterns in drilling data. Finally, a novel method for prediction of karsts while drilling using look-ahead of the drill bit technology is proposed based on borehole acoustic tool. The developed technology can be used to indicate upcoming drilling hazards associated with karsts or any other unexpected formation changes. The concept of this technology is demonstrated through experiments in a state-of-the-art industrial simulator.

Dedication

First and foremost this thesis is dedicated to my beloved parents, Nina and Alexander, whose love for me throughout my life knew no bounds. Next to my sister Anastasia, who has always been my best friend, a source of support, wisdom and knowledge. And last, but not least, this dissertation is dedicated to my wife Ekaterina for all of her tremendous amount of patience, love and support.

Acknowledgments

First I am extremely grateful to my main supervisor Professor Alexey Pavlov for his support, guidance and encouragement during my PhD study. Without his motivation, generosity and patience this thesis would not have been possible. I would also like to thank my co-supervisor Professor Sigbjørn Sangesland, for all the ideas, insightful comments and discussions we had.

Further, I gratefully acknowledge Lundin Energy Norway AS for funding my PhD project, providing valuable field data and access to internal company expertise. All of this enabled this research. I would like to thank Per Haugum and Bård Fjellså at Lundin Energy for their support, professional input as well as openness and willingness to share insights at every stage of the project. In addition, special thanks are given to Eric Claudey from Enhanced Drilling for his valuable support. This research is a part of BRU21 – NTNU Research and Innovation Program on Digital and Automation Solutions for the Oil and Gas Industry (www.ntnu.edu/bru21) and I am grateful for being part of this program.

I am especially grateful to Tonni Franke at SINTEF for valuable scientific discussions, help on numerical and theoretical matters, and for many useful suggestions. I would also like to thank Professor Mai Britt Mørk and Doctor Terje Solbakk from NTNU, for providing expert advice and support on the geological study of the problem. Stewart Clark at NTNU is acknowledged for supporting and improving my work by editing of the language of the papers and thesis. I wish to thank all the lecturers I had during this period, especially Professors Sigve Hovda and Bernt Sigve Aadnøy, at the Department of Geoscience and Petroleum.

I would also like to thank many my fellow PhD candidates and PostDocs from the BRU21 program, with whom I shared my office for three years. I especially grateful to Thiago Silva Lima, Seok Ki Moon, Andreas Teigland and Ivan Alejandro Pirir Ruiz for their encouraging and technical discussions.

Contents

List of Figures

List of Tables

List of Acronyms

ADF	Adaptive Differentiating Filter.
API	Application Programming Interface.
ARC	Array Resistivity Compensated tool.
BARS	Borehole Acoustic Reflection Survey.
BHA	Bottom Hole Assembly.
CFL	Courant-Friedrichs-Lewy.
CML	Controlled Mud Level.
CPI	Computer Processed Interpretation.
CPU	Central Processing Unit.
DIF	Drilling Induced Fractures.
DOI	Depth Of Investigation.
EOW	End Of Well Report.
FEM	Finite Element Method.
GPU	Graphics Processing Unit.
LCM	Lost Circulation Materials.
LIH	Lost in Hole.
LWD	Logging While Drilling.
MAC	Method of Acoustic Comparisons.
ML	Machine Learning.
MPD	Managed Pressure Drilling.
MRL	Mud Return Line.
MUMPS	Multifrontal Massively Parallel Sparse.

MW	Mud Weight.
PDC	Polycrystalline Diamond Compact.
PMCD	Pressurized Mud Cap Drilling.
QTA	Qualitative Trend Analysis.
RAM	Random-access Memory.
RCD	Rotational Control Device.
ROP	Rate of Penetration.
RPM	Revolutions Per Minute.
S&V	Shocks & Vibrations.
SGD	Seismic Guided Drilling.
SPM	Subsea Pump Module.
SPP	Stand Pipe Pressure.
SS	Stick/Slip of BHA.
SWD	Seismic While Drilling.
TST	True Stratigraphic Thickness.
VSP	Vertical Seismic Profiling.
WOB	Weight on the bit.
WR	Windows Radius.

Nomenclature

$\bar{y}_i$	True signal
δ	Required accuracy of the filter
$\hat{y}(t^*)$	Estimates of the signal
λ_{min}	Minimum wavelength
σ	Standard deviation
c	Speed of sound
f_0	Frequency of the source signal
f_{max}	Maximum frequency
h	Mesh element size
h_{max}	Maximum mesh element size
h_{rock}	Mesh element size of rocks
m_i	Noise in the signal
N	Length of the segment
N	Number of elements per wavelength
P_{rock}	Speed of sound in rocks
t^*	Current time instance
T_0	Period of the source signal
t_i	Time instances
$V_n(t)$	Velocity of the transducer surface
W	Sequence of instances
$w[n]$	Sequence of the length of the segment

WR	Window radius
WR^*	Maximal window radius reached in the window adaptation process
WR_{max}	Upper limit for the window radius
WR_{min}	Lower limit for the window radius
y_i	Measurements of the signal

Chapter 1

Introduction

1.1 Background

1.1.1 Drilling in carbonates

Carbonate reservoirs produce a significant volume of the world's total oil and gas [1]. Many of the world's carbonate reservoirs have considerable potential for development and production. However, the history of drilling has shown that the heterogeneous nature and the complexity of rock properties in carbonate reservoirs make them challenging to drill. Karstification processes often affect carbonate reservoirs and cause the development of a number of unique geological features called karsts. Here I refer to a common definition of the karst, introduced to describe the landscape, which contains caves, underground channels, and other features associated with soluble rocks [2].

Encountering karsts while drilling can cause critical safety incidents. Depending on the size of encountered karst, loss of drilling fluid can be uncontrollable resulting in rapid gas migration to the surface and causing well control situations [3]. When fractures and caverns are closely connected as is common in some regions, losses can be treated without any success for a few weeks with subsequent plugging and abandoning of the wells [4].

Such a negative impact of karsts on drilling operations is reported worldwide. Malaysia, Sarawak offsore: based on more than eleven years of drilling experience in carbonate structures total losses were encountered in more than 30% of the wells drilled [5]. USA, Culberson County, Texas: in each case of drilling in the intervals of cave systems, losses that occurred progressed into total losses with well control incidents [6]. Norway, Barents Sea, Continental Shelf: drilling in naturally karstified carbonates resulted in total losses causing weeks of non-productive time, shoot off and Lost in Hole (LIH) of Bottom Hole Assembly (BHA) [7]. Western Offshore fields of India: drilling and completion problems due to mud loss in a number of wells [8]. Philippines, North Senoro Gas Field: well control issues in carbonates, total mud losses followed by gas kicks [3]. Russia, Eastern Siberia: catastrophic mud losses reaching several thousand cubic meters while drilling in carbonates, gas kicks [9].

Overall the problem of drilling in carbonates is serious and costs the industry more than USD 800M per year [10, 11].

1.1.2 Current solutions

There are several ways to mitigate the risks of total mud losses, gas kicks and BHA drops in open cavities. A detailed overview of these methods will be given in Chapter 3. They can be roughly divided into three main groups:

- Pre-drill detection of karsts,
- Karst detection while drilling,
- Minimization of consequences of drilling into karsts.

The first group of methods seeks solutions on how to predict and avoid drilling into karstification objects. It is based on technologies to investigate subsurface structures prior to drilling. Today we benefit from cutting-edge methods within geophysical research. However even with the most advanced geophysical methods it is still challenging to detect karsts and avoid drilling into them.

For example, seismic - one of the most common techniques used nowadays for mapping reservoirs, faults, and structural surfaces - can be effective for the detection of *large* karst structures [12, 13]. However, not all karsts can be detected by seismic technologies. Along with the successful case studies, the main limitation in the seismic detection of karsts is related to the problem of vertical resolution [14]. It has been shown that caves less than $\frac{\lambda}{4}$ (40 m) cannot be detected due to wave interference [15]. In certain regions in the Barents Sea, encountered caves were less than a meter and they were very dangerous for drilling [7].

The second group of methods focuses on karst detection while drilling. Real-time or early detection of karstification objects can lead to timely and more efficient risk mitigation. A wide range of investigative LWD can be used to detect karsts. For example, Borehole Acoustic Reflection Survey (BARS) [16], and ultradeep resistivity tools [17] are among the most promising. Although effective in certain cases [18, 19], the main drawback of LWD tools is that the vast majority provides look-around measurements (also usually at a great distance from the bit) and these tools do not look ahead of the bit. Thus, the area ahead of the bit cannot be investigated by direct measurements. Any relevant measurements from LWD tools come with a significant delay (due to the large offset from the drill bit) and are, therefore, not suitable for real-time decision making on avoiding karsts that can be dangerous for drilling.

The third group addresses methods to minimize consequences of drilling into karsts. Depending on the volume of mud loss, different techniques can be used. For example, the volume of mud loss in some conductive fractures can be successfully controlled by varying the concentration of Lost Circulation Materials (LCM) or by changing the chemical composition of the mud [20, 21]. Usually, these measures have only a short-term effect and

require more and more chemicals and cement materials leading to additional costs and delays [22].

Another approach widely used by the industry to mitigate many of the problematic situations encountered in karstified carbonates is the use of Managed Pressure Drilling (MPD) and its modifications, such as Pressurized Mud Cap Drilling (PMCD). In PMCD, a sacrificial fluid is pumped through the bit nozzles to fill any fractures and caves, while a heavier fluid is pumped into the annulus from the top to maintain the mud cap and prevent gas migration up to the surface. Today this is the most common practice for drilling in carbonates used by drilling companies [5, 23–26].

However, MPD-based solutions have limitations. For PMCD there is an operational necessity for additional equipment installation on the rig site such as the Rotational Control Device (RCD) [27]. Additionally, a significant volume of sacrificial fluid is required for drilling, which makes this technique inapplicable in some regions. In the case of exploration drilling, the rig may not be equipped for PMCD before drilling begins due to underestimation of drilling risks. PMCD does not solve all karst-related challenges. An excessive shock can act on the drill bit when the BHA suddenly reaches the bottom of a cave. It can break the drillstring with possible Lost in Hole (LIH) and stuck-pipe events.

Despite the fact that there are different methods to tackle the challenge of drilling in karstified carbonates, these methods have limitations:

- small, dangerous for drilling karst forms cannot be detected and located before drilling with seismic-based methods
- any relevant LWD measurements while drilling are look-around with a significant delay. They cannot look in front of the bit and therefore cannot be used for avoiding drilling into karsts or even for real-time detection of encountering karsts
- minimization of consequences of drilling in karsts cannot solve the problem of damaging drilling components in cavities. Moreover, the MPD type of drilling, is rarely available in exploration drilling beforehand, leaving the risk of well-control issues unchanged.

These limitations indicate a significant room for further research and development to find methods and technologies for safer drilling in karstified carbonates.

1.1.3 Challenges

This thesis focuses on the challenge of how to predict karsts ahead of the bit and detect karstification objects and zones while drilling. As follows from the overview of the available technologies from the previous section, these challenges are far from solved. Obtaining solutions to these challenges can be vital for real-time decision making and minimization of drilling risks in karstified carbonates.

Early karst detection is a complex multidisciplinary problem and different approaches have to be investigated to tackle this challenge. For example, in this thesis, an extended set

of methods from different research areas is used, including geology, geophysics, drilling, acoustics, signal processing and machine learning. Another challenge related to early karst detection or prediction is the lack of high quality data sets. The number of wells encountering karstification objects is relatively low compared to the overall number of drilled wells. Moreover, not so many of these wells were drilled with proper sensor sets. This makes this problem even more difficult for research.

1.2 Main research questions

To address the described challenges the following research questions require answering:

- Q1: What are karsts and which of them can be considered as dangerous for drilling?
- Q2: Are there any available (geophysical) methods that can be used for early karst detection?
- Q3: Can karsts be detected in real-time from drilling measurements and what measurement patterns correspond to them?
- Q4: Can these drilling measurements be analyzed in an automated manner to simplify the detection of karst patterns in real-time drilling data?
- Q5: What technology can be used to consistently investigate a region ahead of the drill bit and indicate the presence of dangerous karst forms in advance?

This thesis systematically addresses these questions with the overall goal to find better strategies, methods and technologies for safer drilling in karstified carbonates.

1.3 Methodology

The following methodology was used to address these research questions.

- M1: Karstification phenomena were studied to gain insight into current knowledge and to systematize theoretical information based on literature survey. To identify dangerous for drilling karst forms and classify karstification objects from the drilling point of view, an analysis of real field data from one of the fields in the Barents Sea was performed. This provided a better understanding of the karstification problem in the studied region and karstification phenomena in general.
- M2: To investigate technologies suitable for early detection or prediction of karst cavities in drilling, advances in geophysical methods were reviewed concentrating on the detection of geological objects around and ahead of the bit. This analysis and classification of these technologies was based on the overview of academic publications, patents, inventions and commercial solutions used by operator/service companies.
- M3: A detailed study of drilling events was made and end-of-well reports from the available field data from the Barents Sea. This correlated intervals of karstification identified from borehole images with the rig-site events. This analysis provided an overview

of rig-site drilling events for the entire field. Joint analysis of the rig-site events and borehole images was undertaken to find specific behavior of BHA in the intervals of karstification. A detailed analysis of the recorded time-domain data of BHA dynamics and mud flow data in these intervals was compiled to identify signatures or patterns of karstification objects in the corresponding real-time measurements.

M4: Once karst signatures were identified, this work investigated the possibility of karst patterns detection in an automated manner using a special filtering algorithm. The algorithm was applied to the set of drilling data containing fractures, vugs and caves identified by the operator company providing the dataset. These intervals were used as references for comparison and validation of the intervals detected automatically by the algorithm.

M5: Since karst prediction while drilling is challenging with the state-of-the-art geophysical methods, a concept was introduced to investigate a region ahead of the bit. This novel geophysical method showed how the region in front of the bit can be investigated and how dangerous for drilling karsts can be detected in advance. A set of numerical models, which represented a reservoir section of the studied region, was developed to test and validate the method. Different geological scenarios were simulated in the state-of-the art industrial simulator COMSOL Multiphysics® to investigate and find a suitable tool configuration as well as signal processing algorithms to demonstrate the concept. This work demonstrated how dangerous for drilling karsts can be distinguished from not dangerous for drilling objects with the proposed instrumentation setup and signal processing algorithm.

1.4 Contribution

The contribution of this thesis with respect to the formulated research questions is given below.

C1: The analysis of literature on karstification and the field data from Loppa High region in the Barents Sea, provided a description of various karstification objects relevant for drilling and their classification into dangerous and not dangerous for drilling karstification objects. These descriptions and classifications are important for evaluation and validation of various technologies aiming at safer drilling in karstified carbonates.

C2: The analysis of the drilling data (mud logs, drilling reports, site survey reports), drilling mechanics data (surface and downhole measurements), geology (lithology, stratigraphy, biostratigraphy), rock and core (conventional core analysis and core photos), petrophysical reports (Computer Processed Interpretation (CPI), Composite), well logs (wireline, LWD), demonstrated that karstification objects tend to appear in groups. These groups of karsts occur in zones with geological conditions favorable for karstification. Such zones can include both, dangerous and not dangerous for

drilling karstification objects. Encountering any of them while drilling can serve as an indicator of drilling through a karstification zone. This can be used to support decision making for mitigating risks in drilling in karstification zones. The novelty here is utilization of not dangerous for drilling karst objects as indicators of karst zones. These objects can often remain unnoticed in the current drilling process.

C3: The obtained description and classification of karstification objects enabled a review of available technologies and methods that can be utilized for their prediction and/or detection either prior to or while drilling. The contribution of this stage is the classification of available methods and technologies with respect to their ability to detect/predict dangerous for drilling karsts. This classification shows a gap in the available technologies and indicates the most promising directions for research and development to fill in this gap. The summary of methods and technologies is provided in a table which can be used as a reference for selecting the most suitable technologies for drilling in carbonates.

C4: An extensive set of measurements consisting of drilling mechanics, mud flow, geology, core sample, petrophysical and geophysical data was analyzed and enabled the identification of a number of patterns in real-time drilling data corresponding to various karstification objects. These patterns, when detected, can serve as real-time indicators of karstification objects and zones. This information can be utilized by engineers and drilling support centers. Moreover, various automatic data processing technologies can be used to detect karstification zones in real-time and thus support risk mitigation while drilling through karstification zones. The results obtained at this stage are especially valuable, since they are based on in-depth analysis of the field data set from the Loppa High region in the Barents Sea. This is a very rare data set as it corresponds to drilling through karstification objects and it contains a rich set of measurements not usually utilized in drilling. This rare combination makes this data set and the corresponding analysis unique. The methodology developed in this section can be utilized for analysis of similar data sets from other fields. Thus, it can contribute to safer drilling in karstified carbonates when data from other fields become available.

C5: This work proposes and tests a signal processing algorithm for automated detection of the patterns in real-time drilling data corresponding to karsts. This algorithm provides better results than standard data filtering and can help engineers in drilling support centers to detect karstification patterns and other drilling events. The performance of this algorithm is demonstrated on the drilling data from the Loppa High region.

C6: A novel method is developed for prediction of karsts while drilling using look-ahead technology based on a borehole acoustic tool. The method is based on utilizing a pulse generator at the drilling bit and conventional borehole acoustic tool located further up at the BHA. By utilizing sequential measurements along the wellbore while drilling and by comparing these measurements by using an unsupervised ML algorithm, the proposed method can indicate upcoming hazards and other significant changes in the

formation properties. The concept has been validated through extensive simulations in the state-of-the-art industrial simulator COMSOL Multiphysics®. It can serve as a foundation for further research and development of look-ahead bit tools for safer drilling.

1.5 Structure of the thesis

The research has been structured into five goals, distributed over the five chapters in the main body of the thesis.

Chapter II presents, first, a general theoretical background of karstification phenomena with specific focus on the karst-forms that can be encountered in carbonate reservoirs and, second, based on a real field data set introduces the research objective of this thesis: prediction and early detection of dangerous for drilling karst forms.

Chapter III provides insight into advances in geophysical methods aiming at the detection of different geological objects (including karsts) in front of the bit.

Chapter IV analyzes possible patterns in real-time drilling data corresponding to drilling through karstification objects.

Chapter V focuses on the implementation of an algorithm that contributes to more accurate karst-patterns detection through the use of real-time drilling data.

Chapter VI presents and demonstrates a novel technology based on borehole acoustics and machine learning for investigating the region ahead of the drill bit to detect karst hazards or formation changes.

Chapter VII contains conclusions and discussions.

1.6 List of Publications

Paper I

Prediction and early detection of karsts – an overview of methods and technologies for safer drilling in carbonates
Danil Maksimov, Alexey Pavlov, Sigbjørn Sangesland, Bård Fjellså and Per Haugum
Published in the Journal of Energies. October, 2021

Paper II

Drilling in karstified carbonates – early risk detection technique.
Danil Maksimov, Alexey Pavlov and Sigbjørn Sangesland
Published in the Conference proceedings of the ASME 2020 39th International Conference on Ocean, Offshore and Arctic Engineering, Virtual Conference, June 28 - July 3, 2020

Paper III

Automated pattern recognition in real-time drilling data for early karst detection.
Danil Maksimov, Marius Aleksander Løken, Alexey Pavlov and Sigbjørn Sangesland
Published in the Conference proceedings of the 40th International Conference on Ocean, Offshore & Arctic Engineering, Virtual Conference, June 21 - June 30, 2021

Paper IV

Detection of karst hazards while drilling in carbonates. Danil Maksimov, Alexey Pavlov and Sigbjørn Sangesland
Submitted to the Journal of Energies

Chapter 2

Karstification - geological background

This chapter introduces the karst phenomena and discusses surface and subsurface signs of karstification. The geological background provided in this chapter summarizes the main elements of the conducted analysis of more than 100 papers devoted to the karst phenomena. In addition to that, an example of karstified carbonates in the Loppa High region is reviewed. Based on the field data provided, there is an analysis of the types of karstification objects. Their occurrence provides a classification of these objects into dangerous and not dangerous for drilling karsts.

2.1 Karst phenomena

One of the earth's most common minerals is calcium carbonate. Degradation of carbonates, known as karstification, results in the development of caves, vugs, fractures and cracks. There are a number of processes contributing to karstification. Dissolution of soluble rocks by meteoric waters along pathways specified by a geological structure is considered as one of the main mechanisms of karstification [28]. Other important factors for karst development are favorable geology, formation lithology, rock mechanical properties, burial depth and rock fracturing.

Karsts and signs of karstification can be found at different depths. Since the main mechanism of karstification is common for shallow and deeply buried carbonate structures, it is essential to review the common features of karstified landscapes first and then consider subsurface karsts.

2.1.1 Landscape karstification

Karstification of a landscape may be seen by different large and small-scale surface or subsurface objects as shown in Figure 2.1. Karst-classification, presented in this section, will be divided into surface (micro- and macro-forms) and subsurface (sinkhole and caves) categories. This is a conditional division of karsts because some of the karst forms like sinkhole may fall into both categories.

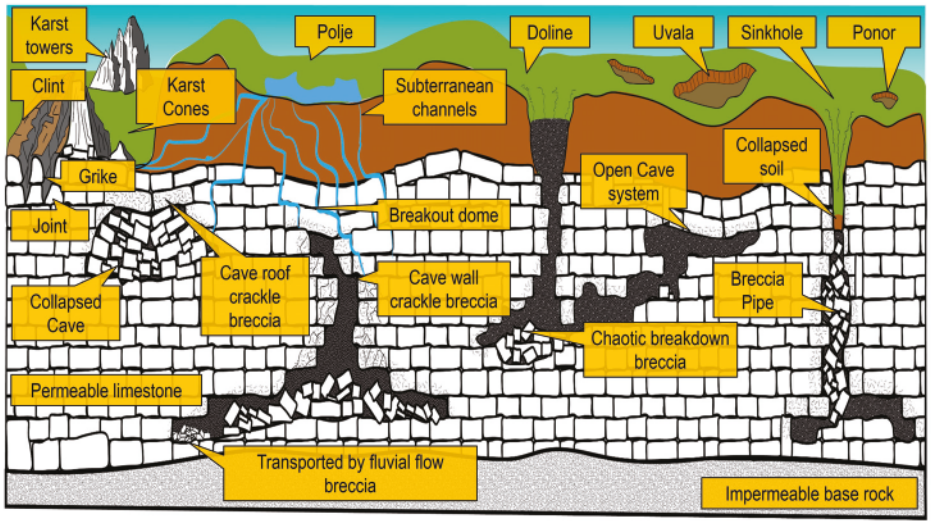

Figure 2.1: Karstic landscape

Surface micro-forms objects can generally be developed in the limestone or other soluble rocks such as carbonate or gypsum. As shown in the Figure 2.1, the typical result of this process is development of some salient features such as division of limestone into blocks (clints) bordered by vertical fractures (gricks) [2]. This is a widespread sign of landscape karstification presented by variety of shapes and sizes, spanning up to tens of meters.

Larger scale surface signs of karstification fall under the surface macro-forms objects category, which are the results of karsts/collapse features. As illustrated in Figure 2.1, round depressions of different scales are the common results of this process. This process underlies genesis of Doline or Uvala (set of Doline) surface signs of karstification. The largest macro-form phenomena is Polje. Typically, it has landforms of a kilometer scale, and is often seen in tectonically active karsts areas. Poljes landscape can be defined as karst basin, with steep peripheral slopes and karstic drainage.

Sinkhole form stands out in a separate class of objects and refers to a phenomenon of preceding cavity collapse with a subsequent development of surface sinks as the cavity becomes filled with soil or coarse-grained material. Depending on the mechanisms of the ground failure and rock type involved in subsidence, different types of sinkholes can be defined.

Depending on the mechanisms of the ground failure and rock type involved in subsidence, six classes of sinkholes were defined: dissolution, collapse, caprock, dropout, buried and suffusion [29]. Figure 2.2 provides a schematic overview of different types of sinkholes.

It should be noted that besides the aforementioned landscape phenomena, there are many other signs of surface karstification, which cannot fit into provided definitions as they consist of complex forms and cannot be described with a few criteria [30, 31]. Furthermore,

in certain cases even surface signs of karstification can be challenging to reveal. For instance, various subsequent processes such as immersion of a landscape caused by tectonics can be accompanied by karstification, which makes detection process complicated.

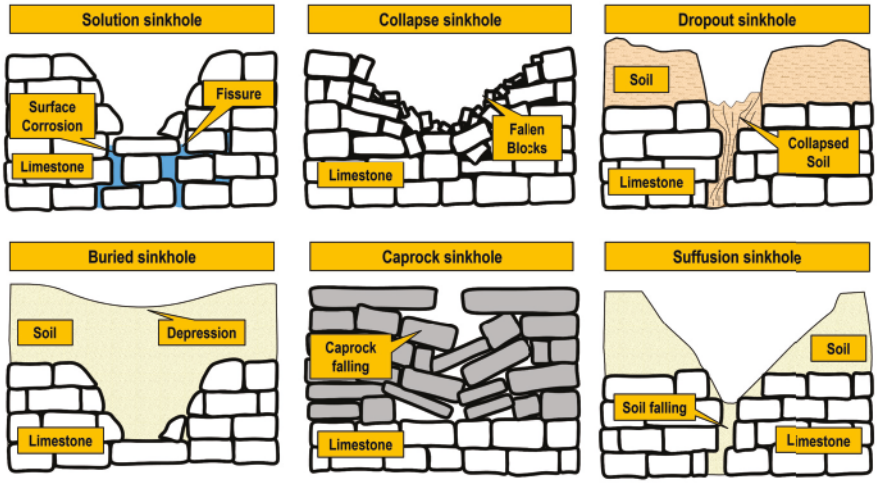

Figure 2.2: Types of sinkholes, inspired by [29]

Having discussed the surface signs of karstification, the following section discusses subsurface karst systems will. These karst systems can be discovered at large burial depths and in certain cases can be dangerous for drilling.

2.1.2 Subsurface karstification

A cave form is a conventional subsurface karst feature of soluble rocks. Based on Bella's [32] classification, the following mechanisms of cave development can be distinguished: chemical erosion (corrosion caves) and turbulent streams erosion (fluvial caves). Corrosion caves are more numerous unlike the turbulent caves and in general are smaller (diameter and length). Frequently, some caves can be a combination of these types of erosion.

Highly permeable channels, formed by the soluble action of water, create a primary network of channels, called anastomotic caves. The channels are typically spread along certain geological features such as fractures or a system of faults, and can penetrate the system of fluvial caves. Besides that, there are isolated cave types, which are not connected to any network. This type of caves is defined as voids. Many objects fall under this definition. Such voids can range from the vug-size small scale, up to the full cave scale. They pose a significant risk in case of suddenly revealing a well path crossing.

Regardless of the processes that cause enlargement of the caves, dimensions of the caves cannot infinitely expand. The resultant cave size has certain limits [33]. One of the main factors restricting the growth of the cave is the elastic limit of the rock masses surrounding

the cave. As soon as a certain limit is reached, the cave starts to collapse. Cave collapse initiates events, that have a serious impact on reservoir properties and are actively used as part of reservoir characterization study. Products of collapse, called cave-collapse breccia are composed of different angular fragments with their interspace filled by finer sediments or matrix particles. There are several cave-related breccia types depending on their texture and foregoing processes as shown in Figure 2.1. Progressive roof collapse with subsequent upward migration of the cave creates a breccia pipe [29]. Ceilings and walls collapse result in chaotic breakdown in a breccia. Cave-roof crackle breccia is formed by stress-contrast fractures of cave-roof rocks. However, brecciated rocks do not necessarily belong to the places of their development. For example, transported by fluvial flow, roof-collapse breccia rocks might be moved to a significant distance from original places of their development. An example of breccia is presented in Figure 2.3.

Figure 2.3: Core plug sample photo of angular breccia. Interval of cave roof collapse. Loppa High region.

Study of the products of cave collapse is important for different purposes, such as quantifying geological processes or reservoir modeling for flow simulators. Moreover, cave-collapse breccia is a direct sign of zones with open or partially filled caves. Drilling through open or filled caves can cause serious well control scenarios due to possible lost circulation of drilling fluid or damage of drill string components due to BHA drops.

Karstification does not always create potentially dangerous objects for drilling. In the oil and gas industry, karstification plays an important role. It is considered as the key process for the development of the permeability and porosity of carbonate reservoirs. In some cases, highly karstified intervals are the pay zones of the well. However, as stated previously, karstification is a complex process and the results of this process can be everything from small-scale porosity to the development of a large cave system. For the industry, on the one hand, porosity plays an important role for reservoir development purposes. On the other hand, there is a high risk associated with crossing a system of caves or vugs while drilling.

The cave form is the most complex structure among all the other landforms discussed in this section. For instance, dissolution caves are characterized by numerous three-dimensional patterns developed within different rock types with a variety of shapes and lengths. The mechanism of cave development can be explained by the influence of any of the following

factors or by a combination them: tectonic, climatic, hydrological, chemical and many others. Different theories exist nowadays in karstology that have been proposed to classify the caves based on the development mechanism. However, many of researchers argue that there is no single theory of genesis which can encompass all the caves, except at a trivial level of explanation [34].

Sometimes it is mistakenly assumed that large cave systems typically occur only at shallow depths, as the rock strength is sufficient to support overlaying sediments. Deeply buried open caves in general are not frequent as the increasing buried depth is directly related to the increased probability of a cave collapse. Nevertheless, there is numerous evidence of deeply buried caves, that are not collapsed and can exist for many centuries in equilibrium with the surrounding rocks. [1]

This section has discussed the main objects of karstification, which can be encountered both on the surface and subsurface.

2.2 Karstified carbonates in the Loppa High region

Karstification is a complex process and can result in objects with different shapes and sizes such as large cavities or small vugs. Some products of karstification can be dangerous for drilling, others are not. To learn more about geometrical properties of karsts deeply buried paleokarst terrain in Alta and Gohta discoveries of the Loppa High region (Figure 2.4) were examined. This analysis is based on the field data provided by Lundin Energy AS.

Figure 2.4: Barents Sea, Loppa High region, Alta and Gohta discoveries

[1] For further reading, I refer the interested readers to a book on problems in theoretical karst science, where there are details of possible factors affecting cave sizes with depth [35].

The seafloor in the studied region consists of complex patterns, formed as a result of considerable uplift and Cenozoic era erosion. Uplift has brought high density rocks close to the seafloor. This creates additional difficulties for seismic studies of the region [36]. This tectonic event led to the development of a complex underlying structure with extensive faulting and significant altitude changes of more than 1000 m (Kobbe formation) as shown in Figure 2.5.

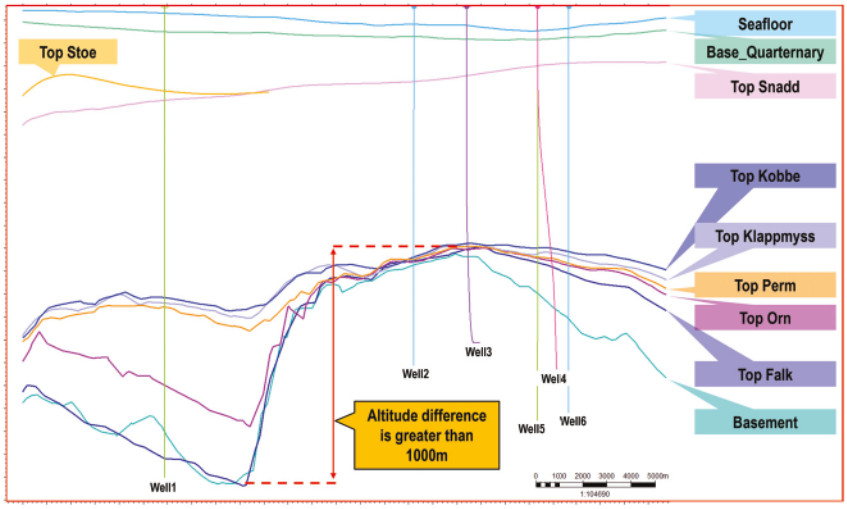

Figure 2.5: Intersection window through Alta and Gohta discoveries demonstrates significant altitude change of more than 1000 m (Kobbe formation)

Deeper layers of naturally fractured carbonates were weathered and buried. This caused karstification and the development of dominant regional karst features with certain properties. The major contributor to karstification is the process of dissolution of soluble rocks by meteoric water [28, 32]. [33] and [29] provide additional background on the mechanisms of karstification and their products.

2.2.1 Methodology of karsts mapping

The first step in the analysis of the field data from the Loppa High region is to identify wells with drilling events that can be associated with karsts, such as mud losses, gas kicks, drilling through cavities (see Step #1 in Figure 2.6). Based on this analysis an overview of rig-site drilling events was obtained for all wells within the region of study. Joint analysis of the rig-site events confirmed the existence of karstification intervals with specific BHA behavior such as reported drilling breaks, high levels of shocks, and mud losses.

Second, intervals of drilling events associated with karsts along the well-paths were localized and identified, as shown in Step #2 in Figure 2.6. This analysis provides a distribution of drilling events along the well-paths for the entire field.

Third, a detailed analysis of borehole images and core samples data was completed (Step #3 in Figure 2.6). Interpretation of borehole image data provided insight into karstification objects which were encountered in carbonates. This analysis allowed the study of some important properties of karsts. This gave a better understanding of the karstification problem in the Loppa High region in particular, and karstification phenomena in general. Moreover, analysis of borehole images reveals additional wells and intervals with karsts, where no drilling events were reported. This step completed the localization of karsts along the well paths. The main outputs are: 1) accurate karst mapping along the well paths 2) description of geometrical properties of karsts 3) revealing additional wells/intervals of karstification.

In the fourth step (#4 in Figure 2.6) I collected a systematized extended set of drilling measurements from the wells drilled in karstified carbonates, including drilling mechanics (surface and downhole measurements) and mud flow data (from CML sensors). This data analysis is used in subsequent analysis of karstification intervals (see Chapter 4).

Figure 2.6: The developed methodology for karst mapping and drilling events analysis

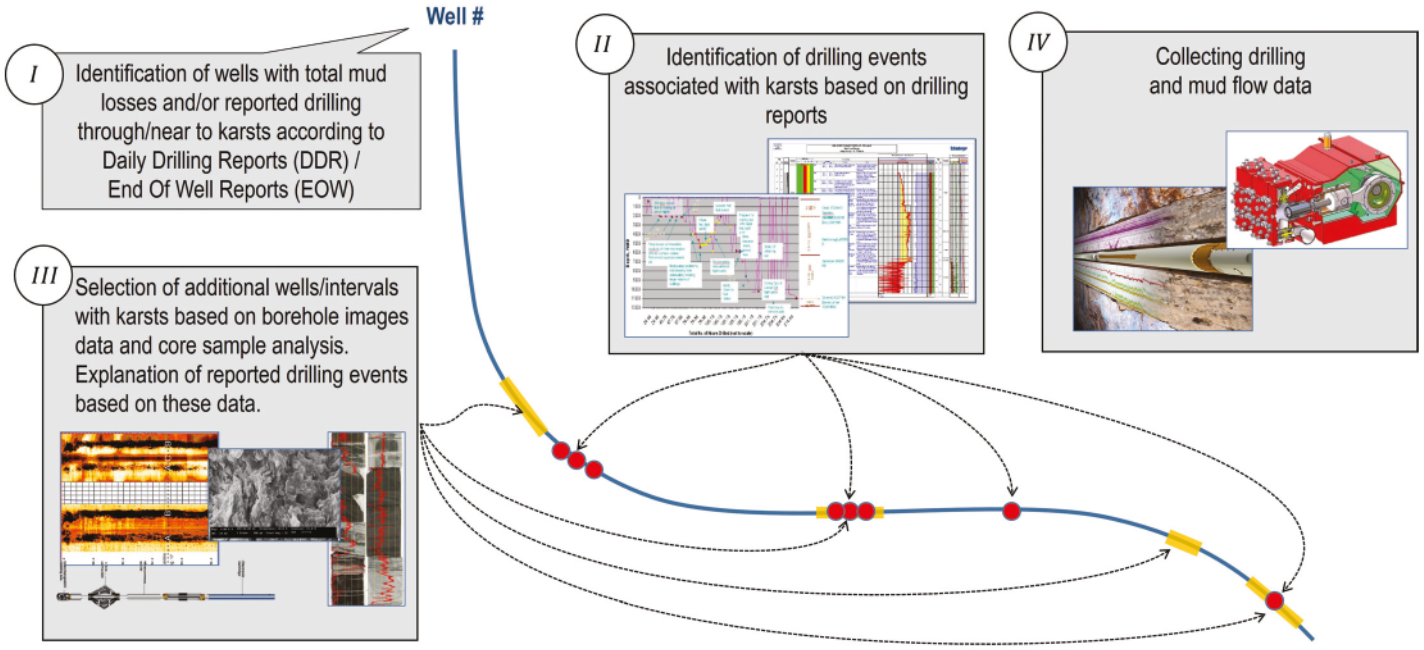

2.2.2 Overview of available field data

For this analysis I got access to drilling data from more than 20 wells drilled in karstified carbonates in the Loppa High region (Figure 2.4). These wells are characterized by an extended set of data available for analysis, including drilling data (mud logs, drilling reports, site survey reports), drilling mechanics data (surface and downhole measurements), geology (lithology, stratigraphy, biostratigraphy), rock and core (conventional core analysis and core photos), petrophysical reports (Computer Processed Interpretation (CPI), Composite) and well logs (wireline, LWD).

This is a relatively rare set of data, since: 1) The percentage of wells drilled through karsts that contain the necessary well log data such as borehole images, real-time drilling measurements, accurate delta-flow measurements is rather small; 2) Such data are typically confidential and rarely can be found in open access. Access to such a data set opens possibilities for detailed analysis of subsurface karstification phenomena.

Based on this analysis an overview was obtained of the different drilling problems encountered in carbonates for the entire field. Tables 2.1 and 2.2 present the collected data and data coverage across the field. A larger-font table can be found in the electronic version of the thesis available online. As can be noted, lower sections of the wells can be characterized by an extensive set of studies, since typically lower sections of the wells were drilled into karstified carbonate intervals.

Table 2.1: Overview of collected data and data coverage (Part 1)

Wells	Section, in (MD)	EOW reports			Daily reports		FIT/LOT	Drilling Mechanics data		LWD tools .las		Wired Pipe Daily or EOW reports		Logging Data							Wireline Data		Special Logging Data			Geological Data		Models
		Drilling	Geological	Mud Loggers	DDR	Mud Loggers		depth	time	depth	time	.pdf	.las	GR	Resis-ivity	Dens.	Poro-sity	Compr Veloc.	Shear Veloc.	Calip.	.pdf	.las	Borehole Images	ELAN	VSP	Well Tops	Faults, Fractures	Geomecha nical
1	26-in. (488-598 m)	+	+	+	+	+	n/a	+	+	+	n/a	n/a	n/a	+	+	n/a	n/a	+	+	n/a	n/a	n/a	n/a	n/a	n/a	+	+	+
	17.5 in. (898-1085 m)	+	+	+	+	+	+	+	+	+	n/a	n/a	n/a	+	+	n/a	n/a	+	+	n/a	n/a	n/a	n/a	n/a	n/a	+	+	+
	12.25 in. (1065-1767 m)	+	+	+	+	+	+	+	+	+	n/a	n/a	n/a	+	+	+	+	+	+	+	n/a	n/a	n/a	n/a	n/a	+	+	+
	8.5 in. (1767-1956 m)	+	+	+	+	+	+	+	+	+	n/a	n/a	n/a	+	+	+	+	+	+	+	n/a	n/a	n/a	n/a	n/a	+	+	+
2	12.25 in. (1102-1774 m)	+	+	+	+	+	n/a	+	+	+	+	n/a	n/a	+	+	+	+	+	+	+	+	+	n/a	n/a	+	+	+	+
	8.5 in. (1774-1922 m)	+	+	+	+	+	+	+	+	+	+	n/a	n/a	+	+	+	+	+	+	+	+	+	n/a	n/a	+	+	+	+
3	12.25 in. (1110-1913 m)	+	+	+	+	+	n/a	+	+	n/a	n/a	n/a	n/a	+	+	n/a	n/a	+	+	n/a	+	+	+	+	+	+	+	+
	8.5 in. (1913-2133 m)	+	+	+	+	+	+	+	+	n/a	n/a	n/a	n/a	+	+	+	+	+	+	+	+	+	+	+	+	+	+	+
4	6 in. (2130-2600 m)	+	+	+	+	+	+	+	+	+	+	n/a	n/a	+	+	+	+	+	+	+	+	+	+	+	n/a	+	+	+
5	26-in. (478-799 m)	+	+	+	+	+	n/a	+	+	+	+	n/a	n/a	+	+	n/a	n/a	n/a	n/a	n/a	n/a	n/a	n/a	n/a	n/a	+	+	+
	12.25 in. (799-1862 m)	+	+	+	+	+	+	+	+	+	+	+	+	+	+	n/a	n/a	+	+	n/a	n/a	n/a	n/a	n/a	n/a	+	+	+
	9.5 in. (1862-2336 m)	+	+	+	+	+	+	+	+	+	+	+	+	+	+	+	+	n/a	n/a	+	+	+	+	n/a	n/a	+	+	+
	8.5 in. (2336-3057 m)	+	+	+	+	+	+	+	+	+	+	+	+	+	+	+	+	n/a	n/a	+	+	+	+	n/a	n/a	+	+	+
6	26-in. (409.5m - 994 m)	+	+	+	+	+	n/a	+	+	+	+	n/a	n/a	+	+	n/a	n/a	+	+	n/a	n/a	n/a	n/a	n/a	n/a	+	+	n/a
	17.5 in. (894-1202 m)	+	+	+	+	+	+	+	+	+	+	n/a	n/a	+	+	n/a	n/a	+	n/a	n/a	n/a	n/a	n/a	n/a	n/a	+	+	n/a
	12.25 in. (1203-1770.5 m)	+	+	+	+	+	+	+	+	+	+	n/a	n/a	+	+	+	+	+	+	+	+	+	n/a	n/a	n/a	+	+	n/a
	8.5 in. (1770.5-2291 m)	+	+	+	+	+	+	+	+	+	+	n/a	n/a	+	+	+	+	+	+	+	+	+	+	+	+	+	+	n/a
7	26-in. (479m - 999 m)	+	+	+	+	+	n/a	+	+	+	+	n/a	n/a	+	+	n/a	n/a	+	n/a	n/a	n/a	n/a	n/a	n/a	n/a	+	+	n/a
	17.5 in. (999-1212 m)	+	+	+	+	+	+	+	+	+	+	n/a	n/a	+	+	n/a	n/a	+	+	n/a	n/a	n/a	n/a	n/a	n/a	+	+	n/a
	12.25 in. (1212-1778 m)	+	+	+	+	+	+	+	+	+	+	n/a	n/a	+	+	+	+	+	+	+	n/a	n/a	n/a	n/a	n/a	+	+	n/a
	8.5 in. (1778-2093 m)	+	+	+	+	+	+	+	+	+	+	n/a	n/a	+	+	+	+	+	+	+	+	+	+	n/a	+	+	+	n/a
8	17.5 in. (899-1222 m)	+	+	+	+	+	+	+	+	+	+	n/a	n/a	+	+	n/a	n/a	+	n/a	n/a	n/a	n/a	n/a	n/a	n/a	+	+	n/a
	12.25 in. (1222-1860 m)	+	+	+	+	+	+	+	+	+	+	n/a	n/a	+	+	+	+	+	+	+	+	+	n/a	n/a	n/a	+	+	n/a
	8.5 in. (1860-2121 m)	+	+	+	+	+	+	+	+	+	+	n/a	n/a	+	+	+	+	+	+	+	+	+	+	+	n/a	+	+	n/a
9	26-in. (483m - 664 m)	+	+	+	n/a	n/a	n/a	+	n/a	+	+	n/a	n/a	+	+	n/a	n/a	n/a	n/a	n/a	n/a	n/a	n/a	n/a	n/a	+	+	n/a
	17.5 in. (664-669 m)	+	+	+	n/a	n/a	+	+	n/a	+	+	n/a	n/a	+	+	n/a	n/a	n/a	n/a	n/a	n/a	n/a	n/a	n/a	n/a	+	+	n/a
	12.25 in. (669-1830 m)	+	+	+	n/a	n/a	+	+	n/a	+	+	n/a	n/a	+	+	+	+	+	+	+	n/a	n/a	n/a	n/a	n/a	+	+	n/a
	8.5 in. (1830-1970.4 m)	+	+	+	n/a	n/a	+	+	n/a	+	+	n/a	n/a	+	+	+	+	+	+	+	+	+	+	+	n/a	+	+	n/a
	6 in. (1970.4-2282 m)	+	+	+	n/a	n/a	+	+	n/a	+	+	n/a	n/a	+	+	+	+	+	+	+	+	+	+	+	+	+	+	n/a
10	17.5 in. (664-669 m)	+	+	+	n/a	n/a	+	+	n/a	+	+	n/a	n/a	+	+	n/a	n/a	+	+	n/a	n/a	n/a	n/a	n/a	n/a	+	+	n/a
	12.25 in. (664-2174 m)	+	+	+	n/a	n/a	+	+	n/a	+	+	n/a	n/a	+	+	n/a	n/a	+	+	n/a	n/a	n/a	n/a	n/a	n/a	+	+	n/a
	8.5 in. (2174-2281.8 m)	+	+	+	n/a	n/a	+	+	n/a	+	+	n/a	n/a	+	+	+	+	+	+	+	+	+	+	n/a	n/a	+	+	n/a
	6 in. (2281.8-2392 m)	+	+	+	n/a	n/a	+	+	n/a	+	+	n/a	n/a	+	+	+	+	+	+	+	+	+	+	+	n/a	+	+	n/a

Table 2.2: Overview of collected data and data coverage (Part 2)

Wells	Section, in (MD)	EOW reports			Daily reports		FIT/LOT	Drilling Mechanics data		LWD tools .las		Wired Pipe Daily or EOW reports		Logging Data							Wireline Data		Special Logging Data			Geological Data		Models
		Drilling	Geological	Mud Loggers	DDR	Mud Loggers		depth	time	depth	time	.pdf	.las	GR	Resis-ivity	Dens.	Poro-sity	Compr Veloc.	Shear Veloc.	Calip.	.pdf	.las	Borehole Images	ELAN	VSP	Well Tops	Faults, Fractures	Geomecha nical
11	26-in. (455m - 479m)	+	+	+	n/a	n/a	n/a	n/a	n/a	+	+	n/a	n/a	+	+	n/a	n/a	n/a	n/a	n/a	n/a	n/a	n/a	r/a	n/a	+	+	n/a
	17.5 in. (479-546m)	+	+	+	n/a	n/a	+	n/a	n/a	+	+	n/a	n/a	+	+	n/a	n/a	n/a	n/a	n/a	n/a	n/a	n/a	r/a	n/a	+	+	n/a
	12.25 in. (546-1130m)	+	+	+	n/a	n/a	+	n/a	n/a	+	+	n/a	n/a	+	+	n/a	n/a	+	+	n/a	+	+	n/a	r/a	n/a	+	+	n/a
	8.5 in. (1130-1540m)	+	+	+	n/a	n/a	+	n/a	n/a	+	+	n/a	n/a	+	+	+	+	+	+	+	+	+	n/a	r/a	+	+	+	n/a
12	26-in. (435m - 965m)	+	+	+	n/a	n/a	n/a	+	+	+	+	n/a	n/a	+	+	+	+	+	n/a	+	n/a	n/a	n/a	r/a	n/a	+	+	n/a
	17.5 in. (965-670m)	+	+	+	n/a	n/a	+	+	+	+	+	n/a	n/a	+	+	+	+	+	+	+	n/a	n/a	n/a	r/a	n/a	+	+	n/a
	12.25 in. (670-1622m)	+	+	+	n/a	n/a	+	+	+	+	+	n/a	n/a	+	+	+	+	+	+	+	n/a	n/a	n/a	r/a	n/a	+	+	n/a
	8.5 in. (1622-2177m)	+	+	+	n/a	n/a	+	+	+	+	+	n/a	n/a	+	+	+	+	+	+	+	n/a	n/a	n/a	r/a	n/a	+	+	n/a
	6 in. (2177-2842m)	+	+	+	n/a	n/a	+	+	+	+	+	n/a	n/a	+	+	+	+	+	+	+	n/a	n/a	+	+	+	+	+	n/a
13	24 in. (489-800m)	+	+	+	n/a	n/a	+	n/a	n/a	+	n/a	n/a	n/a	+	+	+	n/a	+	n/a	n/a	+	n/a	n/a	r/a	n/a	+	+	n/a
	12.25 in. (800-1805m)	+	+	+	n/a	n/a	+	n/a	n/a	+	n/a	n/a	n/a	+	+	+	n/a	+	n/a	n/a	+	n/a	n/a	r/a	n/a	+	+	n/a
	8.5 in. (1805-2800m)	+	+	+	n/a	n/a	+	n/a	n/a	+	n/a	n/a	n/a	+	+	+	n/a	+	n/a	+	+	n/a	n/a	r/a	+	+	+	n/a
14	26-in. (343m - 823m)	+	+	+	n/a	n/a	n/a	+	n/a	+	n/a	n/a	n/a	+	+	n/a	+	+	+	n/a	n/a	n/a	n/a	r/a	n/a	+	+	n/a
	17.5 in. (823-1545m)	+	+	+	n/a	n/a	+	+	n/a	+	n/a	n/a	n/a	+	+	n/a	+	+	+	n/a	n/a	n/a	n/a	r/a	n/a	+	+	n/a
	12.25 in. (1545-2022m)	+	+	+	n/a	n/a	+	+	n/a	+	n/a	n/a	n/a	+	+	+	+	+	+	+	n/a	n/a	+	+	n/a	+	+	n/a
	8.5 in. (2022-2818m)	+	+	+	n/a	n/a	+	+	n/a	+	n/a	n/a	n/a	+	+	+	+	+	+	+	n/a	n/a	+	+	+	+	+	n/a
15	26-in. (443m - 680m)	+	+	+	n/a	n/a	+	+	n/a	+	n/a	n/a	n/a	+	+	n/a	n/a	+	+	n/a	n/a	n/a	n/a	r/a	n/a	+	+	n/a
	17.5 in. (680-1622m)	+	+	+	n/a	n/a	+	+	n/a	+	n/a	n/a	n/a	+	+	n/a	n/a	+	+	n/a	n/a	n/a	n/a	r/a	n/a	+	+	n/a
	12.25 in. (1622-2300m)	+	+	+	n/a	n/a	+	+	n/a	+	n/a	n/a	n/a	+	+	+	+	+	+	+	n/a	n/a	+	+	n/a	+	+	n/a
	8.5 in. (2244-2985m)	+	+	+	n/a	n/a	+	+	n/a	+	n/a	n/a	n/a	+	+	+	+	+	+	+	n/a	n/a	+	+	+	+	+	n/a
16	17.5 in. (610-1222m)	+	+	+	n/a	n/a	+	n/a	n/a	+	n/a	n/a	n/a	+	+	n/a	+	+	+	n/a	n/a	n/a	+	+	n/a	+	+	n/a
	12.25 in. (1222-2136m)	+	+	+	n/a	n/a	+	n/a	n/a	+	n/a	n/a	n/a	+	+	+	+	+	+	+	n/a	n/a	+	+	n/a	+	+	n/a
	8.5 in. (2136-2226m)	+	+	+	n/a	n/a	+	n/a	n/a	+	n/a	n/a	n/a	+	+	+	+	+	n/a	+	n/a	n/a	+	+	+	+	+	n/a
17	26-in. (394m - 460m)	+	+	+	n/a	n/a	+	+	+	+	n/a	n/a	n/a	+	+	n/a	n/a	n/a	n/a	n/a	n/a	n/a	n/a	n/a	n/a	n/a	+	+	n/a
	17.5 in. (460-1122m)	+	+	+	n/a	n/a	+	+	+	+	n/a	n/a	n/a	+	+	n/a	n/a	+	+	n/a	n/a	n/a	n/a	n/a	n/a	n/a	+	+	n/a
	12.25 in. (1122-2046m)	+	+	+	n/a	n/a	+	+	+	+	n/a	n/a	n/a	+	+	+	+	+	+	+	n/a	n/a	+	+	n/a	+	+	n/a
18	8.5 in. (2034-2925m)	+	+	+	n/a	n/a	+	+	n/a	+	n/a	n/a	n/a	+	+	+	+	+	n/a	+	n/a	n/a	+	+	+	+	+	n/a
19	26-in. (326m - 445m)	+	+	+	n/a	n/a	+	+	n/a	+	n/a	n/a	n/a	+	+	n/a	n/a	n/a	n/a	n/a	n/a	n/a	n/a	n/a	n/a	n/a	+	+	n/a
	17.5 in. (645-1322m)	+	+	+	n/a	n/a	+	+	n/a	+	n/a	n/a	n/a	+	+	n/a	n/a	n/a	n/a	n/a	n/a	n/a	n/a	n/a	n/a	n/a	+	+	n/a
	12.25 in. (1322-2033m)	+	+	+	n/a	n/a	+	+	n/a	+	n/a	n/a	n/a	+	+	+	+	+	+	+	n/a	n/a	n/a	n/a	n/a	n/a	+	+	n/a
	8.5 in. (2033-2925m)	+	+	+	n/a	n/a	+	+	n/a	+	n/a	n/a	n/a	+	+	+	+	+	+	+	n/a	n/a	n/a	n/a	+	+	+	n/a
20	26-in. (422m - 480m)	+	+	+	n/a	n/a	+	+	n/a	+	n/a	n/a	n/a	+	+	n/a	n/a	n/a	n/a	n/a	n/a	n/a	n/a	n/a	n/a	n/a	+	+	n/a
	17.5 in. (480-1122m)	+	+	+	n/a	n/a	+	+	n/a	+	n/a	n/a	n/a	+	+	n/a	n/a	n/a	n/a	n/a	n/a	n/a	n/a	n/a	n/a	n/a	+	+	n/a
	12.25 in. (1122-1836m)	+	+	+	n/a	n/a	+	+	n/a	+	n/a	n/a	n/a	+	+	n/a	n/a	n/a	n/a	n/a	n/a	n/a	+	n/a	n/a	n/a	+	+	n/a
	8.5 in. (1836-2025m)	+	+	+	n/a	n/a	+	+	n/a	+	n/a	n/a	n/a	+	+	+	+	+	n/a	+	n/a	n/a	+	+	n/a	+	+	n/a

2.2.3 Mapping of logged karstification objects

All the above-mentioned wellbore information was gathered and aggregated into a single industrial software platform - Techlog Wellbore Software ® [37]. It allowed the uniting of various types of field data to conduct a joint analysis of different types of data. An example of this analysis is shown in Figures 2.7, 2.8 and 2.9. For each wells displayed in the figure well tops were assigned according to geological reports. This gave an understanding of the geological section where each well was drilled. Well tops are plotted on the first track and displayed in Measured Depth.

The second track shows the Mud Weight (MW) which was used for drilling specific intervals of each of the studied well. These data were gathered from daily drilling- and End Of Well Report (EOW) wellsite reports. This gave an overview of the MWs used to drill each of the formations. It was used in estimation of average values of mud weights used across the field for each of the formations drilled. This part of the analysis allowed the removal of intervals of mud losses when the MW was significantly higher than the average MW used to drill the same interval on other wells. Keeping such intervals of high MW can lead to misinterpretations of the real causes of mud loss events.

Based on in-depth analysis of rig-site events reported in mud logging, drilling and well-site reports, specific intervals of the communicated drilling problems were marked as shown in Figures 2.7, 2.8 and 2.9. This gave an overview of drilling problems that encountered corresponded to drilling through carbonate sections.

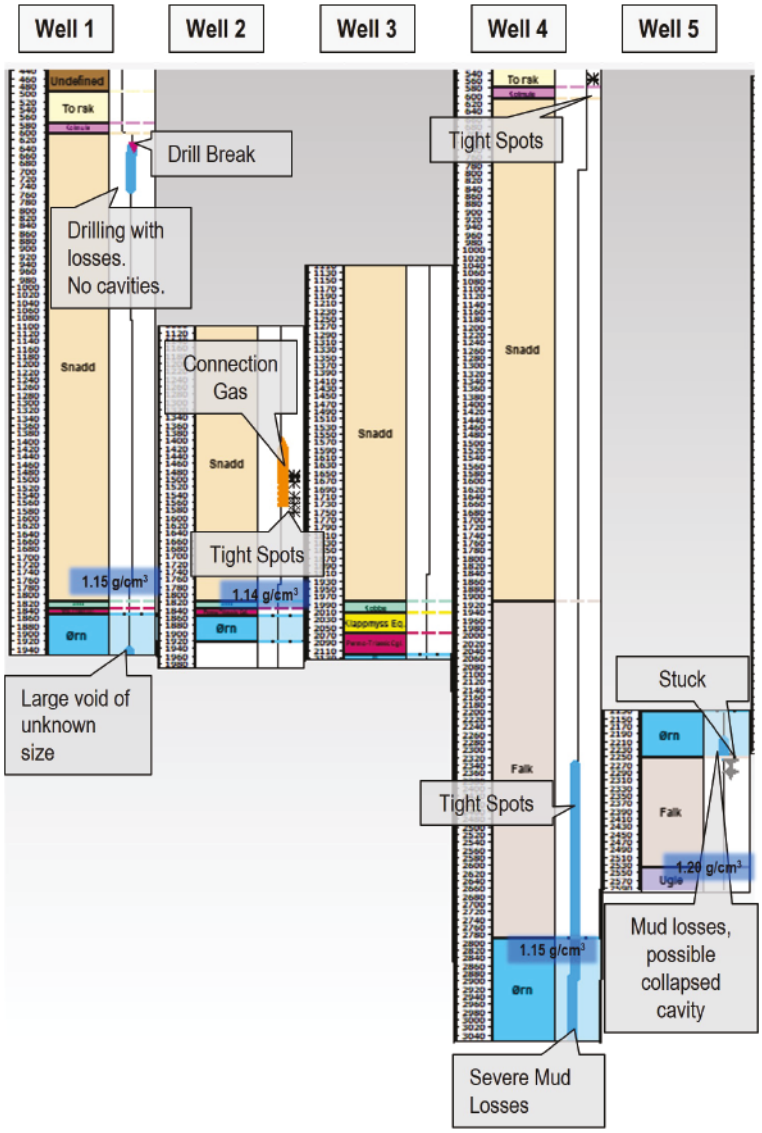

Figure 2.7: Audit of drilling events in the intervals of karstification (Wells 1-5)

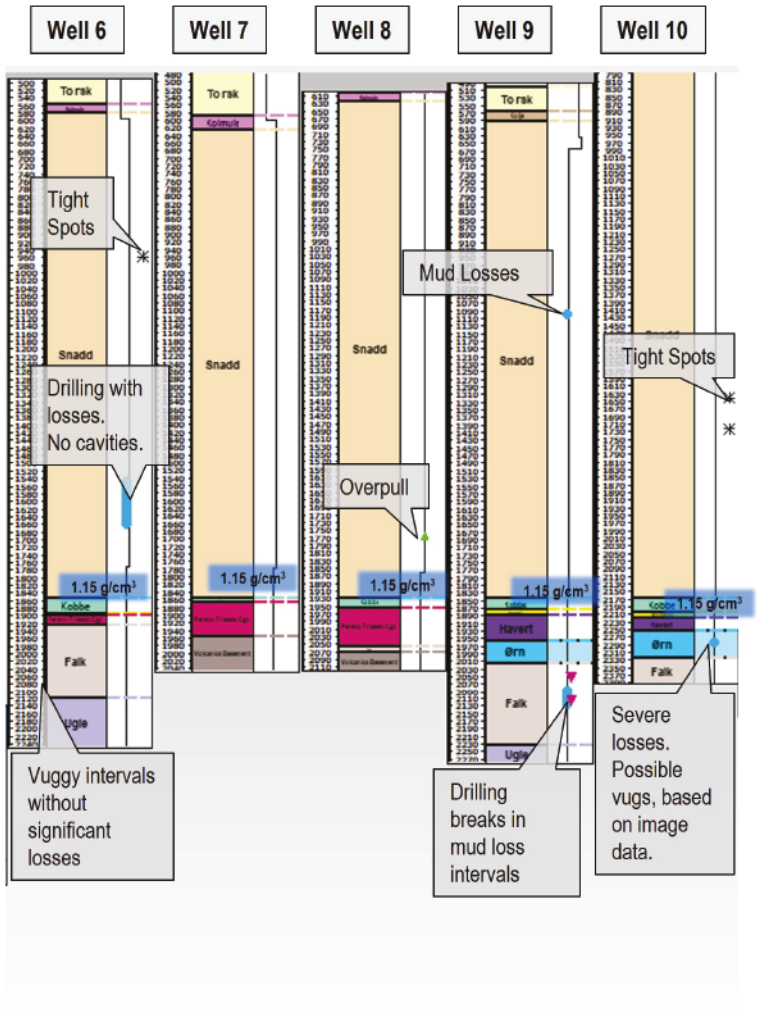

Figure 2.8: Audit of drilling events in the intervals of karstification (Wells 6-10)

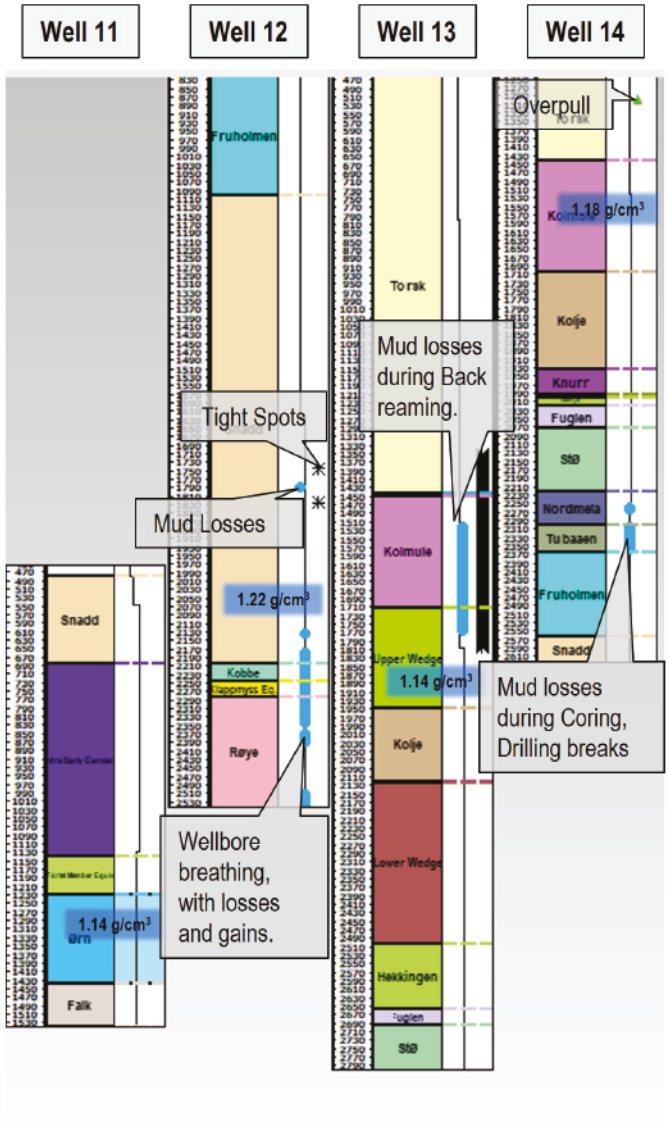

Figure 2.9: Audit of drilling events in the intervals of karstification (Wells 11-14)

An analysis of borehole image data was done. Interpretation of image data typically is intended to determine the magnitudes, azimuths and geometrical properties of numerous geological features along the wellbore paths, including studying of vugs, breccias, caves and other karst forms. Borehole imaging can be presented as the “unrolling” of a wellbore picture along the well path as shown in Figure 2.10. This study uses borehole images for: 1) mapping intervals of karstification such as open fractures vugs and caves; 2) determination of geometrical properties of karsts. This helps to get insight into root causes of some of the drilling events that occurred in carbonate sections such as drilling breaks and mud losses. Moreover, borehole image analysis enabled the identification of additional intervals of karstification. An example of this analysis is shown in Figure 2.12.

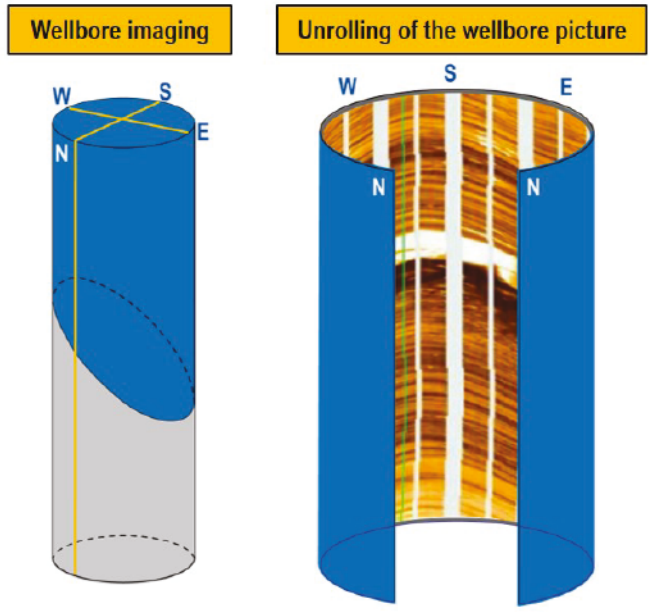

Figure 2.10: Borehole imaging - visualization of the borehole environment

This work included an analysis of core samples. Core analysis provides essential input for the evaluation of karstified intervals mapped by borehole images. The studied cores were drilled near cave intervals. Analysis of these core samples indicates that cave structures are surrounded by intervals with breccia and fluvial channels. Examples of core samples from such intervals are given in Figure 2.11. The shown interval of fluvial channels underlies a cave.

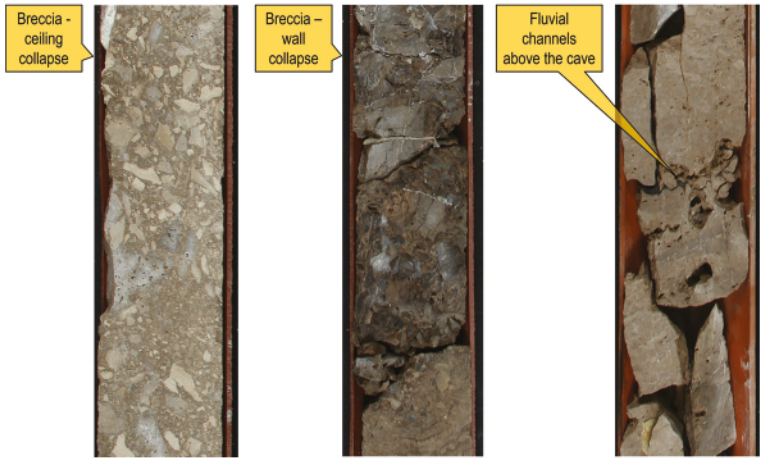

Figure 2.11: Photography of core sampled intervals of a carbonate section. From left to right: breccia originated from ceiling collapse, a breccia originated from wall collapse, interval of fluvial channels discovered above a cave

2.2.4 Analysis of mapped karstification objects

A comprehensive study of the borehole images and drilling events has been performed for the entire region of study for 20 wells. An example of this analysis is shown in Figure 2.12, where some of the discovered events are plotted along the well trajectories. The visualization of events and mapped intervals of karstification is conducted in the Petrel Software Platform ® [38]. The presented well intersection window allows well trajectories to be displayed along a selected *slice* of a 3D geological cube. The slice-line in this example intersects wells drilled through the intervals of karstification. Since some of the wells are located at a significant distance from each other, it is difficult to plot them in an appropriate scale for a figure. To obtain better visualization, in Figure 2.12 only a subset of the 20 wells which are located close to each other are presented.

As follows from Figure 2.12 as well as from the analysis of all the remaining wells, karstification objects and the corresponding drilling events, minor or major, are often encountered in sequences corresponding to karstification intervals rather than as individual objects.

This confirms the hypothesis that geological conditions favorable to development of a single karst object extend over zone region and can reult in generation of a number of karstification objects in that region.

Therefore, encountering karstification objects while drilling, even though they can be not dangerous for drilling, can serve as an indicator of the region with a high likelihood of encountering other dangerous for drilling karst objects. Detection of different karst-forms while drilling may provide a vital information about possible regional drilling risks. How to detect them from real-time drilling data will be discussed in details in Chapter 4. In the

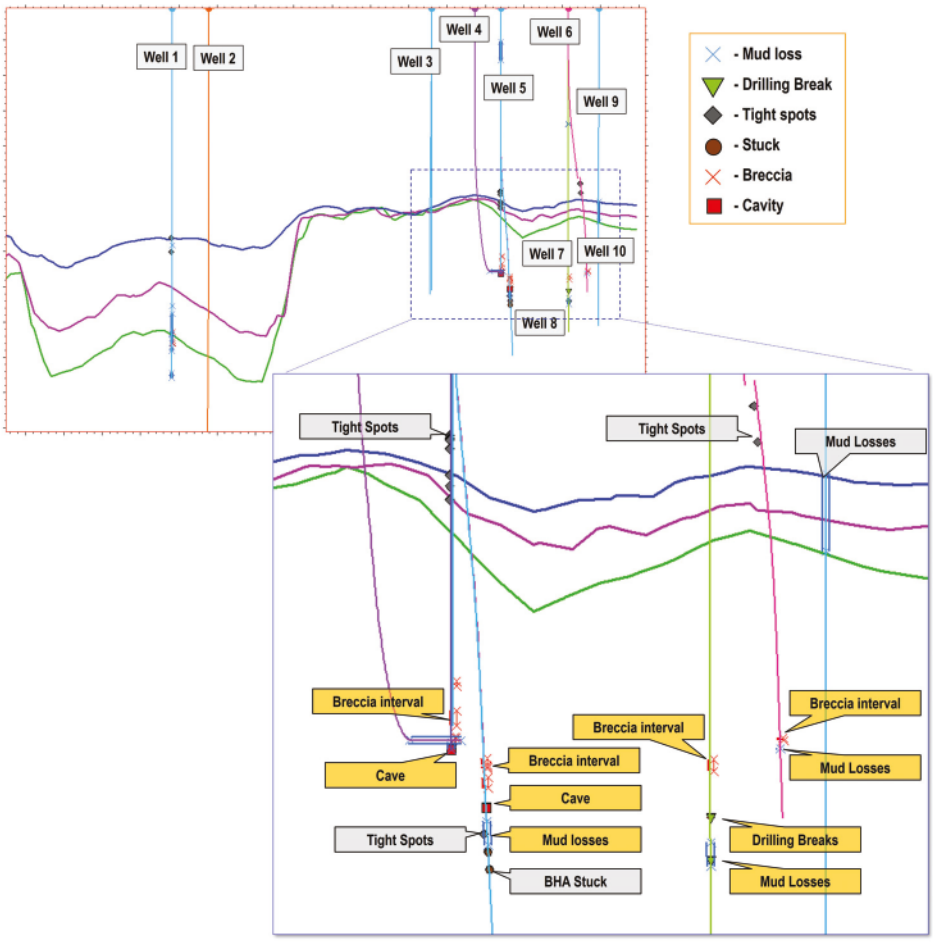

Figure 2.12: Drilling events in the karstification intervals

next chapter parameters of dangerous for drilling and not dangerous for drilling karsts are considered.

2.2.5 Classification

Dangerous for drilling regional karst features

A comprehensive analysis of borehole images, and the history of drilling, revealed that karsts larger than 0.5 m pose significant risks for drilling since they led to a partial or total loss of drilling fluid, compromising drilling safety [7]. In some cases, Bottom Hole Assembly (BHA) components were broken due to excessive shock loading when the drill bit suddenly touches the bottom of a cave. As an example let us consider some parameters of a karstification cave that caused drilling problems (Figure 2.13).

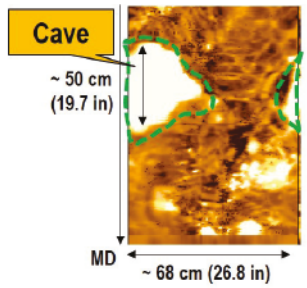

Figure 2.13: Example of a cave

The exact geometrical size of this karst is unknown. However, its interpretation from the borehole image defined the geometrical size as more than 50 cm in length with a circumference of 21.6 cm (8.5" section of the well). Overall, the average size of the caves in the studied region is in the range of 0.5 and 2 m. These karst forms are challenging to detect with the state-of-the-art geophysical methods as will be shown in Chapter 3. This thesis focuses on the development of solutions for early detection of karsts sized 0.5 - 2 m.

Not dangerous for drilling dominant regional karst features

Based on the analysis of drilling events from the entire field, vugs and natural fractures with the following dimensions are considered as not dangerous for drilling within the studied region.

Dominant regional karst features:

1. Vugs are typically dissolution cavities produced by meteoric or diagenetic fluids. Vugs can indicate a lithology- or texture- selective nature of the dissolution process. Borehole geologists often refer to a broader meaning and define them as a pore space that can be detected by the imager (typically $> 0.5\ cm^2$ area of the borehole wall). In this work, the value of $0.5\ cm^2$ is considered as the smallest vug size and the maximum visually estimated value of not dangerous for drilling is a vug of $10\ cm^2$. Image example of cm to dm scale vugs and the vugginess intensity of the Lower Falk formation is shown in Figure 2.14a.
2. Natural fractures are probably formed by the interaction of foliation planes with the recent stress field or tectonic events. Four types of conductive fractures were distinguished in the studied region, depending on their open/closed nature and their circumferential span: Drilling-induced fractures (tensile sector of the borehole wall), vertical to subvertical and open fractures. Aperture results are distributed in a log-normal bell shape in the 0.2 - 20 mm range. Image examples of drilling-induced, irregular conductive fractures and closed conductive fractures are shown in Figure 2.14b, 2.14c, 2.14d.

In this section dominant regional karst features are conditionally divided into dangerous and not dangerous for drilling groups. The next chapter presents an overview of the methods for early detection of the dangerous for drilling karst forms discussed in this section.

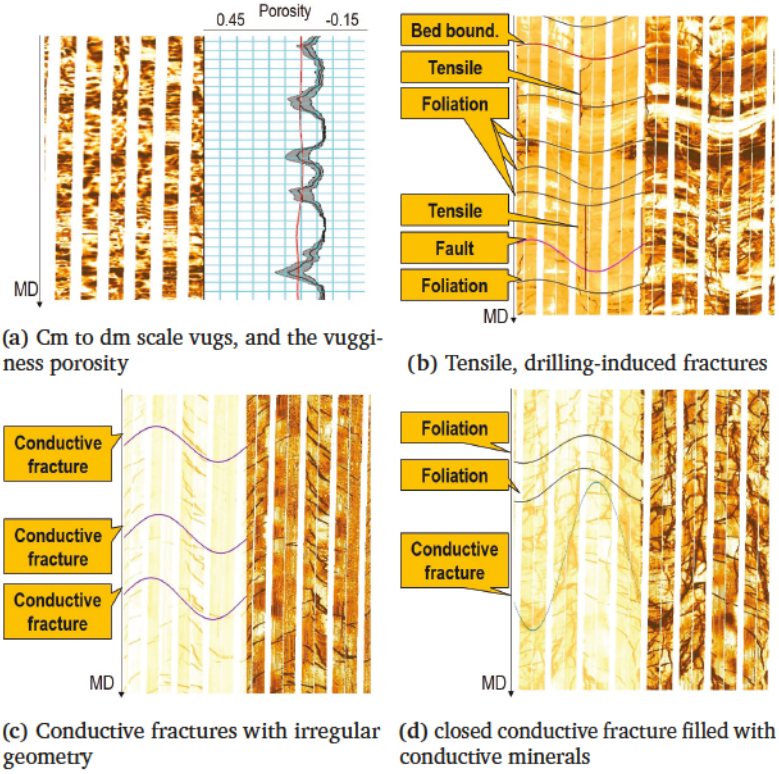

(a) Cm to dm scale vugs, and the vugginess porosity

(b) Tensile, drilling-induced fractures

(c) Conductive fractures with irregular geometry

(d) closed conductive fracture filled with conductive minerals

Figure 2.14: Comparison of dominant regional karst features

2.3 Summary

This chapter is based on a literature review that has considered karst phenomena and has discussed surface and subsurface signs of karstification. A rare set of field data from the Loppa High region was analyzed. It was concluded that karsts come in groups in karstification zones. A single karst object can be an indicator of a karstification zone and thus indicates a high likelihood of encountering other karsts, including dangerous for drilling karsts. The dominant regional karst features were classified into groups of dangerous and not dangerous for drilling. This can be used for evaluation of available technologies and for the development of new methods proposed later in this thesis.

Chapter 3

Geophysical methods for prediction and early detection of karsts

3.1 Introduction

The prediction or detection of dangerous for drilling karstification objects ahead of the bit is an important issue. There are numerous geophysical methods for measuring and evaluating downhole conditions in the wellbore. However, due to limitations and the technological challenges inherent in these methods, there is still no efficient and reliable technology for the prediction or early detection of drilling hazards such as karsts ahead of the drill bit.

This chapter reviews methods and technologies that can be used for the prediction and early detection of karsts. In particular, acoustic, resistivity and seismic approaches are considered as well as inventions and technologies developed and published over the past 40 years. This chapter identifies the advantages, limitations and gaps in the existing technologies and discusses the most promising methods for karst detection and prediction.

There are different methods to mitigate the risks of drilling in karstified regions. As shown in Figure 3.1 three main groups are defined, depending on when risk minimization occurs. The first group is aimed at minimizing drilling risks at the pre-drill stage by identifying potentially dangerous intervals that need to be considered before drilling begins. One of the ways to reveal dangerous karst objects before drilling and estimate the risks of drilling through them is based on geological analysis. In many cases, there are different surface and subsurface signs of karstification that can be detected in the pre-drill stage. These signs can be employed to identify such regions and intervals to optimize well placement and well path.

Another method, that provides insight into potentially dangerous intervals for drilling is the offset well analysis. Intervals with karstification signs that are dangerous for drilling can be defined based on well-site reports, drilling history, and incident analysis of the offset wells. These intervals, in accordance with different approaches to discrete properties distribution, [39], can be propagated into inter-well space and projected on the planned

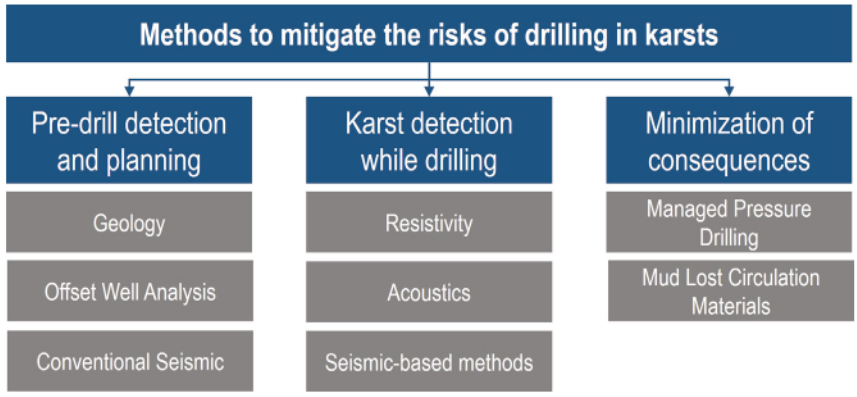

Figure 3.1: Methods to mitigate the risks of drilling in carbonates

well path. In case the planned well path crosses the projected high-risk interval, its drilling trajectory and/or drilling program can be revised for drilling risks minimization.

Seismic imaging is the last method in this group. This the standard technique for mapping reservoirs, faults, and structural surfaces. Seismic detection of karst structures can be very efficient for early drilling risk minimization by providing the most complete picture of the main subsurface objects [40].

The second group represents methods of karst detection while drilling. In some cases, it is challenging to minimize drilling risks at the pre-drill stage. As is the case in exploration drilling, when uncertainties might exist due to limitations of pre-drill methods of karst detection. Thus, to increase the accuracy of karst feature detection, real-time measurements should be used.

There are three main real-time approaches that can be utilized for early karst detection. The first approach covers resistivity methods of karst detection based on ultra-deep look-around and ahead of the bit measurements. The second approach unites a number of measurements, which utilize the principle of reflected acoustic signal detection from interfaces. Unlike conventional seismic, these methods use different wavelengths, which helps to detect small karst features. The third approach investigates seismic-based methods. This set of methods is separate from the conventional seismic methods group as they measure seismic reflections while drilling. These methods are based on the principle of downhole generation of seismic waves, which gives a number of advantages over conventional seismic methods.

The last group addresses methods to minimize the consequences of drilling into karsts. One of the main challenges of drilling in carbonates is potential mud losses of different severity. This often occurs when a well path crosses highly permeable channels, faults, or caves. Depending on the volume of mud losses and geometrical sizes of the channels, some can be successfully plugged by LCM [41], [42]. However, severe mud losses are frequently encountered in large fluvial channels or caves which cannot be plugged with LCM and may

lead to well control incidents [5]. The solution widely used by the industry is MPD and its modifications. In this case, the well is converted to PMCD and drilling can be continued with controllable pumping of sacrificial fluid and drilling cuttings into caves, fractures, and other highly permeable zones. The efficiency of this approach was demonstrated by a number of wells drilled in carbonates [24], [25], [43], [26]. However, MPD-based solutions for drilling risks minimization have limitations. First, additional equipment should be mounted on the rig, such as a rotational control device and modified riser joints. Second, in some regions, it is impossible to supply the required significant volume of sacrificial fluid to pump into well. Third, there are might be government restrictions on well conversion into PMCD . These factors might impose limitations on the use of PMCD . The methods described in this group are beyond the scope of this dissertation. The methods described in this group are not considered in this thesis.

The scope of this chapter is to analyze different geophysical methods and evaluate their ability to detect karsts either before drilling begins or while drilling, before the drill bit hits a karst. Therefore, I follow the first and second groups of methods from Figure 3.1. This analysis can contribute to better utilization of existing technologies and enhance understanding of possible technologies for future development. Thus I evaluate the effectiveness of various methods for early karst detection. By systematically analyzing various types of available measurements based on different principles, I effectively constrain the range of concepts and summarize their areas of applicability. This can provide a starting point for identifying relevant measurements for each specific case to minimize the risks of sudden karst encounters. I have examined the role of the existing state of the art and highlighted examples in which conventional geophysical methods can provide a valuable outcome for decision making. The physical principles of measurements discussed in this chapter are an important aspect for proper evaluation of geophysical methods for detecting signs of karstification.

One of the contributions of this work is the identification of the most representative types of geophysical, geological, and seismic studies that enable us to identify intervals and zones with the highest probability of karst detection before drilling into them. The presented contribution can be used to narrow available pre-drill and real-time data and focus on the most representative methods capable of giving the most accurate early detection of karsts.

3.2 Pre-drill prediction of karsts

Risk avoidance and minimization measures at the early stage of well planning is an essential component in risk management, which can predefine overall drilling and completion efficiency. Wellbore profile and trajectory optimization to find the safest trajectory and ensure that a number of potentially dangerous geological features will be avoided can greatly enhance drilling safety. To design the safest well path, it is important to identify the spatial distribution and geometrical properties of drilling hazards based on available pre-drill data.

In this section, I first introduce the geological signs of karstification phenomena and then consider pre-drill methods of risk minimization such as projection of dangerous intervals on the new well path and seismic imaging of karsts.

3.2.1 Geological signs of karstification

The process of karstification of a landscape may result in a variety of developments in large or small features both on the surface and beneath as was discussed in Section 2.1. This has important implications for evaluating the possibilities of dangerous karst form developments in the region of study. Starting from the identification of landscape signs of karstification, geologists and other specialists in geoscience, can utilize the geological data, typically available before drilling begins, to determine what type of rock underlies the soil. Then, further analysis moves towards the detection of broken rocks which originate from a cavern, fractured zones, and vugs. A joint analysis of the available geological data can be done to improve the localization of potential karstified areas. An important element in this analysis is the detection of vugs and breccias which might be associated with the development of caves and/or overall karstification of the interval.

The detection accuracy of karstification objects at regional or local scales has a significant dependence on the quality and coverage of input geological data. For instance, in the case of limited input data, a study of only landscape signs of karstification cannot reveal spatial positions of karsts at significant depths. At the same time, a joint study of the geological section, through regional tectonics and sedimentation processes evaluation, can improve the accuracy of karst detection. Consequently, the geological method of karsts detection can serve as the first step to obtain an overall picture of karst distribution along with revealing the main areas of karstification.

3.2.2 Projection of drilling risks on planned well-path

Gaining experience from drilling offset wells and transferring it to a planned well path are the two most critical components in well planning. The detailed analysis of recorded geophysical logs from offset wells can reveal some signs of karstification as mentioned in the previous section. Having found such signs, and, thus, identified karst intervals, the next step might be to examine whether there is a probability to intersect the same intervals in the new well trajectory.

This can be done as follows. In most cases, we cannot model caves and vugs deterministically, as we cannot obtain their geometrical properties with sufficient resolution in three dimensions. Instead, modeling of such objects can be done stochastically with statistical equivalence to the observed distribution of karsts along the wellbore. Sequential Gaussian simulation [44] is a commonly used geostatistical method aimed at solving similar tasks of property distribution, by creating stochastic models of spatial phenomena.

This approach is often applied for discrete fracture network modeling and helps to populate individual fracture parameters such as size, shape, orientation, aperture, and coordinates obtained from well fracture characterization data. Besides, the same approach is used for volumetric rock property distribution such as porosity, permeability, density, and many other parameters that can be incorporated into a 3D geological model in the interwell space.

A similar approach can also be used for prediction of karst distribution. The simplest model of karst distribution can begin with setting the positions of caves randomly in a pre-defined volume with a known density. Then, based on the calibration data of the exact cave positions, obtained from geophysical study and/or offset well analysis, cave geometries and any other desired parameters can be incorporated into the model. The output of this model can be a projection of karsts into a new well trajectory. There are more sophisticated approaches to discrete property distribution, which can be used to model different levels of karst structure complexities. This example demonstrates the possible application of stochastic methods to model the distribution of karsts in carbonates.

Some limitations of this method should be noted. First, the statistically-based prediction of karsts on the planned well path depends on whether or not karsts were identified in the offset wells. Second, due to the possible lack of geophysical studies on the offset wells, many karst features might be unforeseen and therefore cannot be included in the stochastic distribution. Third, there are a variety of stochastic methods with different settings, that might project dangerous intervals differently. Detailed analysis of these methods is beyond the scope of this study, but these methods should be considered for well planning in carbonates to minimize the possible risks of sudden karst encounters.

3.2.3 Seismic methods of karst detection

Seismic imaging is the most common technique for mapping reservoirs, faults, and structural surfaces. Along with the standard seismic applications, this is an effective instrument to reveal geological objects and risks of drilling through them. There are many successful examples of detecting karsts based on seismic reflections. Peiling et al. [13] present seismic reflection characteristics of a deeply buried karstic carbonate. Their paper explores Ordovician carbonate rock, composed of caves, vuggy, and fractured-vuggy reservoirs, located in the central basin in the Tazhong area (China). The study concludes that the strong flake-like reflections have a direct relationship with the inter-layered karstification, which includes caves, vuggy and fractured objects.

Jianxun Zhao et al. [12] investigate how carbonate karsts can be mapped based on high resolution 3D seismic. In their study, more than 20 different seismic attributes were produced during processing. It was concluded that the amplitude and energy attributes have the highest correlation coefficients with calibration data (well log data). Along with the successful case studies of mapping the diagenetic networks of karsts based on seismic

indicators, there are many challenges associated with pre-stack time and depth migration.

Caves are typically small-volume objects and deviation from original pre-stack time migration imaging points can result in the significant inaccuracy of cave position estimation. Typically for small targets, pre-stack depth migration must be used. There are different methods and algorithms for depth-migration. An extensive work and analysis of depth migration algorithms for cave detection has been done by Wang Xiaowei et al. [45]. The results found that there is a significant shift of 30-70 m up-dip between Kirchhoff pre-stack depth migration and reverse time migration algorithms. This strengthens the idea that conventional seismic has significant limitations due to serious uncertainties generated by the depth-migration algorithms. The significant influence of the depth-migration algorithm on karst mapping is the main drawback of conventional seismic methods for detection of karsts.

On the other hand, reflections from cave-like small structures are different from the reflections from extensive interfaces. Small objects typically generate diffractive waves, which propagate with wide scattering and azimuth directions. As these signals are often weak, they can be affected by different types of noise and, therefore have a low signal to noise ratio. Imaging such small objects requires advanced acquisition and processing approaches. This problem has been investigated by [46, 47].

On top of that, the fundamental limitation of seismic detection of karsts is linked to the problem of vertical and horizontal resolutions [14, 48]. In seismic detection of karsts both, vertical and horizontal resolutions are important due to the nature of the problem of unknown scale. Nijian Wang et al. [15] explore the capability of seismic imaging to detect artificial karst caves, gradually increasing in height from 8 to 316 m. With the given model parameters, the velocity of 4000 m/s, and the source dominant frequency of 25 Hz, it has been shown that caves less than $\frac{\lambda}{4}$ (40 m) cannot be separated due to wave interference [15].

As discussed earlier, some karstic features are relatively small (up to a few meters) and fall beyond the resolution of state-of-the-art seismic methods. Such small cave systems or fluvial channels might be dangerous to drill through, as the total permeable volume is typically large enough to totally absorb drilling fluid, as will be demonstrated with an example in Chapter 4. Thus, the main drawback of conventional seismic imaging for karst detection is linked to its inefficiency to detect small objects that must be taken into account to minimize drilling risks. So, instead of conventional seismic methods for karst detection, in Section 3.3.3, I examine seismic-based methods with a better vertical resolution that can be more suitable for karst detection.

3.3 Real-time detection of karsts based on geophysical measurements

In the previous section, methods of pre-drill karst detection were discussed that can be utilized for drilling risks minimization in the well-planning stage. This section is devoted to methods of real-time karst detection while drilling.

3.3.1 Resistivity measurements

Looking ahead of the bit has been an object of research since the 1990s and is ongoing [49]. The unpredictable environment in front of the bit can pose significant risks for drilling. On the one hand, there is a risk of missing geological targets due to an unexpected dip in the geological structures. On the other hand, there is a risk of underestimating or encountering drilling hazards due to the lack of measurements ahead of the bit. Resistivity-based methods can successfully meet some of these challenges. Generally, geosteering tools are rarely based on direct measurements in front of the bit. Even the innovative ultra-deep geosteering resistivity tools measure behind the bit, by looking laterally around the wellbore [50]. However, in some applications, resistivity propagation tools can utilize the drill bit as an electrode to focus an electromagnetic radiation pattern in front of the bit. Below, both types of tools are discussed and the application of resistivity measurements for karst detection is examined.

Ultra-deep resistivity measurements

Rock property characterization by measuring its electrical resistivity is common in wireline and LWD services. On September 5, 1927, a crew working for Schlumberger recorded the first resistivity log [51]. From that moment, the study of rock resistivity has found a wide application in the oil and gas industry. Resistivity measurements are taken as follows. The coil-type transmitter emits an electromagnetic field at certain frequencies. Generally for LWD tools this is 2 MHz and 400 kHz [18]. Receiver coils are placed in the electromagnetic field and voltage is induced to each of the receivers as the transmitter fires. The tool configuration from the [51] is schematically shown in Figure 3.2. As the speed of wave propagation is very challenging to measure directly, instead, receivers sample amplitude and phase shift of the electromagnetic waves, emitted by the transmitter at certain frequencies. Once the phase shift and amplitude are registered, two rock properties can be estimated – attenuation and phase shift resistivities. To convert raw attenuation and phase shift measurements, the relative dielectric constant is approximated to a constant function of resistivity, obtained from empirical testing of hundreds of core samples [18].

For deep boundary detection, conventional LWD-resistivity tools have been significantly modified by transmitter-receiver spacing increase and by introducing tilted sources of

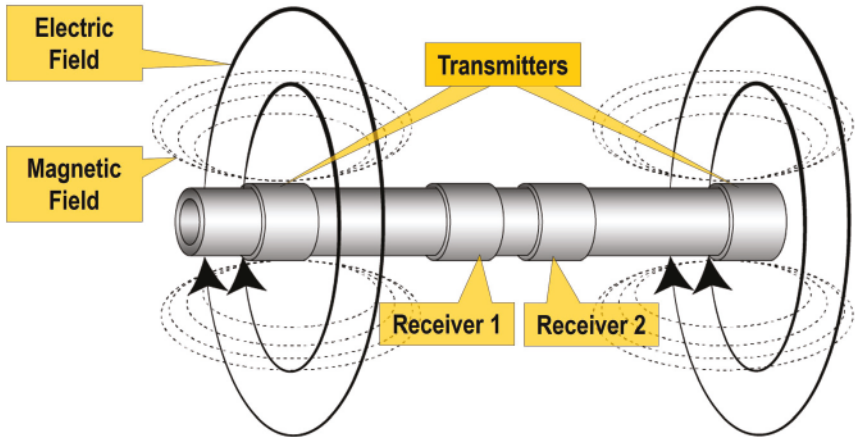

Figure 3.2: Schematic diagram of receivers and transmitters placement in the resistivity tool

electromagnetic waves. These improvements enable remote boundaries detection including identification of their spatial positions around the tool.

In practice, remote boundary detection with ultra-deep resistivity tools is challenging. As already indicated, LWD-resistivity tools cannot provide direct measurements. Instead, the inverse problem needs to be solved. The relation between resistivity measurements recorded by the tool and the distance to the boundary has strong non-linearity [52], therefore to define the distance to the boundary, the formation model needs to be updated to describe resistivity measurements obtained by the tool and relate them to the expected geology [17]. This approach is called front modeling and consists of modeling, comparing, and updating the formation model. Thus the described front-modeling approach cannot solve the problem of karst detection ahead of the bit as the expected karst structure should be initially included in the model.

Recent case studies demonstrated that ultra-deep resistivity tools can detect geological structures at significant distances ranging up to 70 m away from the tool [19]. However, such Depth Of Investigation (DOI) is achievable only in favorable conditions. The DOI is used to describe the depth, below which geophysical data cannot be used for interpretation of physical properties of the earth [53].

The current induced in the formation by the transmitters, propagates through the least resistive path. In the case of a low-resistivity medium, the current remains in the region closest to the wellbore, which leads to a shallow depth of investigation. For a high-resistivity medium, the current spreads over larger distances. This effect results in the reduced vertical resolution and better depth of investigation, as the current spreads deeper into the formation. Thus, the depth of investigation for resistivity methods is not a constant parameter and to a high extent depends on the resistivity of the formation and conductivity of the mud.

There are several advantages with the discussed ultra-deep resistivity approach for karst

detection: significant depth of investigation in favorable conditions, possibility to detect karsts with high contrast interfaces, and controllable electromagnetic radiation pattern. In spite of these advantages, there are drawbacks to this method when applied to early karst prediction, as this approach is based on look-around measurements and front-modeling algorithms. Thus, it is challenging to predict the presence of certain geological features in front of the bit without any direct measurements ahead of the bit. The significant dependence of DOI on the formations and the electrical properties of the drilling mud reveals the limitations of the method, as the distance of detection might be reduced considerably.

It can be concluded that ultra-deep, look-around resistivity measurements, should not be neglected for the purpose of karst detection. Due to a significant volume of rock, investigated around the tool, there is a probability of the detection of some karsts with sufficient electric contrast. Their presence might also be an indicator of possible karstification in the drilling interval and can be used in transferring drilling experience from offset wells as stated in Section 3.2.2.

Resistivity measurements ahead of the bit

There have been attempts in the industry to measure formation properties in front of the bit. To implement this idea, the drill bit was utilized as an electrode to propagate electric current ahead of the bit. The first near-bit resistivity tool was developed by Brian Clark in 1994 [54]. The tool configuration from the [54] is schematically shown in Figure 3.3.

As can be seen in the figure, the drill bit cannot be isolated from the BHA completely, as there is a contact with the bearing section of the rotary steerable system or with the mud motor [55], depending on the configuration of the BHA. Therefore, with an increased length of the electrode, it becomes challenging to distinguish responses from multiple, chaotically distributed points of contact with borehole walls.

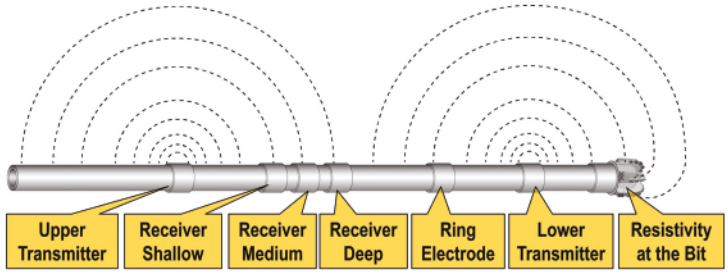

Figure 3.3: Resistivity at the bit tool schematic (based on the Brian Clark Patent [54])

However, with today's sophisticated hardware and data-processing improvements, resistivity at the bit is actively used for high-contrast boundary detection close to the bit in the *decimeter* range [56]. Most often, resistivity at the bit measurements provides core sample point selection, or stop-drilling warning when the well is approaching a shale layer [57].

Despite that, the limited depth of investigation and non-azimuthal quantitative measurements make it impossible to apply the resistivity at the bit for karst detection. Too shallow measurements in front of the bit leave no room for steering the well path away from a karst in case of successful detection.

An example of resistivity response in an interval of caves is shown in Figure 3.4. The displayed well logs belong to one of the recent discoveries in the Loppa High region (Norway, Barents Sea).

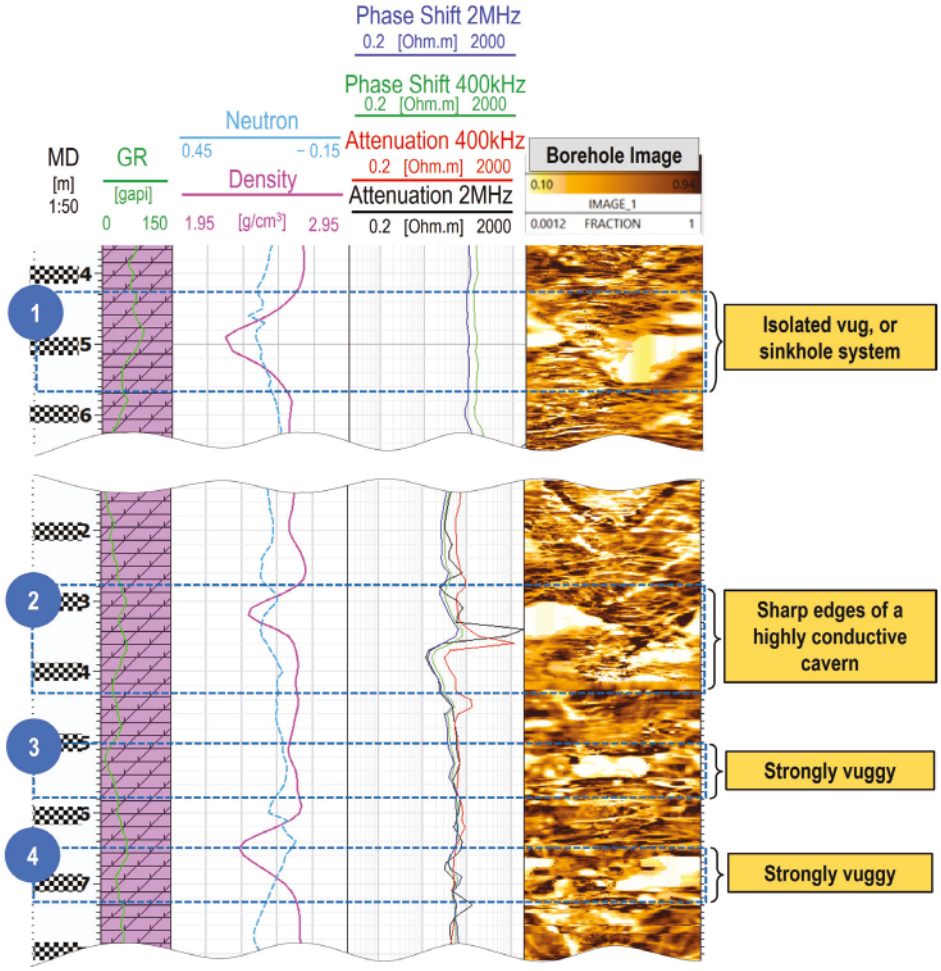

Figure 3.4: Example of resistivity measurements in vug and cave intervals. Courtesy of Lundin Energy

To demonstrate resistivity responses to karstification objects, in the given example cave depths based on borehole image data were localized. [1] [2]

In this example logs were recorded by the conventional Array Resistivity Compensated tool (ARC) tool. As can be seen from Figure 3.4, in zones 1, 3, and 4, resistivity measurements remain constant and it is challenging to identify that the well is crossing the caves. These intervals demonstrate the resistivity response in the case of the low-contrast environment, when the dielectric properties of the rocks surrounding the cavities and dielectric properties of the fluid, saturating the cavities are equal. Additionally, it can be noted that regardless of the depths of investigation, the deepest resistivity measurements (400 kHz attenuation resistivity) have the same readings as shallow measurements. This might be evidence that the resistivity contrast plays a crucial role in cavity detection regardless of the transmitter frequencies.

Unlike previous intervals, in Zone 2 in Figure 3.4, cave boundaries can be seen by the peak resistivity values in deep and shallow resistivity measurements. This demonstrates the main limitation of the resistivity-based approach – high dependency on the formation properties around the cavities. This, in turn, might have a negative effect on the overall reliability of advance cavity detection based on the resistivity measurements as some of the caves cannot be detected.

In conclusion we can say that resistivity methods of karst detection have their advantages, such as minor sensitivity to downhole noise, predictable pattern of electromagnetic radiation around the tool, advanced methods of data interpretation, and many others. However, this method has a number of drawbacks that are essential for karst detection such as high dependence on the resistivity properties of drilling mud, surrounding rocks, and inter-karst space-filling material properties.

3.3.2 Acoustics measurements

This section considers the principle of conventional sonic measurements around the tool and also reviews sonic-based measurement application for remote object detection.

Propagation of acoustic waves in a porous media is of considerable interest for different domains in the oil and gas industry. Studies of acoustic wave propagation in porous media were initiated by Biot in 1956 [58]. The first sonic tool was developed in 1958. This was a simple device that consisted of a monopole transmitter that generated a sound wave and two receivers to detect the wave traveling through the formation. The method of the propagation of elastic waves described in [58] is shown in Figure 3.5.

[1] Image tools are very accurate in terms of the detection of many geological features, crossed by the well path. Borehole imaging can provide the exact boundaries of vugs, breccias, caves, and other karst forms. However, this method cannot be used for early karst detection due to very shallow look-around measurements and significant bit-sensor offset.

[2] A common practice is to transform phase shift from degrees to resistivity since dielectric permittivity is considered to be related to resistivity. Similarly attenuation is converted from dB/m to Ohm.m which is more convenient for the analysis resistivity units

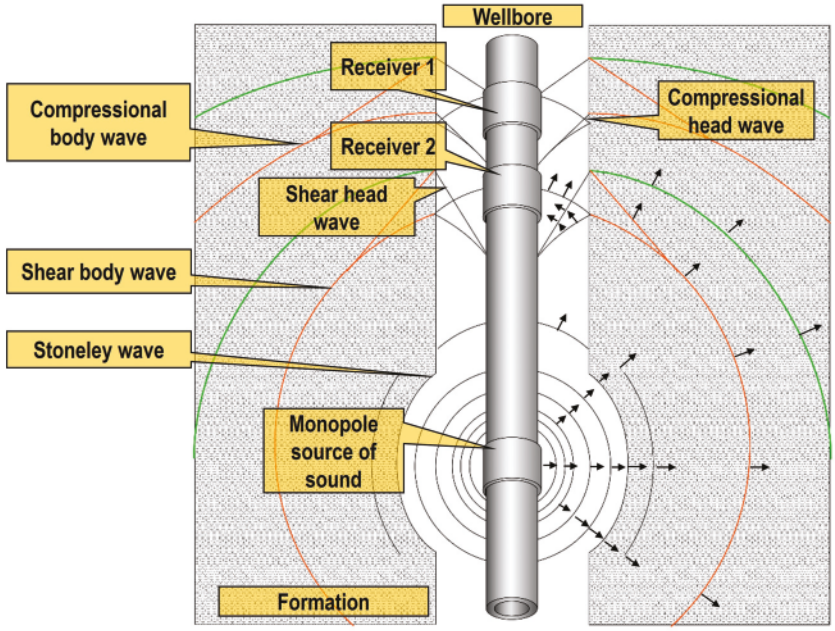

Figure 3.5: Waves traveling in the case of monopole source of sound.

As can be seen, several types of waves can be created in the mud, borehole, and formation. Since the pressure pulses reach the borehole wall, pressure waves generate compressional and shear wavefronts (body waves) that propagate further in the formation. The wave propagation in the formation causes pressure disturbances in the drilling fluid. The advancing compressional and shear body-waves create head waves. To generate shear and fluid mode (Stonley) head waves, body waves must propagate faster than the head waves in the fluid. Depending on the wave propagation speed, fast formations (shear velocity faster than mud velocity) and slow formations (shear velocity slower than mud velocity) can be defined.

The arrival time difference, detected by two receivers divided by the known distance, gives an interval transit time or slowness of the formation around the tool.

Changes in wave slowness and frequency can be used to estimate different formation properties. For example Stonley wave slowness and frequency change can be used in estimation formation permeability [59]. Compressional and shear data are crucial for determining wellbore strength, in-situ stress and rock mechanical properties [60].

The depth of investigation of the described tools depends on the formation slowness, the distance between transmitter and receiver, and the presence or absence of an altered zone in the formation. In general, the depth of investigation for the majority of sonic tools stays within an invaded zone of several centimeters (~3-6 cm) away from the borehole.

Borehole Acoustic Reflection Survey (BARS)

Returning to the problem of remote object detection, significant changes in the hardware of the discussed sonic tools were made, such as the introduction of array-receivers and new types of transmitters, acoustic logging progressed towards full sonic waveform analysis [61]. The difference in frequencies between BARS (f 10 kHz) and conventional seismic (f 100 Hz) as well as the different signal detection techniques enable higher resolution of borehole reflection imaging of the near-wellbore space.

In contrast to seismic studies, where registration and processing of a signal reflected from geological boundaries are studied, in the sonic seismic survey, there are a number of challenges. First, refracted and reflected waves are weaker compared with the direct arrival waves, thus wavefield separation becomes a crucial stage in data processing. Second, instead of seismic geophones, more sensitive receivers are used, which are capable of recording a wider range of waves. This requires additional data filtering for BARS signal processing.

The BARS method is based on separating the waves propagated along the wellbore from the waves spread deeply and reflected back from the boundaries of distant geological objects. Initially, standard sonic tools were utilized for deeply reflected signal detection. Such tools were equipped with an array of receivers and a monopole source of sound as described earlier. To map the positions of reflections around the tool, azimuthal measurements were introduced, which became an important step in expanding the range of applications of sonic tools. The hardware in the modern sonic tools for reflected signal detection described in [61] typically consists of three monopole transmitters, two dipoles, and an array of receivers, as illustrated in Figure 3.6.

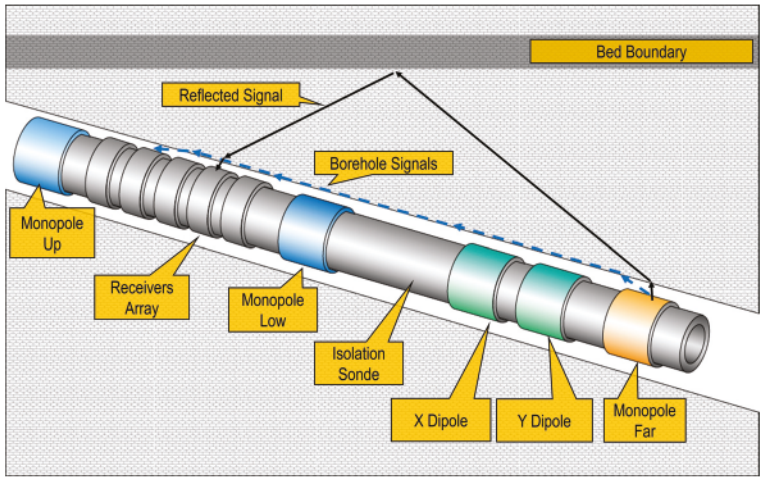

Figure 3.6: Tool Schematic for Borehole Acoustic Reflected Survey. Bed boundary detection.

Directional acoustic measurements are achieved by cross-directional dipole emitters. The introduction of azimuth measurements facilitates the detection of geological object positions with respect to the high side of the tool. This, in turn, enables the use of acoustic tools for geosteering, which has several advantages compared to resistivity-based geosteering methods, discussed earlier. In the case of a low-contrast resistivity environment, sonic-based geosteering has proved to be a good alternative method for well placement and is suitable for boundaries detection at a distance up to 10-20 m away from the borehole [16, 62]. Unlike the resistivity methods, the depth of investigation of acoustic measurements is significantly less affected by properties of the surrounding medium such as rock electrical conductivity and others. The main advantage of BARS over resistivity-based methods is the detection of karsts and cavities regardless of the conductivity or other properties of the karst-filling fluid.

Based on the example from the Loppa High region, the discovered average sizes of the caves have dimensions of 0.5-2 meters of a True Stratigraphic Thickness (TST). Though they are relatively small for seismic methods objects, they might be detected by BARS, as they fall into the resolution limits of the method (along the well resolution of 0.3 m).

Moreover, the BARS object detection distance of 10-15 m gives a sufficient volume of investigation, which can significantly increase the possibility of karstification object detection, around the tool. Discovering such objects might be crucial information for further drilling decisions: detection of a single karst form might be evidence that other karst forms may also exist within the same region and could be suddenly discovered during drilling. Overall, the discussed method can be considered as a reliable solution for karst detection around the wellbore.

However, despite a number of advantages, there are some limitations. First, drilling must be stopped to provide favorable conditions for BARS acoustic surveying. Second, this technology provides only look-around type of measurements and not look-ahead. The main problem of object detection in front of the bit remains unsolved, since sonic tools are located at a considerable distance from the bit and the waves do not propagate ahead of the drill bit. Thus it is still challenging to predict the presence of dangerous drilling objects while drilling.

3.3.3 Seismic-based measurements

So far, I have considered acoustic methods of karst detection by tools developed for reflection detection around the well. In this section, I focus on acoustic measurements ahead of the bit.

To the best of the author's knowledge, currently there is no ready-to-use solution specially designed or adapted for karst detection in front of the bit. However, over the past few decades extensive work has been done in this area. The principle of measurements ahead of the drill bit is significantly different from the look around measurements, described in the previous section. This section gives a brief review of prior work that is appropriate for karst detection (patented inventions, academic work and commercially available solutions). The inventions below are conditionally grouped based on the common receiver / detector placement and wavelengths, used by the method.

Downhole excitation of seismic waves

From our perspective this section gives the most significant inventions in the area of downhole excitation of seismic waves with a brief discussion of the basic principles of sound wave generation / detection.

Some of the early inventions focused on the challenging problem of downhole sound source development with certain specifications. The source should be small enough to be lowered downhole and at the same time, have sufficient power to generate high energy seismic waves, which can be registered by surface detectors. The reason for downhole positioning of the sound source instead of surface positioning is because better vertical resolution is achieved. An additional benefit of downhole excitation of seismic waves is that almost all wave modes can be captured. A number of inventions have been dedicated to the downhole excitation of seismic waves in different ways.

One example of downhole seismic-wave excitation of sound waves is described in the invention by Brett in 1994 [63]. It was suggested to mount a mass on a rotating part, inside the collar. When this apparatus is lowered downhole, the mass can be rotated to generate the signal, which can propagate around, and ahead of the drill bit. Due to centrifugal force, the rotating mass is designed to be in contact with the wellbore, which increases the effectiveness of signal propagation. The reflected signal can then be recorded by geophones placed on the surface.

Another principle of mass excitation was proposed by Paulsson in 1986 [64]. Instead of rotation of the mass, excitation of seismic waves is activated by triggering the mechanism that redistributes the pressure inside the air chambers in the apparatus, leading to moving the striking mass downwards. Thus, seismic energy is produced with less destructive stresses on the wellbore walls compared to the previous example. A similar approach for generating seismic waves by striking mass was proposed by Pascal Dedole in 1984 [65]. A device used a striking mass to hit elements inside the body that had a retractable platform to push the

apparatus against the wellbore wall. Striking mass in this invention is excited by an electric motor. Due to a firm coupling with the formation with this apparatus, a powerful seismic pulse can be generated.

A downhole periodic seismic source was proposed by H. Hardy in 1983 [66] and described in the patent [67]. The goal was to develop a downhole, nondestructive, high resolution, seismic tool suitable for studying fluid zones in hydrothermal magma systems encountered in deep holes. A downhole hydraulic seismic generator system was used for transmitting energy of vibrations into the earth surrounding a borehole. An electric servovalve regulated a high pressure hydraulic fluid flow traveling between the upper and lower chambers. The valve was controlled and powered from the surface with the standard logging cable, which is an advantage with this approach. This prototype was succesfully tested in a shallow zone and showed that this type of oscillator can generate downhole low-frequency seismic waves (10–100 Hz).

To the extent of my knowledge, the devices described in [63–67] were never used for commercial work.

A compressible fluid-driven downhole seismic source was suggested in another invention proposed by H. Hardy in 1989 [68]. The source device was capable of periodically generating horizontally propagated shear waves. The fluid generated torsional oscillations of the mass inside the device acts on the housing, thereby a seismic source produces waves. The oscillator was driven by a fluid rotary valve mounted in a sleeve which fits inside or in-between an existing bottom hole assembly.

An important result from the downhole seismic tests was obtained by B.Paulsson in 1988 [69]. The casing-cement bond strength was measured after the test of different types of seismic sources. The most significant damage (decrease of cement bond strength up to 30%) recorded for the airguns the least damage in the cement strength was obtained for the downhole hydraulic vibrators. An important conclusion was made regarding the use of impulsive sources. Very strong tube waves are generated by impulsive sources which became a new source of body waves with different acoustic impedances at different parts of the well. These body waves hide any arrivals after the direct P-wave arrival. It was shown that the hydraulic vibrator source is most efficient as it generates fewer tube waves.

Experimental comparison of airguns and explosives was done by S. T. Chen et al. in 1989 [70]. It was confirmed that airguns produce stronger tube waves compared to explosive sources and explosive charges can produce enough downhole energy without significant damage to the borehole.

A comparison of borehole seismic sources under consistent conditions was performed at the Texaco geophysical test facility in 1991 [71]. The goal was to evaluate the relative performance of a wide variety of downhole seismic sources such as small explosive sources, air- and water-guns, hydraulic and pneumatic borehole vibrators. The sources that have been tested operate with various principles and in the past it was difficult to examine their advantages and disadvantages as they were deployed in different fields and their

performance differed. The test facility allowed geological and regional differences to be eliminated. The survey depth levels, setup of receivers and test well were the same for all of the sources tested. One of the conclusions that was made is that all of the sources produced identifiable P-waves. S-waves are challenging to detect as reflections are obscured by numerous arrivals of the Mach waves generated by well-tube waves.

Despite the variety of methods of mass excitation, the common principle for this group of inventions is downhole seismic waves generation by the movement of a mass. The potential disadvantage of the methods described in this section is connected with difficulties of sound radiation pattern control, and therefore focusing the area of investigation ahead of the drill bit. Moreover, a serious impact on the wellbore walls by intensive mass movements can be dangerous since it can lead to wellbore damage. When the wellbore is damaged, pieces of the formation can fall around the drillstring leading to pack off of the annulus and/or jam of the drillstring (hole bridging).

Directional sound waves generation

This section is devoted to the inventions aimed at propagating directional sound waves in front of the bit with a controllable frequencies range. These inventions use a different principle of sound waves excitation, and their detection of reflections. Special attention in this section is given to acoustic signal focusing in front of the bit.

In the invention patented by John B. Farr and Ronald W. Ward in 1973 [72], it was suggested to constantly measure phase delay during drilling from a mono-frequency source of seismic waves, installed next to the drill bit. As the frequency of the source is pre-defined, it is possible to estimate travel time and the speed of sound between the source and receiver. The reflected signal, in this case, might be registered close to the bit, which can help to detect geological objects ahead of the bit.

A similar apparatus is described in the invention by Alf Klavness in 1975 [73]. A seismic pulse generator is suggested placed close to the drill bit. Obtained seismic data may be used to determine drilling conditions in advance. In the invention, proposed later by John Beresford in 1995 [74], sound waves are generated by excitation of the drill bit and detected by an acoustic sensor located inside the bit. To perform an acoustic survey when drilling is stopped, the drill bit with the excitation device is separated mechanically from the rest of the BHA, and the bit is pushed against the bottom of the wellbore to ensure that there is sufficient contact between the transmitter and the rock.

The invention proposed by James Legett in 1995 [75], is based on an apparatus and methods for obtaining acoustic measurements by many segmented transmitters and receivers which allow directional focus of acoustic energy with respect to the axis of borehole. The arrangement of transmitters allows acoustic measurements to be made ahead of the drill bit and provides information concerning formations that have not been drilled by the bit.

A comparable apparatus with some modifications is described in the invention by Holger

Mathiszik and Joachim Oppelt in 2003 [76]. The invented apparatus has an array of directional sources of sound waves that could emit acoustic signals in the selected direction and with the defined frequencies. The controllable frequency range enabled the selection of useful spectra of acoustic wave frequencies. This is different from the spectrum of acoustic waves generated by the drill bit. The signal reflected from geological boundaries, is then detected by geophones and hydrophones mounted on the apparatus. In some inventions, it was suggested to use tilted sound transmitters to ensure that acoustic waves will not interfere with the components of the BHA. For example the patent submitted by Rasheed Wajid in 2011 [77] describes an apparatus that can measure geophysical and petrophysical properties of the rocks based on transmitters and receivers that are inclined, with respect to the tool axis. It enables angular and axial focusing of the signal to study rock properties ahead of the bit.

To the author's knowledge, the devices described in [72–77] were never used in commercial work. Due to various difficulties, both from the hardware manufacturing and from the subsequent signal processing points of view, these inventions remained theoretical developments. However, they are important, since they demonstrate possible directions of the technologies developed for early detection of reflective interfaces in front of the bit.

3.3.4 Seismic while drilling

This section discusses a different means to tackle the same challenge of how to propagate and detect reflected signals ahead of the bit. There have been many attempts to propagate acoustic signals at a considerable distance in front of the bit to detect reflections from remote interfaces. Approaches that were different from those discussed above were presented in the early 1930s [78]. It was suggested to utilize the energy, generated by the bit while drilling and use it as a source of seismic waves. As roller-cone drill bits became widespread, researchers demonstrated their interest in this area. In 1985, the algorithm for instantaneous acoustic logging in a borehole was patented [79]. The proposed Seismic While Drilling (SWD) signal acquisition principle described in [79] is shown in Figure 3.7.

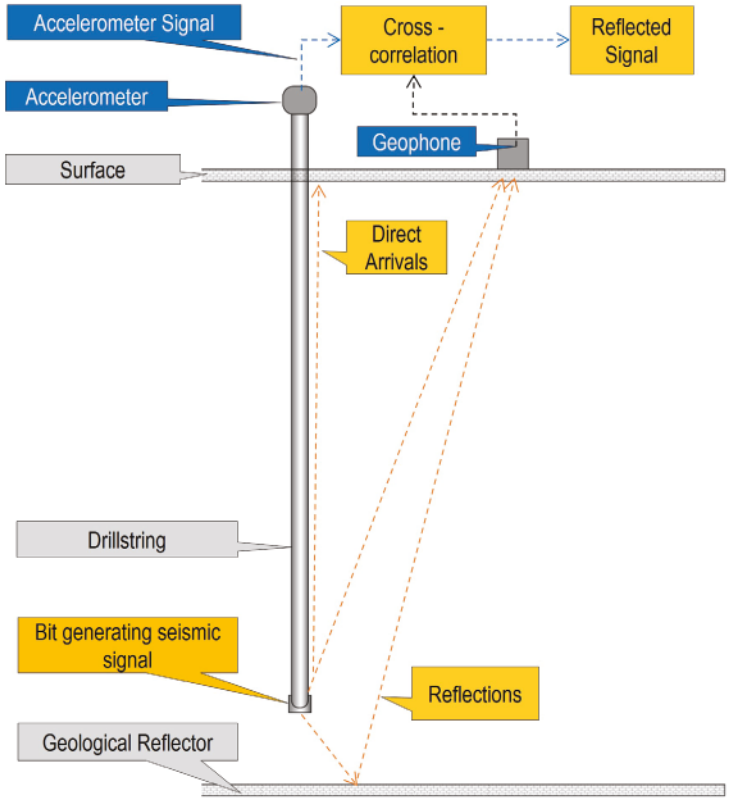

Figure 3.7: Schematic view of Seismic While Drilling signal acquisition. Based on [79]

In the proposed signal acquisition principle, drilling bit is used to generate acoustic impulse. Reflected from a geological interface signal then propagates back to the surface and can be detected by a geophone. To estimate the travel time of the signal that passes through the formation, cross-correlation technique is used. Cross-correlation between the signal that propagates through the drillstring and the reflected signal passing through the

formation is used to estimate the time shift and the speed of sound in the formation. To detect the signal that propagates through the drillstring, accelerometers are mounted on top of the drillstring as shown in Figure 3.7.

However, in reality, this process is more challenging since the speed of sound propagation in metal is significantly dependent on the BHA and drillstring component lengths, diameters, drill pipe wall thickness, etc. Thus inaccuracy of speed of sound propagation measurements in metal introduced inaccuracy in the estimation of the formation speed of sound. Analysis of seismic waves, generated by the roller-cone bit was quite popular in that period.

Many attempts have been made to increase the accuracy of direct arrivals measurements. Farr and Ward in 1973 [72], implemented a top drillstring sensor. Later, Yves Ollivier in 1993 [80] invented a device that was installed and rotated together with the drillstring. These inventions helped to register shocks, experienced by the BHA during drilling, almost without attenuation.

Along with the improvements in the signal-processing techniques, the described inventions used surface-located geophones. In this regard, the source of seismic energy (drill bit) should be preferably a low-frequency source with a long wavelength. This limits the resolution of the Seismic While Drilling (SWD) method, which can be roughly estimated at about 15-20 m. It has a better resolution compared with the conventional seismic study. Additionally, as stated earlier, it is challenging to obtain an accurate reference signal based solely on the measurements of drillstring vibrations. In 1992 [81] to address this issue the Atlantic Richfield Company in 1992 [81] proposed using a set of sensors, positioned similarly to sonic tools at a small distance from the bit to detect seismic waves emitted from the bit while drilling. This was intended to improve both the resolution and the depth of investigation in front of the bit along with the improvement of weak reflection detection from distant objects.

It is important to mention that these inventions were not theoretical. In the 1990s a number of experiments were performed confirming the viability of the seismic while drilling approach. For instance, in 1992 an experiment confirmed the possibility of signal extraction, generated by the source of sound with unknown properties (drill bit). To detect this signal, a total of 12 km of 40 channel geophones were placed on the ground at one of the onshore rigs in Germany. Data were recorded during 5 hours of drilling up to 3735 m depth. The technique described in [82] showed that it can be used to detect reflectors ahead of the bit based on SWD measurements. Extensive work was done by James Rector and Bob Hardaj in the study of radiation patterns and seismic waves generated by SWD [83].

In 1991, Western-Atlas published interesting results obtained from wells drilled in North America [84]. The experience from operating companies was that the proposed type Tomex® SWD survey (Baker Atlas) would not lead to constantly satisfactory results. In general, the results were inconsistent even with the use of roller-cone bits in favorable conditions (hard / medium formations, vertical well trajctory, long teeth of roller-cone bits).

Later, the French Institute of Petroleum (IFP) introduced the TRAFOR® system using

electrical wired pipe technology for fast data transmission of downhole data. This system was used for drill-bit seismic profiling [85].

In 1996 following these works, Miranda et al. [86] developed SEISBIT®. This system uses a selective data processing technique depending on current drilling conditions.

Starting from this time the DBSeis® system was presented by Schlumberger. The SWD system performs recognition of drilling through the estimation of the spectral difference between drilling and non-drilling events. The data from 12-36 geophones were digitaly processed (beam-forming) to separate the noise from the bit signal [87].

After a series of successful and unsuccessful experiments, the 90th attempt in this direction was continued. An important experiment devoted to studying the drill bit pattern was performed by Chabot in 2002 [88]. The aim was to obtain seismic maps of the surrounding formations. On the one hand, the experiment has demonstrated the advantages of a bit-seismic approach for remote feature detection. On the other hand, it has been shown that there is a significant limitation in the SWD method, as the BHA vibrations during drilling have high amplitude, which complicates the process of weak reflection detection from geological objects.

In 2002, Comelli et al. [89] proposed a methodology to increase the signal-to noise ratio of SWD signal. The proposed idea was to utilize mud-logger surface measurements to describe downhole process. In this way, the type of rock drilled and the drilling parameters can be taken into account and related to the signal from the bit.

In 2008, Flavio Poletto [90] presented the results of an experiment where test drilling was performed to study the pattern of waves generated by the drill bit. The experiment confirmed that the drill bit can generate both compressional and shear waves. Besides that, it demonstrated that the signal, generated by the drill bit, can propagate to significant distances in front of the bit and reflected signals can be detected by receivers.

To avoid hazardous situations during drilling, a similar principle of seismic while drilling was proposed by Espen Birger Raknes et al. [91] in 2017. The proposed method uses the seismic diffraction response from the borehole for imaging the well-path using surface seismic detectors. It was claimed that no extra tools are needed and the well can be imaged while drilling. The main application of this approach was in relief well drilling where this method can reduce the accuracy for the intersecting the blowing well. The numerical simulations of the approach have shown good results and seismic while drilling images were used to identify the exact position of the drill bit. The approach was tested on a synthetic well on data from the Kvalhovden area, east Spitsbergen, Norway.

In summary, despite the number of SWD advantages over conventional seismic, the bit-seismic study has not become popular due to the following reasons. First, there is no methodology for interpreting seismic signals from the drill bit in deviated and horizontal wells. The primary cause explaining existing challenges in interpretation is related to the unwanted, randomly distributed additional sources of seismic waves generation at numerous points of drillstring contact with the wellbore walls. The necessity to deal with

these additional seismic sources becomes especially important for wells with high deviation, extended horizontal sections, and intervals with high dogleg severity.

Second, roller-cone bits can produce high-energy seismic signals. Today, the vast majority of the wells are drilled with Polycrystalline Diamond Compact (PDC) bits, which are quiet in comparison with roller-cone bits and cannot produce high-energy signals. Such low-energy signals are more difficult to detect, which limits the applicability of the SWD method.

Third, the SWD method demonstrated reliable results only during rotary drilling, as in this mode the bit can produce a more powerful signal than in the sliding mode of drilling. Today's most used mud motors and Rotary Steerable Systems do not contribute to producing high energy signals by the drill bit, which also constraints further development of the discussed methodology.

In the next section I consider a method of employing downhole high-resolution seismic surveying without wireline logging. This can increase the accuracy of geological objects detection as the high-resolution seismic data can be acquired by the tool installed in the drilling BHA.

VSP while drilling

Due to a number of difficulties, associated with the discussed SWD methods, further development of look-ahead acoustic methods was based on a different principle.

Traditionally, in Vertical Seismic Profiling (VSP) receivers are installed on the wireline BHA and seismic sources are placed on the surface of the ground. To perform a wireline seismic survey (checkshot) the tool is lowered to a certain depth, and once the surface source of seismic waves is fired a downhole tool records the travel time, required for seismic waves to reach receivers. Knowing the depth of receivers, the interval velocity of the formation can be estimated. Thereafter, the time-depth conversion depths of geological reflectors can be estimated, including those, located in front of the bit. A significant drawback with this method is the time cost required to do a seismic survey. Drilling has to be stopped and the drillstring must be pulled out of the hole to run wireline seismic logging.

In 1999, Halliburton patented an invention aimed to overcome the problem of inefficient rig-time usage [92]. The invention was proposed to detect seismic waves by the downhole apparatus located in the drilling BHA. This apparatus can also detect reflections from the boundaries ahead of the bit and can thus enable significant rig-time savings. This technology was further developed and, similar to Halliburton's invention, the principle was implemented in early prototypes created by Schlumberger in 2001 [93]. This led to the development of the seismic drilling tool, which became an alternative to the conventional VSP by providing the same quality of data much faster. Interested readers are referred to references [94–96] for details about seismic waveform processing techniques used in VSP while drilling. The seismic guided drilling concept described in [93] is shown in Figure 3.8.

In this concept, a set of sensitive seismic receivers is mounted on the downhole seismic

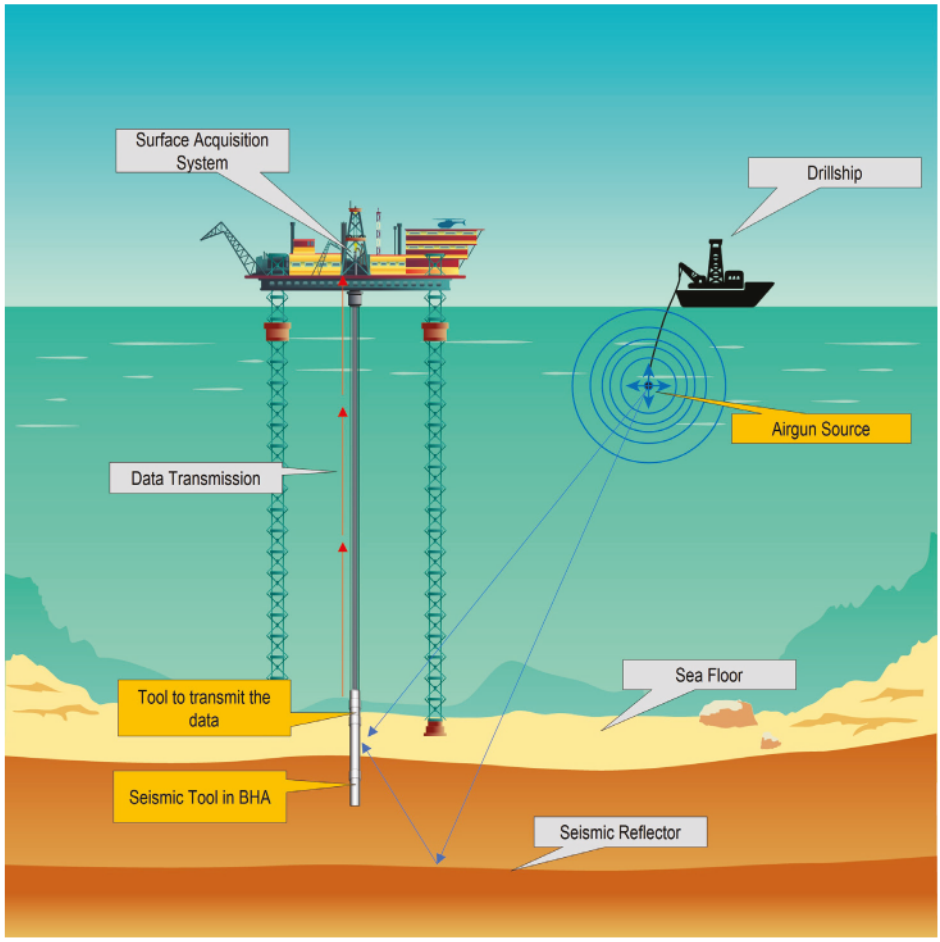

Figure 3.8: The seismic guided drilling technology. Based on the concept described in [93].

tool. The downhole tool processes the incident energy and utilizes a special algorithm that is based on a series of checkshots that compares signals from repeated firings to make sure that arrival time and shape of waveforms are similar. This logic helps to filter out noise and perform an initial quality check of the checkshots. As the tool gathers a pre-defined number of similar waveforms, it starts to stack them together. When the mud circulation is on again after the drill-pipe connection, data are transmitted to the surface through the mud pulse telemetry. The same process is repeated at each survey station. Field tests of this system were successfully performed in the Gulf of Mexico [97].

An example of the SGD technique for carbonate cave detection was demonstrated by the successful detection of Ordovician caves, buried at 6000-8000 m depth in the Tarim Oilfield in China [98]. The challenge was to improve the accuracy of carbonate cave detection. Caves, in this example, have a different genesis mechanisms leading to the development of

“tremendous storage spaces” [99]. The seismic responses to such large paleo karst caves are evident as “strong amplitude anomalies in legacy seismic data and are characterized as “string of beads” with different sizes and shapes [100]. These huge cave systems, contained almost 600 million bbl of oil extracted from the beginning of production (open caves trapping of the oil) [101]. These huge cave systems are incomparably larger than caves, discovered offshore Norway and Tarim caves are still open as drillers have recorded numerous "bit drops" sometimes exceeding 10 meters [99].

The SGD is a powerful technique for the detection of large karsts. However, taking into account the wavelengths generated by surface airguns the resolution of this method is not sufficient for detecting small karstforms ranging from half a meter to several meters. As discussed earlier, the detection of small forms of karstification is equally important along as large karst forms detection. Small karsts might be equally dangerous to drill through.

3.4 Summary and conclusions

In this chapter I have reviewed methods and technologies that can be used for prediction and early detection of dangerous for drilling karsts. All these methods have been published in the last 40 years. The methods can be categorized into pre-drill and while-drilling karst detection methods. They are summarized, together with their advantages and limitations in Tables 3.1 and 3.2 respectively.

The discussed pre-drill group of methods for karst detection focuses on the identification of potentially dangerous intervals before drilling begins. This analysis is based on already available data.

Analysis of geological information can provide an overall picture of the regional karst forms distribution, their possible depths of occurrence and can help in the estimation of the most probable geometrical sizes of regional karst forms. The main limitation of this method depends on the coverage and quality of input data. For example when there is a lack of geophysical or seismic data, studying only surface signs of karstification cannot be so effective in the estimation or prediction of subsurface karst properties.

Offset wells analysis is an efficient method for karst intervals prediction on a planned well trajectory. Different algorithms can be used to transfer gained experience of drilling from the offset wells. This method is effective if there is evidence of karstification which was observed/logged/interpreted based on the offset wells analysis. Since many karstification objects can be undetected in the offset wells due to lack of geophysical studies or if previously drilled wells were not crossing any karsts, projection of drilling risks related to karsts onto the new well trajectory is not possible. Moreover, if the offset well is located at a significant distance from the planned well, projection of karstification intervals can be inaccurate.

One of the most common studies used for the detection of different geological objects and structures is conventional seismic. This method can provide the most complete picture of the main subsurface geological features including general karst distribution, depths of

extended zones of karstification and geometrical dimensions of major karsts. However with conventional seismic, smaller dangerous for drilling karst forms cannot be detected. In addition, there is an inaccuracy/uncertainty in the estimation of the exact subsurface positions of objects based on conventional seismic. These uncertainties in the exact position of karsts detected with conventional seismic leaves the chance of crossing karsts during drilling.

The discussed karst detection while drilling group of methods focuses on the utilization of different types of measurements to investigate the region at or ahead of the drill bit.

Resistivity-based methods such as ultra-deep and resistivity at the bit are not efficient in the detection of karsts with low resistivity contrast. This makes the detection of low-contrast geological objects including karsts challenging. The depth of investigation and accuracy of the methods utilizing resistivity type of measurements strongly depend on the electrical properties of the formation and drilling mud properties.

Geophysical methods utilizing acoustic surveying such as Borehole Acoustic Reflection Survey (BARS) are promising in the detection of deep interface reflections regardless of the electrical properties of the formation. High vertical resolution and sufficient depth of investigation make this group of methods suitable for karst detection while drilling. Despite a number of advantages, these measurements are look-around and thus cannot be used for investigation of the region at or ahead of the bit for early detection of karst hazards.

Some of the methods that utilize seismic measurements are very promising, e.g. seismic guided drilling methods. They can provide detailed seismic maps of the region ahead of the bit with higher resolution than conventional seismic. This significantly increases the probability of karst forms detection in front of the bit. The major limitation of these methods is linked to the relatively low wavelengths that are used in surveying. Low wavelengths are a limiting factor for the detection of smaller dangerous for drilling karsts, which are encountered, e.g. in the Barents Sea.

As summarized in Figure 3.9, while being effective some cases, the reviewed methods for the prediction and detection of dangerous for drilling karsts suffer from the following limitations:

- Small dangerous for drilling karsts are the most challenging objects to detect with pre-drill and while drilling karst detection methods
- Study of geological drilling or offset wells data solely depends on the quality and coverage of input field data, and thus cannot guarantee an accurate prediction of karsts, leaving the risk of well control issues in carbonates unchanged
- Any relevant resistivity, acoustics or seismic-based methods can hardly be used for avoiding drilling into karsts or even for real-time detection of encountering karsts

These limitations indicate room for further research and development within methods and technologies for safer drilling in karstified carbonates.

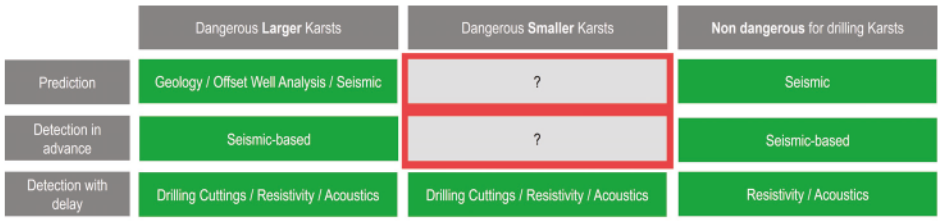

Figure 3.9: Methods to mitigate risks of drilling in karsts

Future work on this subject should concentrate on the development of an acoustic system that will utilize the methods of sound wave generation and registration discussed in this study. A first step in this direction is found in Chapter 6 where I present a novel concept utilizing some of the principles discussed in this section.

Table 3.1: Pre-drill karst detection methods

Method	Look Ahead	Advantages	Limitations	Karst prediction
Geological (Section 3.2.1)	N/A	1. Early detection of surface and subsurface signs of karstification 2. Overall picture of the geological region	Karsts detection depends on the coverage and quality of input geophysical data	Yes
Offset wells Analysis (Section 3.2.2)	N/A	1. Gained experience and dangerous intervals for drilling from the offset wells can be transferred to planned well-path 2. Additional sensors/measurements are not required for the analysis	1. Karsts prediction on the planned well depends on whether or not karsts were defined on the offset wells 2. Many objects may be unforeseen on the offset wells due to lack of geophysical studies, or geological heterogeneity 3. Different methods can project dangerous intervals differently	Yes
Conventional Seismic (Section 3.2.3)	Yes	1. Earth subsurface images 2. The most complete picture of the main subsurface objects 3. General karst distribution/spatial positions can be revealed	1. Inability to identify small karst forms 2. Possible inaccuracy of the exact subsurface objects' positions identification	Partially

Table 3.2: Karst detection while drilling methods

Type of measurements	Abbreviation	Method name	Look Ahead	~DOI	Tested	Advantages	Limitations	Early karsts detection
Resistivity-based	n/a	Ultra-deep Resistivity (Section 3.3.1)	No	Up to 70m	Yes	1. Significant boundary detection distances 2. Possible to detect karsts with high resistivity contrast boundaries 3. Predictable radiation pattern. Less affected by drilling noise.	1. DOI and accuracy depending on the formations' and drilling mud electrical properties 2. It is challenging to detect low contrast geological objects 3. High bit-sensor offset	No
	RAB	Resistivity at the bit (Section 3.3.1)	Yes	Up to 0.1m	Yes	1. Directed ahead of the bit measurements 2. Measurements while drilling	1. Shallow Depth of Investigation 2. Non-azimuthal quantitative measurements 3. Challenging to detect low contrast geological objects	No
Acoustics	BARS	Borehole Acoustic Reflected Survey (Section 3.3.2)	No	Up to 20m	Yes	1. High vertical resolution 2. DOI is almost unaffected by formation properties 3. Deep interface reflections can be separated from the other ones	1. Look-around measurements 2. Sensitive to downhole noise, preferably should be taken during not-drilling periods	Yes
Seismic	n/a	Downhole excitation of seismic waves (Section 3.3.3)	Yes	Up to 2000m	No	1. Powerful seismic pulse attempted to be generated downhole 2. Potentially higher resolution than conventional seismic 3. Low-reflections might be detected	1. The unpredictable wave radiation pattern 2. Challenging to focus the signal ahead of the drill bit 3. Dangerous for the wellbore walls	No
	n/a	Directional sound waves generation (Section 3.3.3)	Yes	Up to 100m	No	1. Focused acoustic signal ahead of the bit 2. Small bit-sensor offset 3. Controllable frequencies range	1. Hardware manufacturing challenges 2. Difficulties of signal processing 3. Unwanted reflections from downhole inner/outer-parts	No
	SWD	Seismic While Drilling (Section 3.3.4)	Yes	Up to 300-500m	Yes	1. Detailed seismic maps of surrounding formations, including measurements ahead of the bit 2. Higher than conventional seismic resolution	1. Small karsts can be missed due to radiation pattern, detection challenges 2. Not applicable for deviated, ERD wells 3. Not applicable for low-energy modern PDC bits	No
	SGD	Seismic Guided Drilling (Section 3.3.4)	Yes	Up to 30-50m	Yes	1. Seismic measurements can be obtained without wireline logging 2. High accuracy of large cave detection	1. Limited resolution due to seismic wavelength utilization 2. Not applicable for small low-reflected objects	Yes

Chapter 4

Karstification patterns in real-time drilling data

It is important to detect karsts as early as possible in order to improve drilling safety in intervals of karstification. As was shown in the previous chapter, the use of the state-of-the-art geophysical methods cannot always guarantee prediction or even real-time detection of dangerous for drilling karsts or karstification zones encountered in the Barents Sea. This chapter presents a novel method for real-time detection of karstification objects and zones with high likelihood of encountering dangerous for drilling karsts. The method is developed based on analysis of field data from 20 wells drilled in karstified carbonates in the Loppa High region.

4.1 Introduction

The lack of available technologies to predict, detect and prevent drilling into dangerous for drilling (smaller) karsts motivates the study presented in this chapter. As follows from the analysis given in Chapter 2, geological conditions that lead to forming a dangerous for drilling karst extend over some distance around that karst and lead to development of other karstification objects in that area. These karstification objects may not be dangerous for drilling. Yet, they can serve as indicators of drilling through an interval with geological conditions favorable to the development of karsts and thus, with a higher likelihood of encountering dangerous for drilling karsts. Early or real-time detection of such intervals can be used for timely risk mitigating actions such as rigging up of Managed Pressure Drilling (MPD) equipment, Lost Circulation Materials (LCM) chemicals rig-logistics, optimization of the well path and well geological targets.

Karstification objects may be detectable from real-time drilling data. A minor mud loss, for example, may correspond to drilling into such a karstification object. If one can find patterns in real-time drilling measurements corresponding to karstification objects, these patterns can be used for real-time detection of karstification zones.

This chapter continuous the in-depth analysis of the field data, started in Chapter 2, for the wells drilled in the Loppa High region. The analyzed data correspond to a very rare combination of drilling through karstified carbonates with logged borehole images and accurate mud flow-rate measurements. This combination enables the detailed analysis presented in this chapter, which identifies and presents patterns in real-time drilling data corresponding to various karstification objects. These patterns can either be used by engineers for manual detection of karstification objects (and intervals) or they can be employed by advanced analytics tools, e.g. based on machine learning, for automatic detection of karstification objects (and intervals) from real-time drilling data.

The methodology employed in this chapter is shown in Figure 4.1. The input is the karstification objects mapped in Chapter 2 (Steps #I -#IV in Figure 2.6). There is then an analysis of the logged real-time drilling measurements corresponding to these objects and intervals (Step #V in Figure 4.1. As it was shown in Chapter 2 (Figure 2.12) in some cases drilling breaks and tight spots were encountered in the intervals close to cave or breccia intervals. This determines the need for a detailed study of drillstring mechanics data to find indicators of karstification zones or objects. The results of this analysis will be discussed in Section 4.2. Since drilling in breccia intervals is often accompanied by mud losses with varying volumes, Section 4.3 examines whether the profile of mud loss changes can be linked to karsts.

The output of this analysis is a presentation of patterns in drilling mechanics and mud flow measurements corresponding to various karstification objects. To the best of the author's knowledge, no such analysis has been reported in the literature on drilling in karsts. In fact, the percentage of wells encountering karsts and, at the same time, containing the necessary well-log data (e.g. borehole images) is rather small. This leads to a general lack of in-depth studies of karst phenomena in drilling. This chapter attempts to fill in this gap and presents a methodology that can be utilized in further studies of karsts in drilling.

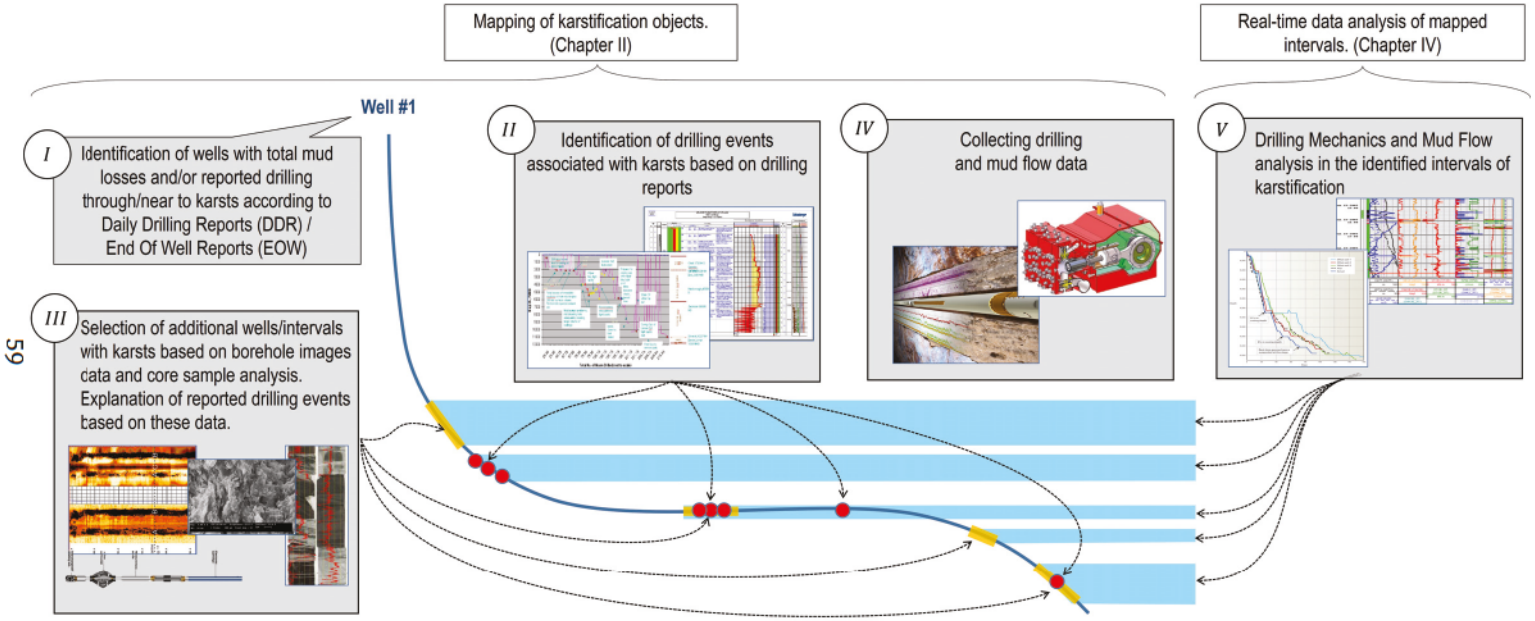

Figure 4.1: The developed methodology for karst-patterns detection in drilling data

4.2 Detection of karsts based on drilling mechanics

This section considers a set of real-time drilling measurements, which can demonstrate specific responses of drilling mechanics in the intervals of karsts. This set of measurements may be used as the first set of indicators for real-time detection of zones with a high likelihood of encountering karsts. Although in this section the focus was primarily on the drillstring dynamics, hydraulic data will be also considered as an auxiliary factor for better understanding of drilling events.

First there is a brief discussion of the measurements that will be studied in this section. Among the surface measurements considered in this analysis there is focus on 1) Rate of Penetration (ROP) - distance drilled per time unit, derived from the block position measurement, 2) Hookload - the weight on the hook to control the weight applied on the bit (Weight on the bit (WOB)). Hydraulic measurements, which will be studied in more detail in the next section, are also mentioned here. They include mud flow rates in and out of the wellbore. Their difference, called delta-flow, indicates mud gains or losses in the wellbore. Accumulated, they lead to changes in the fluid volume in the mud tank. For more information on how these measurements can be used, readers can refer to [102–104].

The downhole set of measurements provide an opportunity to study the efficiency of transferring surface energy downhole. They are a vital source of information about drillstring behavior [105–107]. These sensors are mounted on the drillcollar close to the drill bit [108]. Since the sensors are located very close to the drill bit, they can be utilized to evaluate in real time possible changes in drilling mechanics in the intervals of karstification.

Drilling measurements, either surface or downhole, are affected by changes in the downhole conditions (e.g. formation properties) and in operational parameters specified by the driller. Since we are interested in formation properties, only time intervals where the operational parameters specified by the driller remain constant were studied. This helps to eliminate changes in drilling measurements, which are not related to geological signs of karstification.

Drilling in carbonate reservoirs is frequently accompanied by a high level of Shocks & Vibrations (S&V). This measurement will be the first drilling mechanics measurement to focus on when identifying responses to drilling through karstification objects. Another measurement focused on the Rate of Penetration (ROP) in the intervals of karstification.

Typically, there are a number of drilling parameters, which have considerable influence on the ROP. This influence is far from simple and its complete analysis lies outside the scope of this chapter. However, ROP is an essential parameter for karst detection as it is directly linked to rock properties. This principle underlies many studies devoted to drillability [109, 110]. An implication of these studies is that for constant drilling parameters, fluctuations of the ROP while drilling are most probably related to rock properties. For early karst detection, as will be illustrated later, ROP variations might be an indicator of drilling through different karstification objects such as breccias, vugs or caves. Even though variations in ROP and

S&V are closely related to rock properties, one often needs to consider the whole picture, including other measurements to detect karstification objects from the measurements.

A number of examples are presented that demonstrate the effects of karstification objects on drilling mechanics measurements. These examples also support the conclusion in Chapter 2 that there are various signs of karstification around karsts which in certain cases can be detected through real-time measurements.

A first example is drilling in the Ørn Formation (Well #a). This formation is dominated by marine, shelf / platform carbonates with bryozoan bioherm build ups and shallow marine, supra-tidal carbonates. Initial analysis of drilling events in Well #a reveals the following cases. Drilling measurements logged in this well are shown in Figure 4.2, with the corresponding measurements summarized in Table 4.1.

Table 4.1: List of measurements for real-time karst patterns detection

Measurement	Abbreviation	Unit
Depth of the bit	Bit Depth	[m]
Downhole Torque	Torque	[kN*m]
Difference between Inflow and Outflow	Delta Flow	[l/min]
Position of the block	Block Position	[m]
Revolutions of BHA Per Minute	RPM	[rev/min]
Rate of Penetration	ROP	[m/hr]
Stick/Slip of BHA	SS Min/Max/Avg	[rev/min]
Stand Pipe Pressure	SPP	[bar]
Weight on Bit	WOB	[tonne]

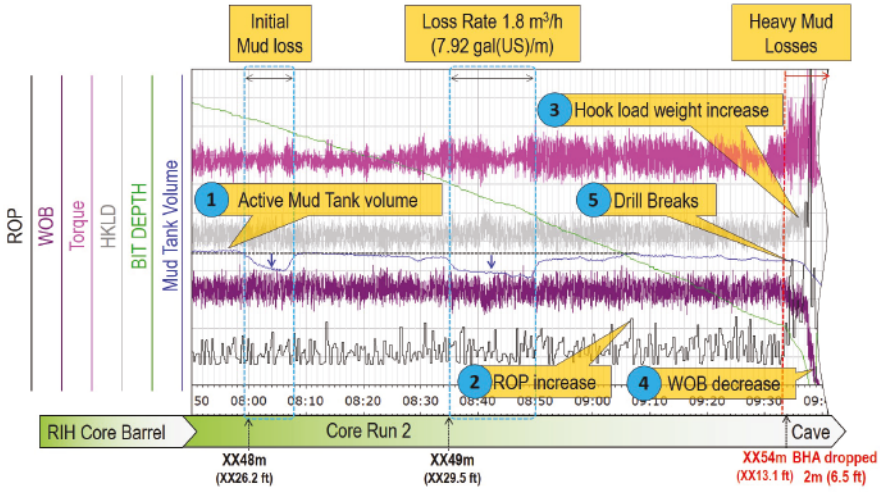

Figure 4.2: Drilling mechanics data in the interval close to cave (Well #a)

During the core-sampling run, the Bottom Hole Assembly (BHA) dropped 2 m without Weight on the bit (WOB). The initial loss rate was 40 m^3/h and escalated to the total mud loss situation. A full well control incident came into effect. This sequence of events demonstrates the result of drilling into an open cave. However, the most important research information here are the signs of karstification in the interval above the discovered cave. As this cave was discovered during coring of Well #a, there is rather limited information for drilling mechanics analysis, for example, there is no information about S&V and there is no borehole image data available for this interval. This means that other sources of information are required: drilling fluid measurements and core samples.

A number of small mud losses were observed in the interval more than 10 m above the cave. The possible presence of a conductive system of vugs and/or the presence of a breccia zone could therefore be assumed, as mentioned earlier.

This assumption is confirmed by the core-sample photos, which were acquired after Core Run 1. As shown in Figure 4.3, the interval of 20 m above the cave is presented by brecciated dolomites, cemented clasts of different size and shape. In the interval 15 m above the cave, it can be noticed cm-scale round to oval conductive spots, which could be interpreted as vugs, probably formed due to dissolution of the massive facies by corrosive fluids. The core sample closest to the cave is 10 m above the cave and has weakly cemented carbonate.

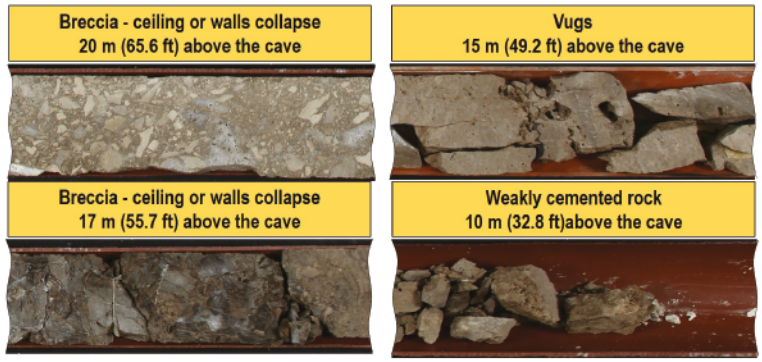

Figure 4.3: Core-samples photos of the interval proceeding the cave (Well #a)

Surface and downhole drilling measurements versus time are shown in Figure 4.2. This is a common representation of drilling data in time domain to analyze the performance of the BHA or study the drilling process. The list of measurements used in the examples below is given in Table 4.1.

In this example recurring mud loss events can be noticed at a distance of 6 and 5 meters from the cave marked with arrow number 1 in Figure 4.2. These intervals correlate with fluctuations of WOB: a small decrease in the first mud loss interval and a considerable decrease in the second interval of mud losses. Since the rest of the drilling parameters remain the same when the WOB changed, this might be a sign of drilling through intervals with different mechanical properties. Before the cave interval, there are a number of sharp

ROP increases, with simultaneous growing of the hook load (arrow #3) and WOB decrease (arrow #4), which can be interpreted as drill breaks pointed out by arrow #5 in the figure, caused by drilling through karstification objects.

The next example demonstrates drilling in Well #b through an interval of conductive patches, which are interpreted as large vugs, probably formed due to post-depositional (e.g. karstic) carbonate dissolution. The interval is identified based on borehole imaging, where dark areas in the acoustic image represent a low-amplitude response (Figure 4.4). This interval is interpreted as carbonate with large vugs facies, dm-scale, conductive, irregular features. As can be seen in Figure 4.4, there is a rapid increase in the S&V in the interval of vugs, marked with arrow #1. The drilling regime remains constant within this interval, as can be seen by the constant value of the hookload. However, the high torque (arrow #2) and ROP (arrow #3) are clearly evident which leads to the conclusion that these changes in S&V might be related to the vugs facies. As in the previous case, this example also demonstrates an increase in ROP, which might be explained by faster drilling through small cavities inside the rock (vugs).

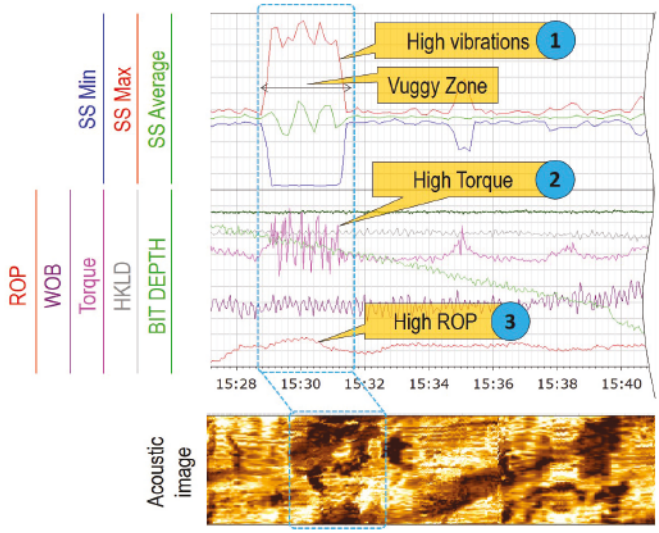

Figure 4.4: Drilling mechanics data in the interval of fracture and vugs (Well #b)

The third example (Well #c) illustrates drilling through a 6 m vuggy interval of cm-scale vugs framed by two erosive surfaces as shown in Figure 4.5. The length of the interval helps to assess drillstring dynamics in the extended vugs zone, without any other geological features crossed by the well path, as can be seen in the borehole image. These conductive patches are interpreted as large vugs, which are probably formed due to post-depositional (e.g. karstic) carbonate dissolution. The beginning of drilling in this interval is characterized by a drilling break. As pointed out in Figure 4.5, entering the vuggy zone causes high ROP (arrow #2) and a sharp drop in WOB (arrow #3). Drilling within the vuggy interval is

accompanied by a constant high level of shocks displayed on the top track in the figure and colored in green, red and blue curves. The interval of higher levels of shocks in comparison with the outer intervals is marked with arrow #1. This example confirms that a high level of S&V may be associated with an interval of karstification.

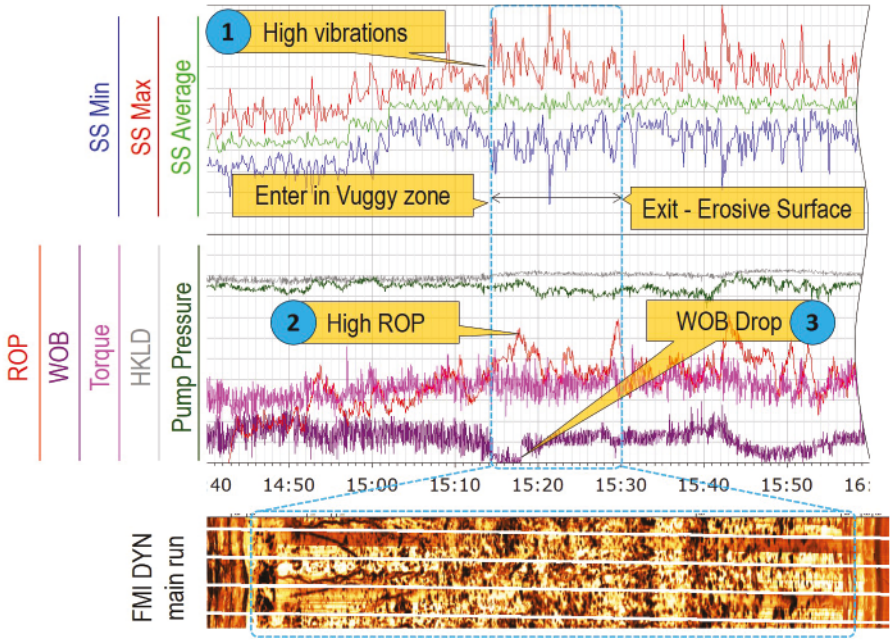

Figure 4.5: Drilling mechanics data in the interval of vugs 6 m thickness (Well #c)

This section has reviewed the key aspects of drillstring behavior in zones of karstification. A high level of shocks, ROP increase, drill breaks within carbonate intervals can often indicate that the well path is going through a karstification object and may be close to other karsts. However, these indicators have drawbacks. As will be discussed in the next section, drillstring dynamics is often not sensitive enough to detect some small-scale features or filled caves, which are also important signs of karstification zones and indicators of intervals with a high likelihood of karsts. The next section considers a set of additional indicators, which can significantly improve the detection of karsts and small-scale geological features that can be missed by drilling dynamics measured by surface and downhole sensors.

4.3 Detection of karsts based on flow-data

Moving the focus from the drilling mechanics data, this section considers a set of flow-based indicators of karsts and identifies patterns corresponding to karsts based on flow measurements. This will concentrate on the problem of karst detection based on a fundamentally different set of measurements, which might significantly increase the accuracy of the detection of karstification objects. This section identifies patterns corresponding to karsts based on flow measurements.

Figure 4.6 illustrates some typical delta-flow profiles corresponding to certain rock properties or drilling conditions. For example, large cavernous intervals can be identified by a step change in delta flow without mud return to the surface. A slow decrease in delta flow can be an indicator of rock matrix permeability caused by the invasion of drilling mud into the formation. Reduction and immediate recovery of delta flow is an indicator of drilling induced fracture initiating subsequent filling with the drilling fluid. A step change of delta flow with slow recovery can be an indicator of an open natural fracture. The discussed details of this characterization based on delta-flow measurements and its applications can be found in [111, 112].

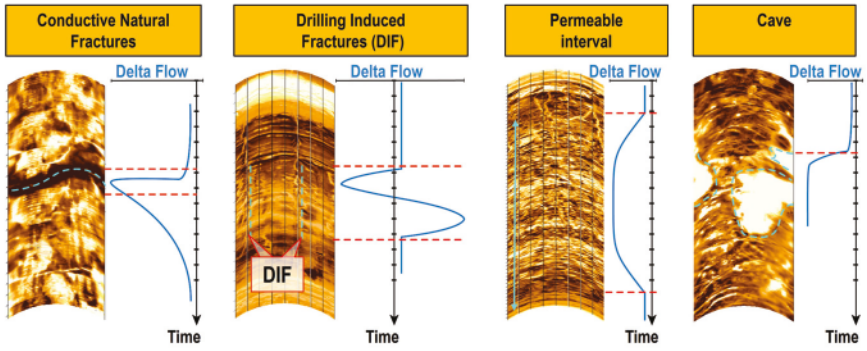

Figure 4.6: Delta-flow profiles and corresponding geological features

Drilling mud is essential for many drilling tasks, from cuttings transfer to transmitting hydraulic energy to downhole tools. It is pumped through main rig pumps to the Kelly hose, enters the drill collars, sprays out of the drilling nozzles and is pushed up in the annulus to the surface mud cleaning system and is then pumped back again. Analysis of the difference between inflow and outflow rates (delta flow) underlies kick/loss monitoring and reservoir characterization methods. The delta-flow analysis presented in this section is based on precise measurements of the inflow and outflow using flowmeters integrated in a Controlled Mud Level (CML) system [113], which was utilized in drilling in the region of study.

Generally, pump performance monitoring is an important component of different control and monitoring systems across many industries. We can now examine real-time Subsea Pump Module (SPM) performance driven by an automatic control system and integrated in

Controlled Mud Level (CML) system. Figure 4.7 shows a schematic placement of different components of the CML system.

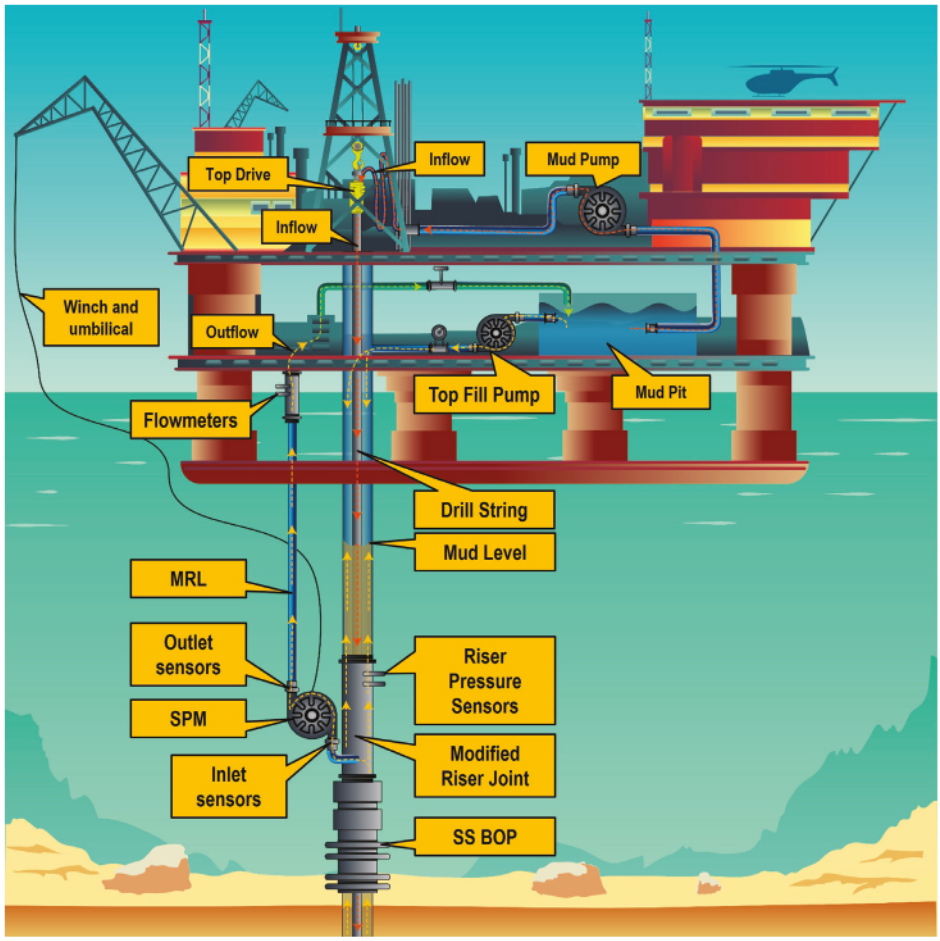

Figure 4.7: CML components

As can be seen, the level of the fluid in the riser is measured by pressure sensors, which serves for tracking changes of the hydrostatic column during drilling. Mud outflow from the wellbore, gets into the SPM. Based on the difference between the desired level of the liquid in riser (specified by the driller) and the actual fluid level, the control system defines the required SPM performance. While the drilling mud is pumped through the SPM module, the pressure and flow rate are measured by sensors, which are installed in the Mud Return Line (MRL). Having discussed, the importance of the information obtained from the delta-flow data, the CML system provides an extensive set of measurements:

- Precise measurements of the inflow and outflow using the flowmeters

- SPM real-time performance measurements: voltage, current, electric mechanical power and shaft Revolutions Per Minute (RPM)
- Riser fluid level

The benefit of the flow-based approach for advance karst detection is based on different types of measurements. In contrast to drillstring dynamics analysis, the flow-based approach can determine not only open caves (e.g. by specific BHA behavior in the intervals of karstification: drill breaks etc.), but also caves filled with clastic material. For instance, in the case of a filled cave, depending on the mechanism of cave genesis and the clastic material property, there may be no clearly detectable changes in ROP that can be linked to drilling through this karstification object.

Figure 4.8 represents the time plot of drilling Well #d, where a combination of two different types of measurements is available. The first and second tracks (from top to bottom) marked on the figure as "standard drilling data" display the same set of measurements as discussed earlier in Wells b and c. A set of additional measurements marked in the figure as "CML Data" is shown in the upper track. The lower track displays the borehole image with marked intervals of vugs and cavity. Interval 1 in the figure represents the response of drilling-based and flow-based measurements in the cm to dm scale interval of vugs. This interval begins with a drilling break, represented by a drop of WOB (arrow #1) with a simultaneous increase in ROP (arrow #2). After that, the ROP profile, the level of shocks as well as other drilling parameters remain constant in this interval. This proves the limitation of the drilling dynamics approach, as it is not accurate enough to detect small changes in the rock properties.

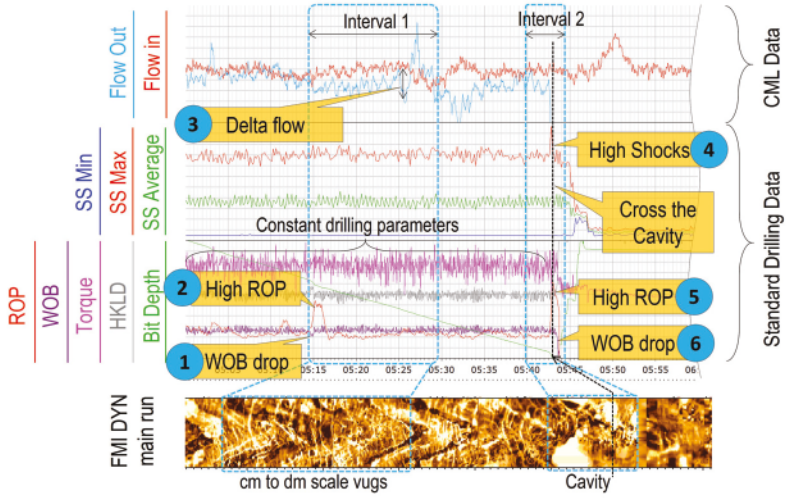

Figure 4.8: Drilling through the intervals of vugs and cave. Standard and flow data (Well #d)

However, analysis of the CML data can reveal some additional information. When the bit passes through a zone with vugs or fractures, drilling mud invades some of the open channels, which results in a consequent decrease in the delta flow (arrow #3). The initial point, when the first difference between the inflow and outflow is noticed correlates with the interval of the vugs facies defined by the borehole image.

Interval 2 illustrates an example of drilling through a cave. The initial depth of the cave boundary is defined by the borehole image and represents the beginning of interval 2. As can be noted, at the depth defined by the borehole image there are no visible changes in any measurements. However, in close proximity to the cave there are spiky changes in the mud losses. Mud losses in the interval of the cave reached 2000 l/min. The clear response can be noticed by a step change in many logged parameters, such as S&V (arrow #4), ROP (arrow #5) and WOB (arrow #6).

The next example demonstrates the response of the drillstring dynamics and delta flow during drilling through bedding planes and Drilling Induced Fractures (DIF) (Well #e). For convenience, the track order and drilling measurements are displayed similarly to the previous example. As can be seen in Figure 4.9, for all three intervals the S&V level remains constant (arrows #1, #2 and #3). The ROP profile at the beginning of each interval (marked with arrows #4, #5 and #6) has similar behavior to the ROP in the karstified interval from the previous example: increased drilling speed can be seen when the drill bit enters the interval. However, the profile of the mud losses is different across these intervals and, for example, in the interval of DIF, there is delta flow followed by recovery, which indicates initiation of DIF and subsequent filling with the drilling mud (arrow #7).

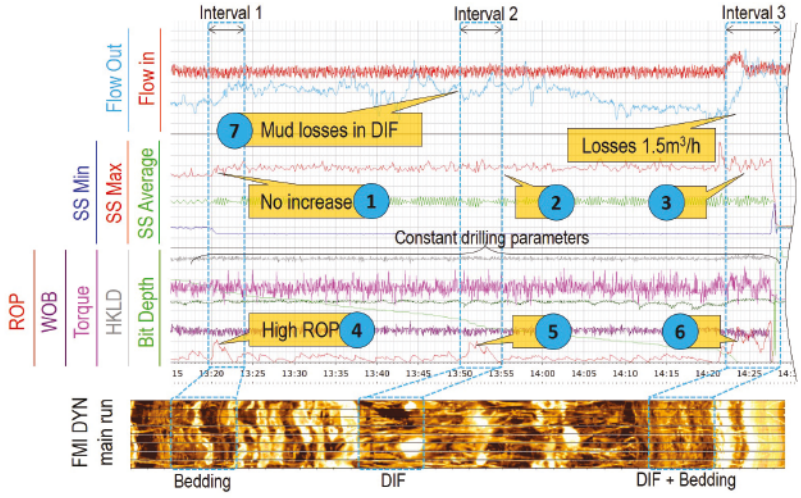

Figure 4.9: Drilling in the intervals of bedding and drilling induced fractures. Standard and flow data (Well #e)

In this section, the applicability of flow-based measurements for karst detection have been discussed. The presented examples demonstrate that drilling dynamics-based and flow-based indicators can complement each other in detecting karstification objects. A delta-flow profile might reveal additional signs of karstification in the intervals that are undetectable through drilling mechanics measurements, such as filled caves or small vugs. Detection of even small forms of karstification can be an important part of early karst detection methodology, as they can indicate drilling in a karstified zone. The studied intervals of vugs are characterized by moderate values of fluid losses (delta flow), without significant fluctuations, in contrast to cave intervals demonstrating a step change in the delta-flow profile.

4.4 Conclusions

This chapter has studied drilling mechanics and mud-flow karst patterns. The analysis is based on data from 20 wells drilled in karstified carbonates in the Barents Sea region. The study included analysis of a complete set of drilling data: drilling events and end-of-well reports, borehole image and core sample data, recorded time-domain data of BHA mechanics and mud flow data.

By correlating logged real-time drilling data with karstification objects or intervals mapped in Chapter 2, this demonstrates that karstification objects generate specific patterns in drilling data. When monitored and detected, these patterns can be utilized as indicators of karstification zones with a high likelihood of encountering karsts. Availability of such indicators can support decision-making process to improve drilling safety. A summary of the identified patterns corresponding to various karstification objects is presented in Table 4.2.

Table 4.2: Patterns of drilling measurements/events corresponding to karstification objects

Karst type	Drilling Break	ROP	S & V	Torque	Mud Losses
Cavities	Often when entering	Step change	Highest lateral vibrations	Highest variations	Step change in mud loss profile
Vugs	Not always detected, size-dependable	Higher ROP while in vugs	Higher compared to other intervals	No/small variations	Constant moderate loss profile
Fractures	Typically no	Increase/ Not always detected	Small/ No increase	No/small variations	Decrease and immediate recovering profile

This work is the first step towards developing tools for detecting karstification zones and mitigating risks related to drilling in karstified formations. Still, with the limited amount of wells available for this study (wells that are located in one geographical area), the presented results should be utilized in the context of all available information and experience.

This study is limited in terms of specific geology and the number of wells available for the analysis. Even in carefully studied fields, the percentage of wells that encountered karsts and at the same time had a full set of necessary well-log data (e.g. borehole images, or accurate delta-flow data) is rather small. Moreover, some of the intervals have to be

additionally excluded from the analysis: only intervals with constant drilling/pump/mud parameters should be kept in order to evaluate the unique patterns of drilling measurements corresponding to karsts and not other possible factors affecting drilling.

Future work on the subject of karst patterns detection from drilling data should be directed towards obtaining and analyzing well data from more wells, including wells from fields with different geology. This will allow the creation of a more complete and statistically reliable picture of real-time indicators of karsts and karstification zones, regardless of the geography of the research region. Such an analysis can be done utilizing the same workflow developed and employed in this chapter.

The obtained results motivate the development and implementation of the algorithm for automated karst pattern detection, which will be discussed in the next chapter.

Chapter 5

Automated detection of karstification patterns in drilling data

5.1 Introduction

Today, the ultimate goal for oil and gas companies is to increase the safety and economic efficiency of drilling. To achieve these goals, significant investments have been made to develop advanced surface and downhole drilling sensors as well as communication technologies. The measurements can potentially provide vital information about the geological properties of the formation and drilling performance/safety. However, most of the measurements are very noisy, making accurate analysis of the drilling data by people or automatic algorithms a challenging task. A solution is the algorithm discussed in this chapter which enables more accurate and timely detection of drilling events (essential for drilling safety and efficiency), as well as contributing to more accurate karst-pattern detection through the use of real-time indicators discussed in Chapter 4. Also, this algorithm contributes to improved drilling risks detection and increased drilling safety.

This chapter is organized as follows. In Section 5.2 an overview of available methods for anomalies detection is provided. Section 5.3 explains the concept of the suggested automated event detection method. In section 5.4 relevant results from the proposed method are presented. Conclusions, discussion and future work are given in Section 5.5.

5.2 Anomalies detection and filtering

A karst encountered during drilling can be considered as an anomaly in the drilled formation. As indicated in the previous chapter, such an anomaly manifests itself in specific patterns in real-time drilling data. One can employ various methods from signal processing to detect these patterns in the real-time data automatically, or to support their detection by an operator. There are multiple of publications on anomalies detection and pattern recognition in time series data. Some of the methods for automatic detection of anomalies (or faults)

can be split into, for example, passive and active.

In active approaches, the process, including normal and faulty phases is described by a set of models. This approach involves injecting a signal, e.g. noise or disturbance into the system to improve the detection of faulty behaviour. Different approaches can be used for anomalies or faults detection within a specified time horizon such as inequality-bounded perturbations [114], bounded additive noise [115], stochastic-deterministic input [116], auxiliary input signals [117] and active incipient signals for multiple faults detection [118]. Despite all the advantages presented in the literature there still a significant complexity and high computational demands of the active faults detection techniques.

In the passive approaches, the signal is compared with either a historical data or modeled data. Faults are then detected as a deviation from the historical or modeled data. Passive approaches are well known. The most common methods are based on models [119, 120], clustering algorithms [121], sliding-mode control [122] or data-driven methods [123]. The main disadvantage of these approaches is that they are based on a model or sets of models. Given high complexity of drilling data, it is difficult to create a model that accurately describes a very complex drilling process and at the same time has a high computational efficiency.

Another group of methods called Qualitative Trend Analysis (QTA), is based on analysis and identification of qualitative characteristics of signals. Initially these methods were based on studying the first and second derivatives of the signals. The goal was to establish a qualitative representation of the signal where the entire signal was divided into segments and each segment was characterized by a convex/concave and/or increasing/decreasing shape [124–127]. Ideally, such a qualitative representation of the signal allows automated patterns detection in time series by incorporating expert knowledge with a qualitative description of a process. However, a simple representation of time series is not always easy due to noise masking important features. The currently available approaches are typically based on piece-wise polynomial functions [128–131], wavelets [132–134], neural networks [135, 136], kernel regression [137, 138] and some other methods. A common feature of these methods is that they require great efforts in selecting and tuning many parameters needed for working with specific types of data. This might be very impractical for the real-time analysis of drilling data. Moreover some researchers indicate that many of these methods will not work with the data outside of the ones used in the original works [124].

Taking into account the complexity of the drilling process and practical requirements on relative simplicity of data-processing algorithms, this thesis focuses at data-driven methods that do not require models. In this case the drilling data was analyzed and the first derivative of the signals was estimated to identify their trends. One of the main challenges in analyzing drilling data is that important information is usually masked by noise leading to masking some important trends and patterns in data. Filtering needs to be applied to get rid of or reduce the noise. Filtering is done by an algorithm that uses the available data points in a signal to calculate a "filtered signal" in which the effect of noise is reduced. A simple

example of a filter is a moving average filter: the value of a filtered signal at time $t*$ is calculated as an average over a number of neighboring data points in the original signal.

There are various filters that can be applied to filter out the noise [139–141]. Filters can be conditionally divided in two groups. One group of filters relies on different methods for smothening the signal such as low-pass [142], Gaussian [143], moving average [144], polynomial fit [145] and spline filters [146]. Another group of filters computes derivatives of noisy measurements to cancel the noise. These filters are based on either analytical [147, 148] or direct numerical differentiation [149, 150].

Despite using a different algorithms to filter out the noise, a common characteristic of many filters is what can be called a window size. It tells how many data points are effectively used in calculating the filtered value. The window size is usually considered a parameter of the filter. It may be specified explicitly or implicitly. For example, for the moving average filter, this will be the size of the sliding window involved in averaging. For filters with infinite support, the effective size of the window is determined by the corresponding weights related to filter bandwidth.

The selected window size of a filter affects filtering of both the noise and the original signal. The higher the window size, the better the noise attenuation properties of the filter, as more data points can be used to "average out" the noise. At the same time, the window size used in averaging/filtering also affects the original signal: large window size results in filtering out fast variations in the signal, keeping only the slowly varying components. Depending on the selected window size, the filter can have very good noise attenuation properties, but poor performance in capturing fast changes in the signal (for large window sizes); or it can capture fast changes in the signal very well, but have low noise filtering properties (for small window sizes). The former one cancels the noise, but wipes out information from the signal. The later keeps the information, but does not unmask it from the noise. One should therefore choose the window size depending on the properties of the signal and the noise.

Signals significantly change during drilling and for some instances one needs a filter with a large window to capture small/slow changes in the signal, while in other cases one needs a small window to accurately capture fast signal changes. This can be achieved by using several filters and switching between them based on the user's judgment. This is not convenient, as it requires experience and multiple actions from the user, as well as introducing an additional human factor in the processing and analyzing of the data. In the next section will be presented a nonlinear filter that addresses these challenges and can both filter out noise and robustly estimate the first derivative of the signal. In addition, it automatically detects instances when the signal experiences fast and noticeable change in the trend, which is convenient for detecting anomalies in drilling data.

5.3 Adaptive Differentiating Filter

In this section an Adaptive Differentiating Filter (ADF) is proposed that automatically adjusts the size of the window to achieve maximal allowable filtering while preserving desired accuracy in capturing fast changes in the signal (as will be explained below). This filter is a modification of the filter described in [151], where it was developed for robotic applications. This chapter describes it and demonstrates through examples how it can efficiently be applied for automated detection of karst patterns in drilling data. This is the main contribution of this chapter.

The filter increases the window size when the noisy signal is slowly varying and thus high-level filtering is needed to capture these small slow changes. It automatically decreases the window when the signal is quickly varying and it is more important to capture these fast changes since the effect of noise becomes less important. In addition to that, the filter estimates the derivative of the signal, which is often very important in detecting and classifying various events from time series. This feature is especially helpful, as the numerical calculation of derivatives is especially sensitive to measurement noise. [1]

To present the filter, a sequence of time instances t_i and the corresponding measurements y_i, $i = 1, ...N$ are considered. The measurement consists of the true signal $\bar{y}_i$ and noise m_i.

$$y_i = \bar{y}_i + m_i \tag{5.1}$$

We assume that m_i has zero mean.

The ADF consists of two operations conducted recursively: 1) signal and derivative estimation (given a window) and 2) window adaptation.

1) Signal and derivative estimation: For a time instant t^*, a window centered at t^* is defined and having a window radius as the sequence of instances $W = [t_i : i = * - WR, * + WR]$, where $*$ corresponds to the index of t^*. To find an estimate of $\bar{y}(t^*)$ and its derivative $d\bar{y}/dt(t^*)$, from the data given in window W, the estimate of the signal $\bar{y}(t^*)$ and its derivative $d\bar{y}/dt(t^*)$ are calculated by solving the least-squares fit problem:

$$\sum_{t_i \in WR} |y(t) - (k(t_i - t^*) + b)|^2 \rightarrow \min_{k,b}. \tag{5.2}$$

Then,

$$\hat{y}(t^*) = b \tag{5.3}$$

$$d\hat{y}/dt(t^*) = k, \tag{5.4}$$

where $\hat{y}(t^*)$ and $d\hat{y}/dt(t^*)$, are the estimates of $\bar{y}(t^*)$ and $d\bar{y}/dt(t^*)$.

2) Window adaptation: at this step there is a check of the accuracy of how the straight-line segment $\hat{y}(t) = k(t - t^*) + b$ approximates the data series over the window W. If

[1] Calculation of the derivative and adaptation of the window determines the name of this filter: Adaptive Differentiating Filter (ADF)

$$(\max_{t_i \in WR} |k(t_i - t^*) + b - y(t_i)| > \delta) \quad \& \quad (WR > WR_{min}), \tag{5.5}$$

i.e. if $\hat{y}(t)$ does not fit $y(t)$ over the window W with the required accuracy δ (which is a design parameter of the filter) and the window radius can be reduced without violating the lower limit for the window radius WR_{min} (specified by the user), then the window radius is reduced, the linear fit function is recalculated, and the condition (5.5) is checked again. This is repeated until either the accuracy requirement is met or the window radius has reached the minimal value WR_{min}. This process is illustrated in Figure 5.1.

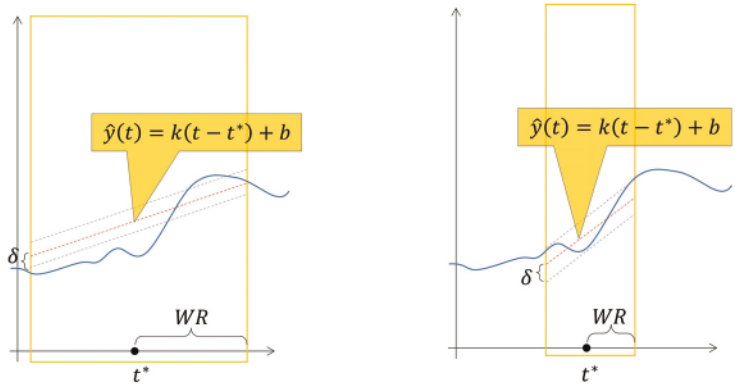

(a) Reduce window radius and recalculate (b) Accuracy is reached

Figure 5.1: Window adaptation from a too large window radius (a) to new window radius where the accuracy is reached (b)

If $$(\max_{t_i \in WR} |k(t_i - t^*) + b - y(t_i)| < \delta) \quad \& \quad (WR < WR_{max}), \tag{5.6}$$

i.e. $\hat{y}(t)$ approximates the $y(t)$ over the window W with the desired accuracy, and the window radius can be increased without violating the upper limit for window radius WR_{max} (specified by the user), then the window radius is increased, the linear fit function is recalculated until and the condition (5.6) is checked again. This process is repeated until it is not possible to increase the window radius without either violating the accuracy of approximation or exceeding the upper limit WR_{max}. This process is demonstrated in Figure 5.2.

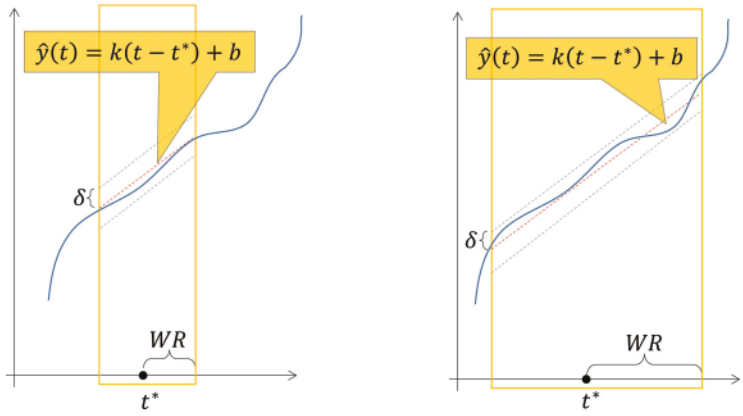

(a) Increase window radius and recalculate **(b)** Maximal window radius is reached

Figure 5.2: Window adaptation starting from windows radius where the desired accuracy of the linear approximation is satisfied (a), to a maximal windows radius having the desired accuracy (b)

The output of the algorithm at this stage is the estimate of the signal and its derivative at time instant t^* and the maximal window radius WR^* reached in the window adaptation process. For the next time instant t^*, the initial window radius is taken as the largest window radius WR^* from the previous step. This significantly speeds up the calculation.

To summarize, the algorithm takes parameters WR_{min}, WR_{max} and δ as inputs and processes the data series t_i, y_i to output estimates of the signal $\bar{y}(t_i)$ and its derivative $d\bar{y}/dt(t_i)$ as well as the radius of the maximal window WR^* corresponding to these estimates.

Parameter WR_{min} determines the minimal level of filtering, as the window radius will always be larger than or equal to WR_{min}. Parameter WR_{min} must be chosen to satisfy the required level of filtering for the particular input data. Parameter WR_{max} determines the maximal level of filtering, as the window radius will always be less than or equal to WR_{max}. Parameter of the the maximal level of filtration WR_{max} needs to be set to the maximal value such that a further increase of this parameter does not lead to a significant improvement in the quality of filtering. It also affects computational cost of the algorithm – it is more costly for higher WR_{max}. Parameter δ must be chosen such that the noise m_i in Equation (5.1) satisfies $|m_i| < \delta$ for all i. In practice this parameter is either known or can be estimated from the data. The closer δ to the actual limit on the noise, the more accurate is the filter for the given WR_{min} and WR_{max}.

As was discussed earlier one of the outputs of the ADF filter is the window radius (Track b in Figure 5.3). It can be seen that the window radius is minimal when the signal experiences relatively fast changes. The small window radius can be used as a flag indicating changes for the detection of drilling events, such as the detection of drilling breaks and mud losses corresponding to karstification objects.

The ADF filter (green line in track c) is adjusted automatically to filter out the noise and follow the behavior of the initial signal (grey line). An overall view of intervals #1 - #4 shows that both main trends and high-amplitude changes in measurements are successfully captured by the ADF algorithm. This is an important property of the ADF algorithm for applications to real-time measurement analysis when it is necessary to capture both small/slow and large/fast changes in the data.

Next, the Gaussian filter was tested for filtering the ROP signal. This filter is based on a user-defined sliding window in which the Gaussian filter is applied. This example tests three sliding window sizes of 1000 ms, 2000 ms, and 6000 ms, as shown in Figure 5.3, tracks *d*, *e* and *f*. With small window sizes (e.g. 1000 ms and 2000 ms) the filter provides a satisfactory filtering of fast varying parts of the ROP signal (intervals #2 and #4 in Figure 5.3, tracks *d* and *e*). However, the filter fails to properly filter slowly varying parts of the ROP signal (intervals #1 and #3 in Figure 5.3). With wider sliding window size (e.g. 6000 ms) the filter provides a good filtering of slow varying parts of the ROP signal (intervals #1 and #3 in Figure 5.3, track *f*). However, as shown in the zoomed window, larger sliding window size, filters out the important fast varying parts of the signal (intervals #2 and #4 in Figure 5.3, track *f*).

A similar performance to the Gaussian filter was demonstrated by the Median filtering algorithm. This method is used to remove spikes using a sliding window across the selected range of data. An output is the median value in the window. Similarly to the previous example the algorithm was tested with three sliding window sizes of 1000 ms, 2000 ms, and 6000 ms, as shown in Figure 5.3, tracks *g*, *h* and *i*. In the zoomed window for sliding window sizes 1000 ms and 2000 ms, fast varying parts of the signal are almost lost (intervals #2 and #4 in Figure 5.3, tracks *g* and *h*). Slowly varying parts of the ROP signal are not filtered (intervals #1 and #3 in Figure 5.3, tracks *g* and *h*). For the sliding window of 6000 ms, the slow varying parts of the ROP signal are filtered properly (intervals #1 and #3 in Figure 5.3, track *f*, track *i*). However, the fast varying parts of the signal are lost (intervals #2 and #4 in Figure 5.3, track *i*).

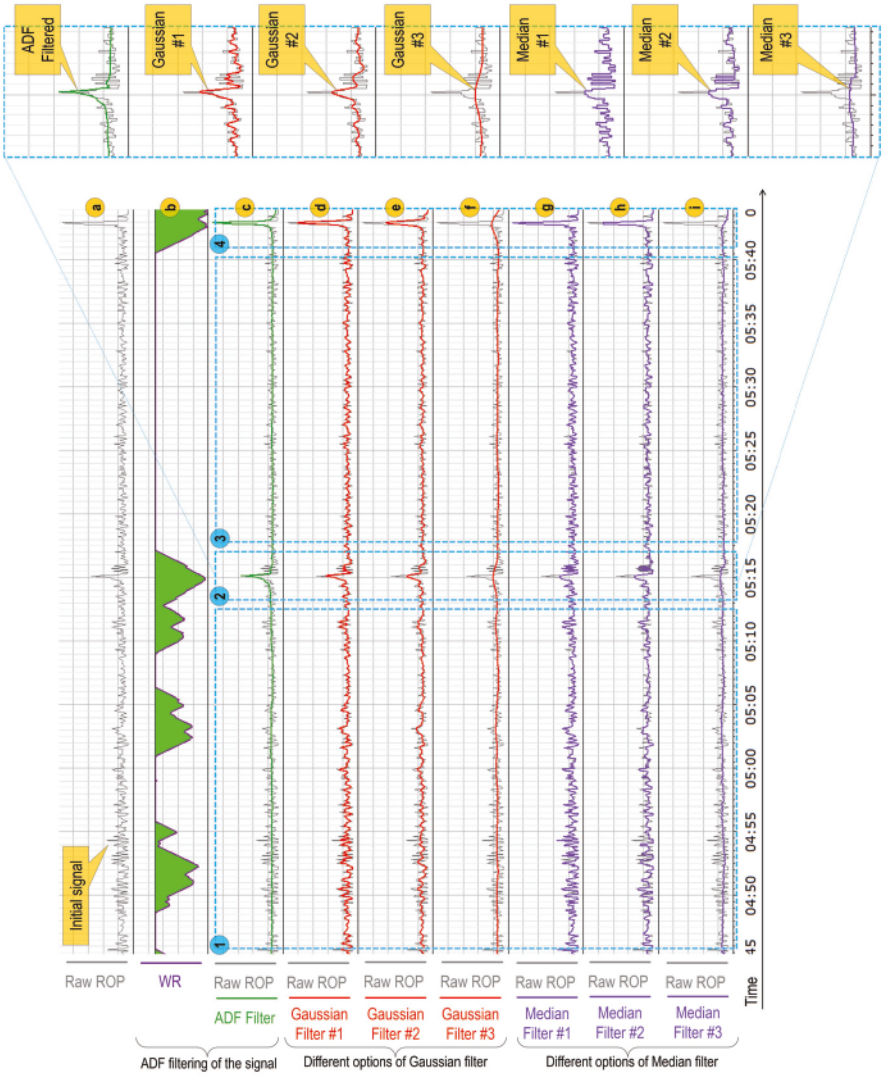

Figure 5.3: ADF algorithm implementation on filtering raw drilling data - ROP

This example demonstrates that the ADF filter provides good filtering of signals with both slow and fast variations. This property makes it more appropriate for applications to real-time measurement analysis when we need to capture both small/slow and large/fast changes in the data. The ADF provides not only the filtered signal, but also an accurate estimate of its first derivative. It is simple, computationally efficient, and has intuitive tuning rules. All together, these favorable properties justify the choice of ADF for automated detection of karstification objects.

5.3.1 Window radius for events detection

The adaptive window radius provides an effective and accurate indication of variations in the time series. As the accuracy of the approximation must be guaranteed, the adaptive window is forced to drop whenever it encounters rapid or large changes in the data signal where the linear polynomial no longer fits the data. By utilizing an appropriate δ value as a threshold for window adaptation, abnormalities in the data may be discovered from a drop in the window radius below a defined threshold. This concept can be taken advantage of to detect changes in the drilling data for event detection.

5.3.2 Pseudo-Code

Below, the workflow of the algorithm is described briefly in the form of pseudo-code.

Algorithm for: Adaptive Differentiating Filter

Input: Raw measurements signal $t, y(t)$

Output: Filtered signal $\hat{y}(t)$, its derivative estimate $d\hat{y}/dt(t)$ and the radius of the maximal window $WR^*(t)$

Parameters: δ, WR_{min} and WR_{max}

while *data in stream* **do**

1. Use current window radius around current time instant
2. Calculate least-squares fit regression estimate over the window
3. Perform window adaption from accuracy check
   - if accuracy is not met, reduce window radius and recalculate until the accuracy or minimum window WR_{min} is reached
   - if accuracy is sufficient, increase window radius and recalculate while the desired accuracy (specified by δ) is maintained and the window radius is below WR_{max}
4. Utilize the already found optimum window radius for the next time instant

end

5.3.3 ADF performance demonstration

Performance of the filter is demonstrated in Figure 5.3 for the case of Rate of Penetration (ROP). In the presented interval, high values of ROP are related to drilling into open karsts leading to Bottom Hole Assembly (BHA) drops (spikes in ROP). In this example a comparison between ADF, Gaussian and Median algorithms of filtering of the ROP data is shown. As illustrated in the figure, ROP measurements are quite noisy and contain both, slow- and fast changes. In practice, these ROP values are obtained by numerical differentiation of the Bit Depth signal.

ADF provides filtered values of both the signal and its estimated time derivative. In this example, we find filtered ROP values by applying ADF to the Bit Depth signal and finding a filtered estimate of the Bit Depth derivative. The filter was implemented in MATLAB™ [152] and then data were exported to Techlog™ [37] for visualization. In this example, parameter δ was selected from observation of the Bit Depth signal, finding an appropriate $\delta = 0.02$.

Minimal and maximal limits for the window radius were selected to be $WR_{min} = 10$ and $WR_{max} = 120$.

5.4 Case study - Automated detection of karsts and fractures

The following section presents results from a case study on automated karst events detection using the adaptive differentiating filter. Here, the ADF is applied to the set of drilling data containing intervals that the operator company reported as containing fractures, vugs and caves.

Figure 5.4 presents a complete set of data, both raw and processed, corresponding to the selected interval. The first track (from top to bottom) displays the borehole image with marked intervals of open fractures, vugs and cave in the depth domain. The second track - "drilling data", displays a typical set of surface and downhole measurements in time-domain such as Torque, Pump Pressure, ROP, delta flow, hookload - the weight on the hook to control the weight applying on the bit (WOB) and downhole WOB measurements. These raw measurements are given to provide an overview of drilling within the discussed interval. Tracks marked with letters a to f represent certain outputs of the ADF algorithm used to detect events related to karstification objects.

Five time intervals will be considered as illustrated in the figure (Events 1 to 5). The sections identified as open fractures are intervals where the operator company encountered mud loss situations. They are marked as Events 1, 2 and 4. Event 3 is interpreted as vug interval. Event 5 illustrates a cavity of more than 50 cm in length with circumference of 21.6 cm. These intervals are highlighted in blue, denoting the start and stop time of each event. These benchmark intervals will serve for validation and evaluation of the ADF algorithm that automatically detects changes in drilling data related to drilling breaks and mud losses.

In this example, drilling was performed with a managed pressure drilling system using a subsea module pump equipped with high-precision sensors of mudflow rate. The measured flow rate can give indications of loss zones, so the calculated delta flow is utilized as one of the inputs for testing the ADF for automated event detection. Drilling breaks within carbonate intervals can often indicate that the well trajectory encounters a karstification object. Thus, I utilized sudden drops in WOB and surges in ROP (drilling break pattern) as an indication of a karstification object and capture these changes with the ADF filter.

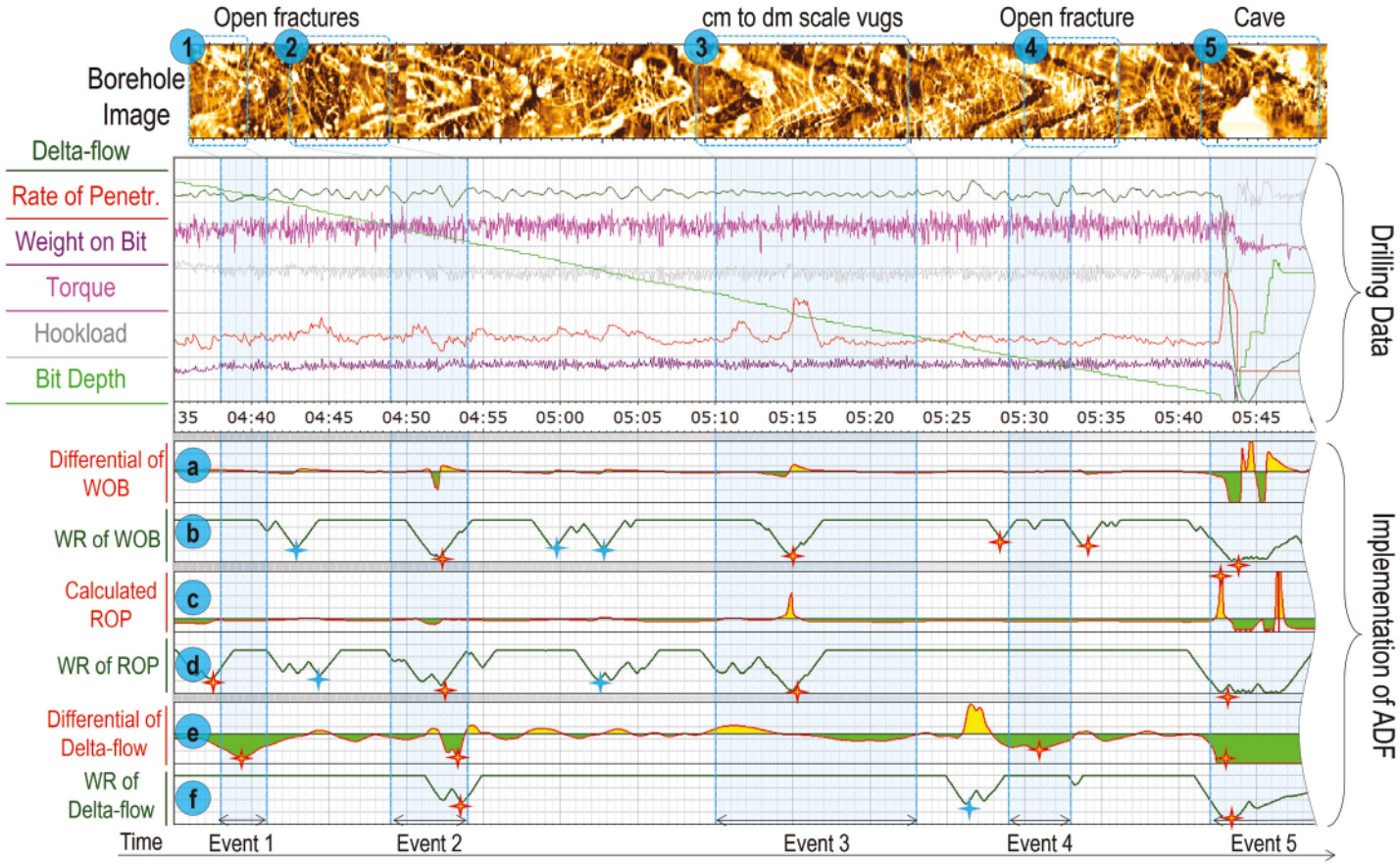

Figure 5.4: ADF algorithm implementation on drilling data

An application of the ADF algorithm for drilling events detection based on three inputs (WOB, ROP) and delta flow is considered in the following sections. The hypothesis of event detection in the ADF algorithm is that the window radius experiences a minimal value when the signal and its derivative experience rapid changes. The corresponding minima of the window radius are marked with stars. Changes in the window radius for the given inputs are displayed in tracks *b*, *d* and *f*. Another consideration which can be used for events detection is the rate of change in the measurements. As was discussed earlier, it is expected to observe a relatively sharp change in the delta-flow profile when the well path crosses a cave. Similar behavior is noted for WOB and ROP measurements (see Section 4.2 for details). For open fractures (fractures with mud losses) the rate of change of the discussed measurements is different from caves. Moreover, it is often the case that open fractures are detected only by delta flow measurements and not by ROP or WOB changes as some of the fractures can be relatively small and might not affect the dynamics of the BHA (see Section 4.3 for details).

For events 1, 2 and 4, benchmarked as open fractures it can be noticed that the calculated rate of change in the delta-flow drops significantly compared to the average level, indicating mud loss situations with sharp drops in the delta flow. For events 3 and 5, which are benchmarked as karst features of different sizes, the window radius of delta flow clearly indicates the interval of a cave (event 5), the detected mud losses (negative values in track e) did not have any sharp changes in the delta-flow, as indicated by no reduction of window radius in track f. For WOB (track b) and ROP (track d) inputs, the window radius reaches its minimum in intervals 2, 3 and 5, indicating quick changes in these parameters.

The main value of the discussed approach in the context of drilling events detection is that it simplifies the process in the detection of suspicious changes in drilling data. For example, it cannot be clearly seen from the raw drilling data (shown in the track "drilling data") that some events were occurring. While the visual analysis of the window radius and the calculated signal derivatives can easily indicate that there are changes in drilling data that might be linked either with regular drilling instances or with drilling through karsts.

This section demonstrated that the ADF algorithm is capable of revealing events in complex datasets such as real-time drilling measurements. Validation of event detection hypothesis exemplified the potential for online karst patterns detection from different real-time input signals such as delta flow, WOB and ROP.

The presented case study shows that the ADF algorithm applied to WOB, ROP and delta flow measurements successfully detects five out of five benchmark intervals corresponding to fractures or karsts. This detection occurred using either one, two or all three measurements. From the results, it is clear that the ADF can be utilized to detect karsts and fractures whenever they cause rapid changes in a measurement or its rate of change. For online drilling event detection, the ADF is robust and reliable, as it is efficient in approximation and detection and applicable to various datasets. This algorithm is highly modular, easy to tune and it can provide reliable results that match with variations that can also be observed.

5.5 Conclusions

This chapter has described the Adaptive Differentiating Filter initially proposed in [151] for robotic applications and demonstrates that it can be effectively applied for automated drilling events detection. In particular, it is demonstrated that it can be utilized for automated detection of patterns in real-time drilling data corresponding to karstification objects. The ADF automatically detects step changes in the delta flow as well as instances corresponding to drill breaks. Both can correspond to encountering karstification objects while drilling in carbonates.

Based on a case-study corresponding to drilling in carbonates in the Loppa High region, it can be concluded that the proposed algorithm generates good results for automated event detection and can efficiently locate change points in measurements corresponding to fractures, vugs, caves and possibly other karst-related events with high precision.

It is the engineer's responsibility to further investigate and evaluate the changes in data indicated by the algorithm, taking into account the totality of available information. In this way, the final responsibility for distinguishing karst patterns from other drilling events is still with the engineer, while the proposed automatic algorithm supports the engineer by detect potential karstification objects and zones.

As future work, automation of selecting filter parameters δ, WR_{min} and WR_{max} can be done. It is important to select these parameters correctly. In this study these parameters were selected by observation/analysis of drilling data. Finding simple rules for selecting these parameters lies outside of the scope of this chapter and is left for further work.

A variant of the proposed algorithm was successfully implemented by the author in Python for subsequent utilization in software platforms other than MATLAB ®. Although it led to significant learning and skills for the author, this part of work is not included in the thesis. It corresponds to implementation/programming aspects which lie outside the scope of this thesis.

Future work can also be undertaken to investigate algorithms for early change detection in drilling measurements including the detection of anomalous trends in data such as losses of drilling fluid and/or significant increase of ROP. Different types of change points detection algorithms can be studied. Such methods are commonly based on the detection of changes in mean [153], variance [154], periodicity [155] or changes in pattern [156] which is more difficult to tackle than the previous ones. An implementation of some of these algorithms for early detection of changes in drilling data will contribute to reducing the time for potential alarms.

Future work includes incorporating multiple inputs for increasing reliability and confidence in the detection of karst patterns and other drilling events, as well as reducing the number of potential false alarms. This will contribute to automation in the detection of karsts and other events to a higher degree and help with more consistent classification of complex real-time drilling data.

Future work can also be focused on combining the method presented in this section with methods for data quality control and improvement. These methods should help to avoid challenges related to common drilling data quality issues. The main drilling data quality issues are typically related to noise of different levels, inaccurate measurements or imperfect sensors, incomplete or missing data due to different sampling frequencies or measurement failures, or invalid data due to measurements taken outside of the sensors operational range or other issues. Therefore, to improve detection of karst patterns and other drilling events one needs to use algorithms for noise filtering, gap filling, range checks and outlier removal.

The research results presented in this chapter also contribute to digitalization and automation of today's manual interpretation of drilling measurements for detecting drilling events while drilling.

Chapter 6

Karst detection ahead of the drill bit based on consecutive acoustic measurements

It is important to detect karsts in advance to avoid drilling into them and/or to prepare risk mitigation actions to increase drilling safety in carbonates. However, with the state-of-the-art geophysical methods early karst detection is still challenging since: 1) logging while drilling (LWD) tools investigate the area around the tool with a large offset from the bit, so we cannot predict the presence of karsts neither ahead of nor at the bit 2) seismic-based methods, including Vertical Seismic Profiling (VSP) and Seismic Guided Drilling (SGD) suffer from low vertical resolution and cannot guarantee detection of small sized dangerous for drilling karsts, see Chapter 3.

This chapter presents a novel geophysical concept to investigate the area ahead of the bit based on acoustic surveying. This concept suggests using an acoustic source at the drill bit and evaluates reflections with a conventional acoustic LWD tool. Contrary to the classical approach, the method is based on consecutive acoustic surveys and their comparison using an unsupervised machine learning technique. Results of this comparison serve as an indicator of the presence of karsts ahead and around the bit.

A set of numerical models was developed, which represents a reservoir section of one of the fields in the Barents Sea to test, further develop and validate the method. These models contain both dangerous and not dangerous for drilling karsts. Numerical simulations of different geological scenarios with randomly distributed fractures and vugs, demonstrates how dangerous for drilling karsts can be sensed and distinguished from not dangerous for drilling objects. With this method one can avoid dangerous scenarios and/or prepare risk mitigating actions.

Simulation results indicate that the same approach can also be used for other applications such as prediction of formation changes, early detection of faults/fractures and pore pressure fluctuations. The proposed concept has been developed and tested based on extensive

numerical simulations. Its verification in a lab-scale setup or in field testing is left for future work.

6.1 Introduction

So far, Chapters 4 and 5 have considered karst detection at the drill bit based on indirect measurements. In other words, no direct measurements in front of the drill bit were utilized to detect karsts. In this chapter a novel method of early karst detection is introduced. This method is based on direct acoustic measurements in front of the drill bit.

Premised on advanced numerical modeling, this chapter presents a method where a drill bit is used as an acoustic signal source to generate and propagate pressure waves ahead of the drill bit. The pressure waves reflected from geological interfaces are then detected with a borehole acoustic tool. Acoustic surveys, sequentially executed at increasing depths, are then compared with each other to detect changes that may indicate the presence of karst objects ahead and around the drill bit. Due to the high complexity of the signals detected by the borehole tool, instead of classical signal processing, I apply an unsupervised machine learning technique – the K-means method [157] – to evaluate the changes/difference between the signals. Specific trends in this difference indicate an approaching anomaly (e.g. karst). Then, a workflow for decision support is developed when such trends are detected. This concept is demonstrated with extensive numerical simulations for different geological scenarios. The concept shows its value for further development and possible implementation for geoscience and drilling engineering.

The chapter is organized as follows. Section 6.2 describes the concept of consecutive acoustic surveying for karst detection ahead of the drill bit, as well as the method of acoustic comparisons and the workflow interpretation of its results. Section 6.3 explains acoustic signal processing and the developed method of acoustic surveys comparison in greater detail. Section 6.4 describes numerical models used in testing and demonstrating the method. In Section 6.2, verifies the concept with numerical simulations in a modeled carbonate well section. Conclusions, discussion and suggestions for future work are presented in Section 6.7.

6.2 Consecutive acoustic surveying

6.2.1 Borehole instrumentation and concept

Borehole instrumentation of the proposed acoustic surveying method is shown in Figure 6.1. An acoustic surveying system comprises a drill bit with an acoustic source to generate acoustic impulses and a Sonic LWD tool to register reflected signals, as shown in Figure 6.1. The impulse is generated when drilling is stopped, but the drill bit is still in contact with the formation. This ensures that the impulse is directly transmitted to the formation and that the noise from the bit-rock interaction does not contaminate the measurements of the reflected signals.

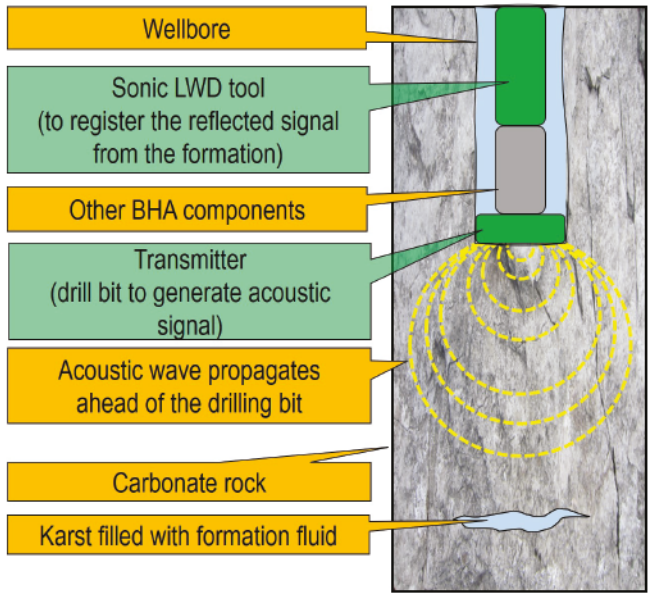

Figure 6.1: Schematic diagram of instrumentation of the method

The acoustic wave generated at the drill bit is traveling away from the source in three directions: upward, horizontal and downward. Reflections of this wave from different geological obstacles, including objects and karsts located ahead of the drill bit, are then measured by the piezoelectric receivers in the acoustic LWD tool. These reflections contain information about the geological obstacles. By taking consecutive acoustic surveys at increasing depths and applying a specific signal processing technique, one can detect approaching geological objects. This is the main concept behind the method.

The main advantages of this approach are:

1. The generated signal propagates ahead of the drill bit, enabling investigation of the area in front of the bit

2. The signal frequency range is lower than in conventional acoustic LWD tools and higher than in seismic methods. Thus the depth of investigation and resolution that are optimal for karst detection can be achieved
3. The approach uses current drilling instrumentation and requires minimum changes in the BHA

6.2.2 Challenges with classical signal processing

The major challenge of karst detection with the described instrumentation setup comes from the difficulties in classical signal processing. A conventional output for acoustic reflections imaging is the spatial positions and geometrical properties of geological objects. However due to the noisy environment and various unwanted reflections from BHA components and minor geological objects, classical acoustic imaging of a geological section can be very difficult. An attempt to utilize a typical acoustic visualization technique has been done to see whether this can help in detecting karsts. Details of this study are presented in Appendix A. From a karst detection perspective, these results pose the question of whether detection of karst hazards ahead of the bit is feasible at all.

Furthermore, due to the nature of the problem, drilling hazards need to be detected and accurately localized at a significant distance ahead of the bit to make the operator aware of possible problems. This process requires fast processing of the reflected signals to meet the real-time demands of drilling operations. This requirement is not always feasible with the currently available methods.

Other problems are caused by multiple reflections from not dangerous for drilling geological objects of different sizes and shapes, located at different depths and positions. The pseudo-random noise generated by these objects masks reflections from dangerous for drilling karst features and also complicates their detection. Specifically, since the characteristics of this ambient noise are unknown, it is challenging to detect whether the received signal contains reflections from dangerous for drilling karst objects in addition to this noise. Without a complex signal processing technique, which can be computationally expensive and difficult for operational interpretation of acoustic surveys, real-time detection of the size and positions of karsts ahead of the bit is expected to fail.

6.2.3 Method of acoustic comparisons

To address these challenges, or rather, to avoid them, instead of using classical acoustic signal processing techniques established for acoustic imaging of formation evaluation, it was suggested a technique that relies on *comparison* of acoustic surveys.

This section proposes a method that avoids the aforementioned challenges inherent to classical acoustic signal processing. It is based on *comparing* consecutive acoustic survey signals. The method stems from a generic anomaly detection technique introduced in [158],

which can be used for detecting equipment failures and other anomalies based on available measurement streams.

The working hypothesis is that the sound reflection characteristics obtained from karsts ("echo" of the pulse information detected by the borehole acoustic tool) will be different in a certain sense from the sound reflection characteristics acquired from any other not dangerous for drilling objects. While the common practice of studying formation properties is through formation images (seismic, resistivity or acoustic), which is very difficult and costly with the described borehole instrumentation, the method applies different principle.

The method is based on consecutive acoustic surveys, illustrated in Figure 6.2. When the well is drilled up to a certain depth, the first acoustic survey is taken (Survey #1 in Figure 6.2). Then, once the well is drilled further, the second acoustic survey is taken (Survey #2 in Figure 6.2). We can then repeat this process of conducting consecutive acoustic surveys while drilling, as shown in Figure 6.2, where surveys from #3 to #8 are taken.

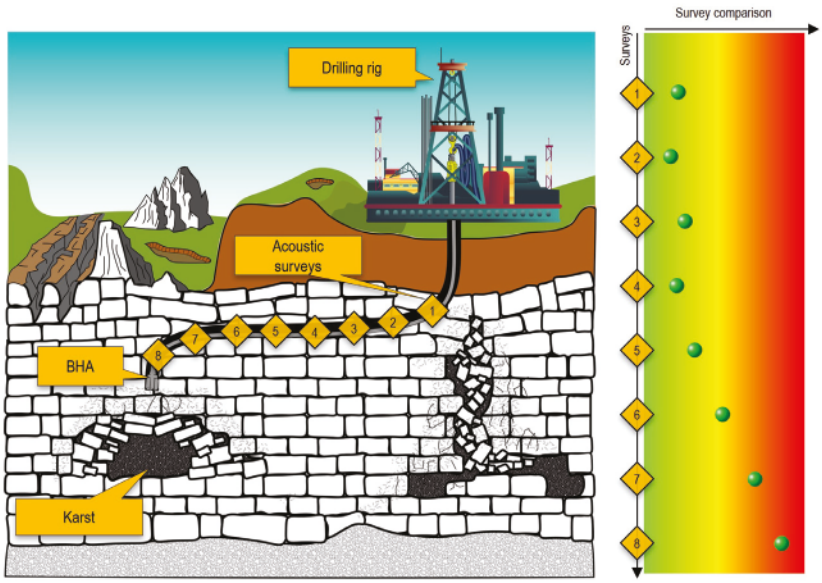

Figure 6.2: Consecutive acoustic surveys along the well path (left) and their comparisons (right)

According to the applied hypothesis, if there are no significant formation changes in the region that has been drilled since the previous acoustic survey, then the difference between the new and the previous acoustic surveys will be minimal. In other words, if drilling is conducted within the same geological formation and there come no new geological objects within the depth of investigation provided by the method, then the current and the previous surveys will resemble each other in a certain sense. Specific ways of how to compare acoustic signals and check their resemblance are discussed further in Section 6.3.

In Figure 6.2, which illustrates the concept with the right-hand plot, equal surveys are expected to be the surveys from #2 to #6. Starting from survey #6, as the well trajectory is getting closer to the karst, each new acoustic survey will contain more reflected components from the karst. These new karst reflections will cause an increasing difference between the consecutive surveys as illustrated in the right-hand side of Figure 6.2 (acoustic surveys #5 –#8). The strongest karst-reflection and thus the biggest difference between the surveys is expected when survey #8 is taken and compared with survey #7. A trend of differences between the neighboring surveys can serve as an indicator of an approaching geological object. This trend can then be interpreted using additional available information, as described in more detail in the next section.

In this concept the distance between acoustic survey stations plays an important role. The longer the distance between surveying stations, the higher the probability of encountering new geological reflectors while drilling. In the case of less frequent acoustic surveys, the values of difference between the surveys can be scattered. A high scattering range between previously recorded surveys, makes it challenging to detect small changes in the upcoming surveys. In the suggested approach the distance between surveying stations can vary (e.g. new survey station can be added when needed). If we expect any potentially dangerous for drilling intervals ahead of the bit, acoustic surveying can be conducted more often. More frequent acoustic surveying can reveal smaller differences between acoustic surveys, thus enabling more accurate detection of an upcoming reflector (interface of geological object ahead of the drill bit). In less dangerous for drilling intervals, or when there is no operational necessity for the detection of geological objects ahead of the bit, acoustic surveys can be conducted less frequently.

6.2.4 Interpretation workflow

The workflow of acoustic surveying and comparison of acoustic surveys consists of the following steps. First, when drilling is stopped, but the drill bit is still in contact with the formation, an acoustic source at the bit generates an impulse signal. Part of the generated impulse propagates ahead of the bit and reflects back. The reflected signal is then detected by a borehole acoustic logging tool such as SonicScope® [159]. Second, instead of a conventional signal processing aimed to visualize geological formation properties, I compare acoustic surveys and estimate the *difference* between them understood in a certain sense, which will be discussed in more detail in Section 6.3. If the difference from the previous acoustic signal is large, it can be explained by several causes, including changes in formation properties, faulting/fracturing or karstification objects. More details on what could be considered as a significant *difference* between the surveys is discussed in Section 6.3.7. Once the difference between the surveys is detected, it is proposed to utilize additional available data, which can be used to explain it. The workflow is shown schematically in Figure 6.3.

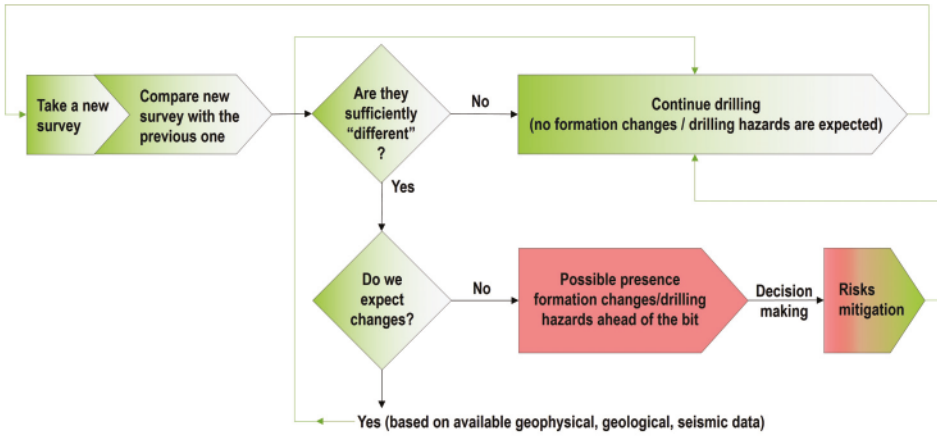

Figure 6.3: The workflow of the acoustic comparisons method

An example of utilizing additional data to explain the difference between acoustic surveys follows. Picking seismic horizons in a seismic study and converting them from time to depth domain results in uncertainties in real horizon depths. Due to the uncertainty of the real depths of geological horizons, on-site interpretation of geophysical data is typically performed by geologists using additional LWD measurements. However due to a high bit-sensor offset, geophysical measurements come with a significant delay. Prediction of an approaching new geological horizon based on such delayed measurements is complicated.

Well site geologists project geophysical *markers* (patterns of geophysical measurements corresponding to a certain geological horizon) from offset wells to solve this problem. Still, without any direct measurements ahead of the bit, advance detection of geological horizons is challenging. With the proposed novel acoustic surveying concept, based on direct measurements ahead of the bit, the difference between the surveys can be detected. Depending on how this difference changes with the depth, it can be possible to predict the approaching to a new geological horizon or geological object as will be demonstrated by simulations in Section 6.4. At this stage additional field data such as geophysical *markers* or seismic interpretation can be used to explain the difference between acoustic surveys. If there is an expected horizon in front of the drill bit, as follows from additional field data (geophysical *markers* or seismic data), then the detected increasing difference between the acoustic surveys will be an indicator of approaching this horizon. This difference can then be used for calibrating the spatial data in the available data, e.g. the seismic model.

Another example illustrating possible utilization of additional field data when the difference between acoustic surveys is observed is the following. If it is not expected from the analysis of available data that the well path will approach a new geological horizon or that formation properties will change significantly, then a possible reason for an increasing difference between acoustic surveys can be associated with encountering a new geological

object. Depending on the region of drilling, various geological features can be expected: karsts in carbonates, overpressure zones in a terrigenous formation, faults in a seismically active region. Depending on the region of drilling, different decisions can be made when a large difference in acoustic surveys is observed. Thus, the combination of the discussed instrumentation setup with the method of acoustic comparisons can be used for risk mitigation while drilling.

The introduced concept of acoustic surveying is not intended to replace existing geophysical methods. It is expected that this concept can provide the best results in terms of early detection of drilling hazards and/or formation changes, when it is used together with other available data and knowledge about the region of drilling. Depending on whether the difference between surveys can be explained or not, different actions can be taken. In some cases the difference between acoustic surveys can be related to approaching a regular (not dangerous for drilling) geological object. In other cases the difference can be an indicator of approaching intervals/objects that are possibly dangerous for drilling.

6.3 Signal Processing

6.3.1 Concept

Each acoustic survey consist of a combination of segments with a certain number of basic shapes. Reflections that come from significantly different formations (e.g. one - from a formation with a large karst, another - from a formation without a karst) will have different features (e.g. basic shapes). Reflections that come from formations with comparable properties will have approximately the same features in shapes. The method of acoustic comparison presented below allows one to detect whether two acoustic surveys (e.g. signals) have different sets of features (apart from the noise coming from minor geological reflections) and quantify the difference in these features.

This method was initially presented in [158] and used for anomalies detection in heart rhythm in electrocardiograms (ECG) [160]. The method of comparing two time series (acoustic signals) consists of eight main steps as shown in Figure 6.4:

1. Take acoustic survey
2. Remove first arrivals (e.g. direct waves from the transducer)
3. Split the survey into segments with overlapping
4. Normalize each segment (windowing)
5. Cluster the segments
6. Generate the library of basic shapes for survey #1
7. Take acoustic survey #2
8. Remove first arrivals
9. Reconstruct the signal from the library of basic shapes (centroids [158]) obtained in step #6
10. Evaluate the reconstruction error
11. Do steps #3-6 for acoustic survey #2 to generate the library of basic shapes for comparison with subsequent acoustic surveys

The main output from these steps is the estimated value of the reconstruction error. Sections 6.5 and 6.6 will provide more details about how this parameter can be used. As illustrated in Figure 6.4, the library of basic shapes of the first signal is used for reconstruction of the second acoustic survey. Once the reconstruction error is estimated for the second survey, as will be discussed in Section 6.3.7, a new library of centroids can be created (see Figure 6.4). More information on how a library of centroids can be created is given in Section 6.3.6. This new library is then used to reconstruct the third survey and estimate the reconstruction error. The details of each step are presented in the next subsections.

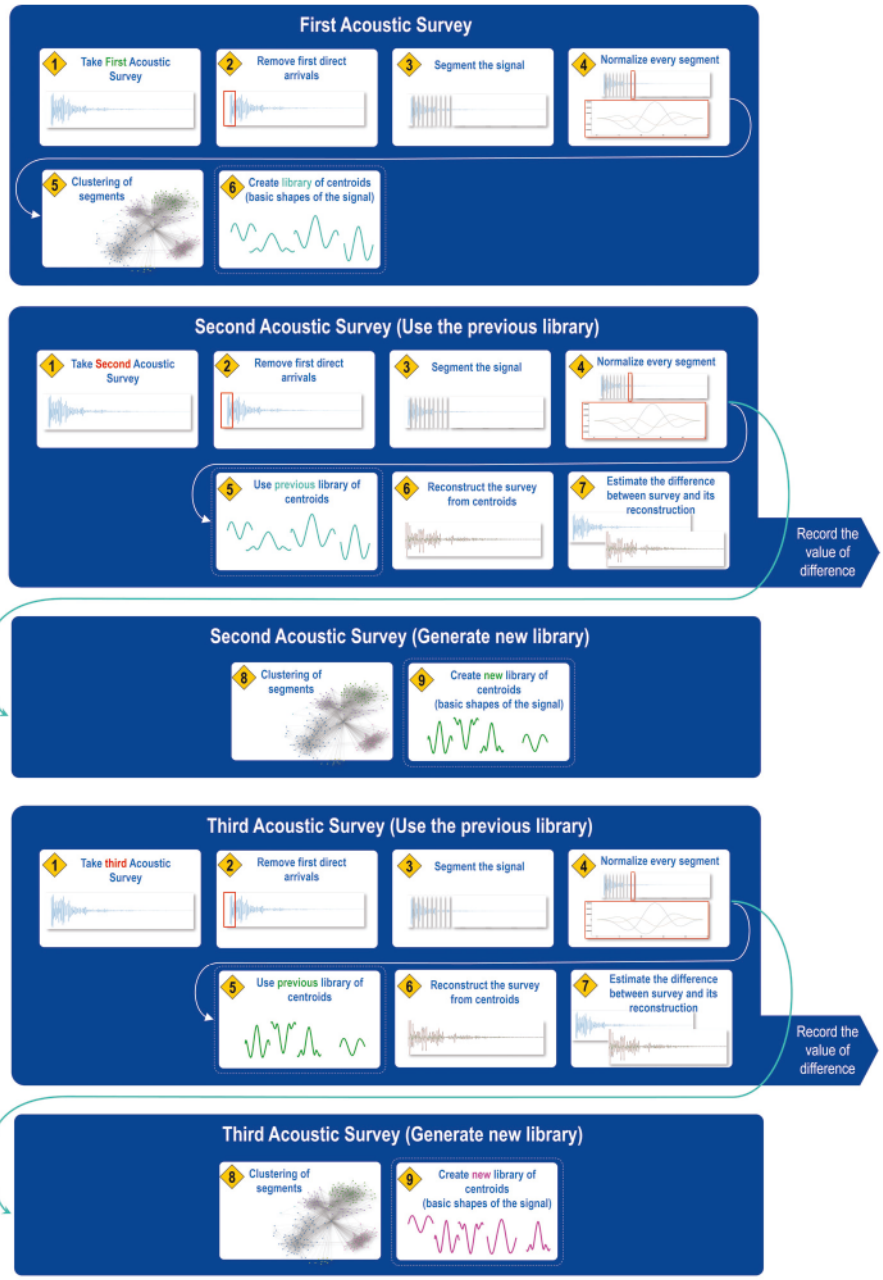

Figure 6.4: K-means for acoustic survey comparison. The main steps

6.3.2 Setup a Python Environment for Machine Learning

The method of acoustic comparisons, discussed in this chapter, requires a computer to handle the computations and the Python environment for AI and Machine Learning. The computer has the following configuration: Central Processing Unit (CPU) — Intel® Core™ i9-9900 processor with 8 cores (3.10 GHz), Random-access Memory (RAM) - 128 GB, Graphics Processing Unit (GPU) — NVIDIA GeForce RTX™ 2080 (11 Gb).[1] To set up Machine Learning in Windows Keras™ [161] and Tensorflow™-GPU packages [162] were used. Keras - is the state-of-the-art deep learning Application Programming Interface (API) developed by Google™ for implementing neural networks. TensorFlow ™ is a library for numerical computations and large-scale machine learning. The following packages were used:

- The distribution of the Python programming language Anaconda [163]
- The parallel computing platform, to use a CUDA-enabled graphics processing [164] (CUDA Toolkit™, version: 11.0.2_451.48_win10)
- The Deep Neural Network library (cuDNN™) - a GPU-accelerated library of primitives [165] (version: cudnn-11.0-windows-x64-v8.0.4.30)

Once new environment is created cuDNN `.bin`, `.include` and `.lib.x64` files can be added to the corresponding Windows path. After that with the following commands a new environment in Anaconda Prompt can be created:

`conda create -c conda-forge python=3.8.5 -n tf`
`conda activate tf` (switch to the new environment)
`pip install tensorflow` (Version 2.4 was used as the most stable one)
`print(tensorflow.reduce_sum(tf.random.normal([1000,1000])))` (The output should indicate that libraries were loaded successfully)
`pip install keras` (version 2.4.3)
install any additional packages if needed for the new environment such as NUMPY [166]

To use Jupyter [167] in the activated environment:

```
conda install -c anaconda ipykernel
python -m ipykernel install -user -name=(name of new environment)
pip install jupyter
```

Once these steps are completed, one can implement examples of code listing provided in this chapter in Jupyter Notebook and run Keras code using Tensorflow™ with Nvidia GPU support.

[1]The method of unsupervised ML used in acoustic comparison (will be discussed in Subsection 6.3.6) is not computationally expensive and can be run with a computer configuration that is less powerful than the one described here. This computer configuration was also used for numerical modeling discussed in Section 6.4 where more computational power was required to meet the needs of the experiment.

6.3.3 Curation of acoustic survey data

The first step in the developed workflow (see Figure 6.4) for acoustic survey comparison is the excitation of the acoustic impulse and the registration of reflected signals as was discussed in Section 6.2.

The second step is shrinking the signal (see Figure 6.4). Since the impulse is generated in close proximity to the receiver (see Figure 6.1), one of the first signals detected by the receiver is the direct arrival from the transmitter. An example of the acoustic survey is shown in the upper part in Figure 6.5. There are different techniques for detecting direct arrivals. Some of them are used in seismic or borehole acoustic signal processing [168–170]. For the sake of simplicity in the implemented workflow the signal is cut at 300 μs as shown in Figure 6.5 (lower part).

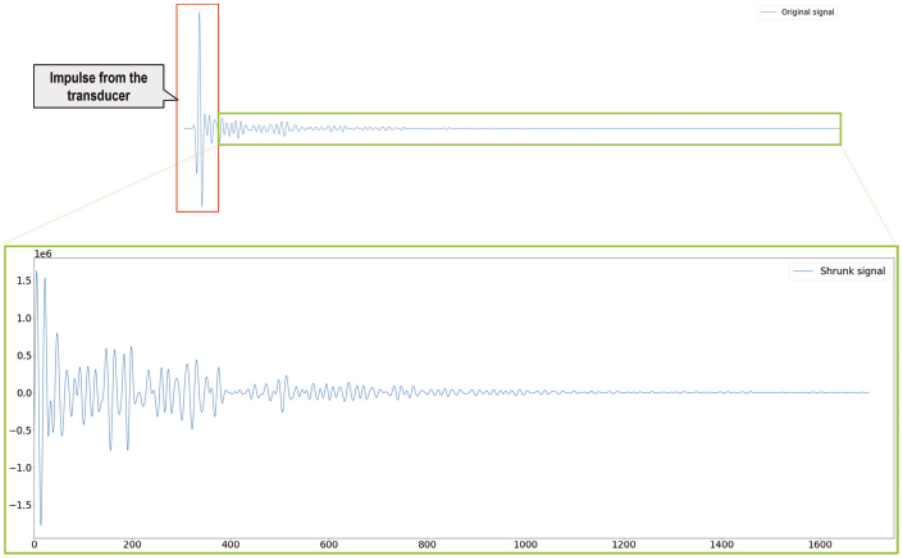

Figure 6.5: Example of simulated reflected signal detected by the receiver (acoustic survey) and shrunk acoustic signal used for signals comparison. The first 300 ms of the signal are cut out

6.3.4 Segmentation

The third step in the signal comparison workflow is the segmentation of the acoustic signal, where the input acoustic signal is split into a sequence of discrete segments (see Figure 6.4). The generated segments are horizontal transitions with half overlapping of each other as shown in Figure 6.6. Sliding length is the horizontal transition and the segment length is the number of data points in each segment.

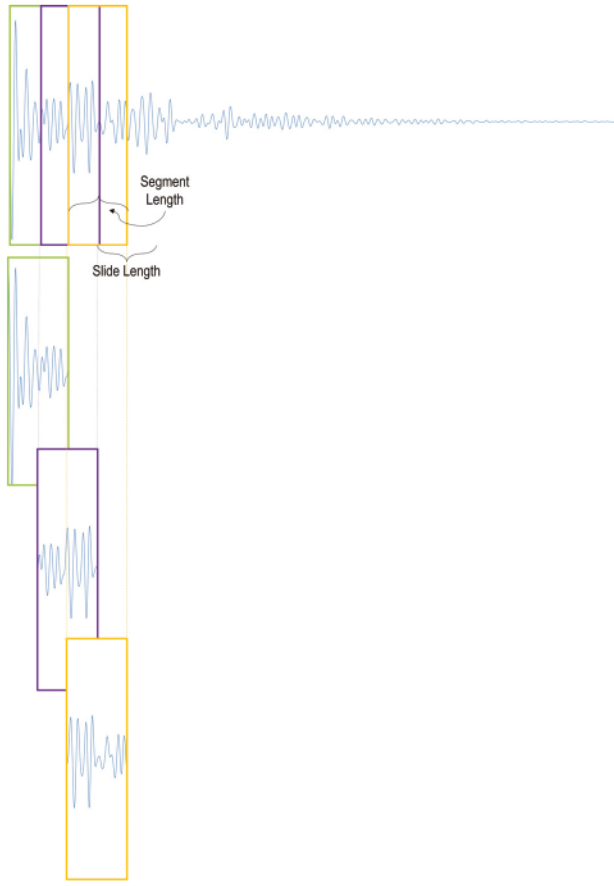

Figure 6.6: Sliding segmentation of the acoustic signal

In the examples discussed in this chapter, each segment consists of 176 data points, representing 176-dimensional space. [2] The result of splitting the signal into equal segments of 25 $[\mu s]$ length is presented in Figure 6.7.

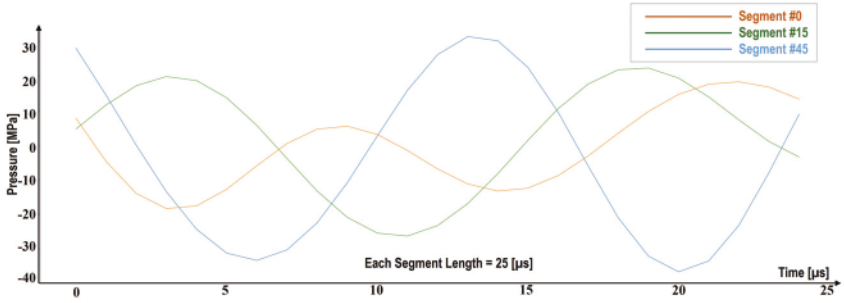

Figure 6.7: Segmentation of acoustic survey into equal segments of 25 μs length. Three segments are shown: #0, #15 and #45

The code used to implement this is:

```
#function:
def slide_box(data, window_length, slide_length):
    boxes = []
    for pos in range(0, len(data), slide_length):
        box = np.copy(data[int(pos):int(pos+window_length))
        if len(box) != window_length:
            continue
        boxes.append(box)
    return box
#implementation:
segment_length = 25
slide_length = int(segment_length/2)
segments = slide_box(data, window_length=segment_length, slide_length=slide_length)
len(segments)

print("␣%␣segments␣are␣generated" % len(segments))
2190 segments are generated
```

[2] Selection of the optimal length of segments is an important aspect in time-series analysis. The smaller the segment size is, the more time series data is split. Depending on the length of the segment, polynomials of different degrees and coefficients are required. In the K-means clustering method, the length of the segment will affect the selection of the number of clusters to use. The higher the number of clusters the higher the influence of polynomial coefficients will be. In this study both the length of the segments and the number of clusters were chosen empirically. The development or implementation of a method to select optimal segment length and number of clusters lies outside the scope of this thesis.

6.3.5 Windowing

The fourth step in the acoustic survey comparison workflow (see Figure 6.4) is windowing. Since the segments do not necessarily start and end at zero as can be seen in Figure 6.7, this can cause discontinuities when a Machine Learning (ML) technique will be used. To reconstruct the waveform from the obtained segments (will be discussed in Section 6.3.7), the learned segments should have zero starts and ends. By applying the sinusoidal windowing function [171] to each of the segments, all the data outside of the window is multiplied by zero. The applied sine window function is defined by:

$$w[n] = sin(\frac{\pi n}{N}) \tag{6.1}$$

, where $w[n]$, $0 \leqslant n \leqslant N$ is the sequence of length N with N being the length of the segment. By applying windowing function to each of the segments, all the data outside of the window is multiplied by zero. The code for the windowing function implementation is:

```
window_r = np.linspace(0, np.pi, segment_length)
window_function = np.sin(window_r)**2
windowed_segments = []
for segment in segments:
    windowed_segment = np.copy(segment) * window_function
    windowed_segments.append(windowed_segment)
```

The result of applying the windowing function to three segments #0, #15 and #45 is illustrated in Figure 6.8. Once the windowing is completed, all the segments are tied together and can be clustered.

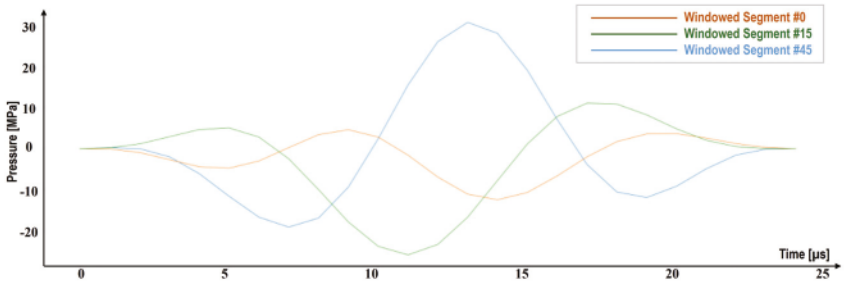

Figure 6.8: Windowing of acoustic segments. Three windowed segments are shown: #0, #15 and #45

6.3.6 Clustering

Clustering algorithms can be useful to uncover the structure presented in time series. The K-means clustering algorithm [172–174] is used in the presented acoustic survey comparison workflow (see step five Figure 6.4). It is useful in data mining tasks since it gives researchers insight into complex data set structures and can reduce the complexity of these data sets. This is especially important when no prior knowledge about the data set is available (e.g. data sets such as the acoustic surveys discussed in this thesis).

Each segment obtained in the previous steps can be visualized as a data point in an N-dimensional space (in our case 176-dimensional space). One can imagine that these points form *clouds* in the multidimensional space. The K-means algorithm splits these clouds of segments into K not overlapping groups (clusters) based on the similarity principle. For the acoustic surveying example studied in this chapter, each cluster will consist of segments with a common shape. An arithmetic mean of the data points in the cluster is called a centroid. In our case, it represents the mean shape of all segments in the cluster.

Figure 6.9 illustrates the main K-means clustering method for the case of two clusters. First, it selects two centroids in arbitrary locations. Then it assigns data points to one of the two clusters based on the Eucledian distance (each point is assigned to a cluster with the minimal distance to the corresponding centroid). After all points are assigned to the two clusters corresponding to their centroids, new centroids are calculated for each cluster (as an arithmetic mean of all points in the cluster) and the process is repeated. The iterations are stopped when the best possible centroid positions (and the corresponding split into clusters) is achieved.

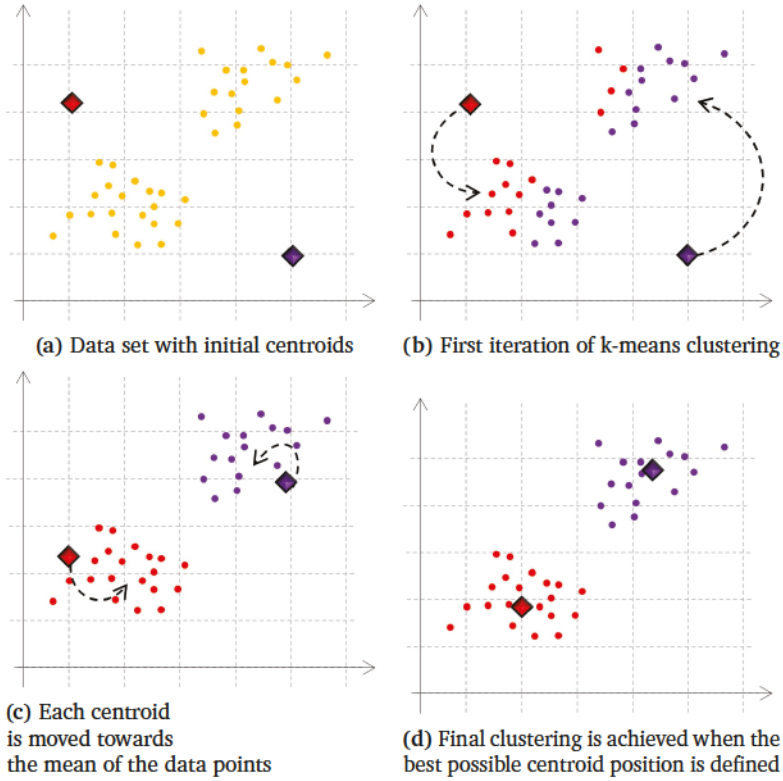

Figure 6.9: K-means algorithm

When processing acoustic survey data, all segments obtained in the previous steps are divided into K clusters and their corresponding centroids are calculated [175]. This set of centroids form the library of main shapes of the signal and are used to reconstruct the signal as will be discussed in the next section. Generating the library of the main shapes is the sixth step in the acoustic comparison workflow (see Figure 6.4).

In this thesis was implemented the K-means algorithm provided in the Keras package. Determining the optimal number of clusters is a known issue in partitioning clustering. Different methods such as average silhouette [176], gap statistic [177] or computing the number of clusters using R language *NbClust* package can be used to select an optimal number of clusters to be used. However, one of the simplest, although, probably, not the most optimal ways to find the optimal number of clusters is an iterative method: in this method, one could gradually increase the number of clusters, until reaching the "optimal" number after which further increase in the number of clusters does not lead to a significant improvement in the reconstruction error of the signal. For the signal discussed in this section the maximum number of clusters was set to 150. The code of utilizing the corresponding K-means function is given below.

```
cluster = KMeans(copy_x=True,
    init='k-means++',
    max_iter=300,
    n_clusters=150,
    n_init=10,
    random_state=None,
    tol=0.0001,
    verbose=0)
cluster.fit(windowed_segments)
```

A nearest centroid estimated for one of the windowed segments is shown in Figure 6.10.

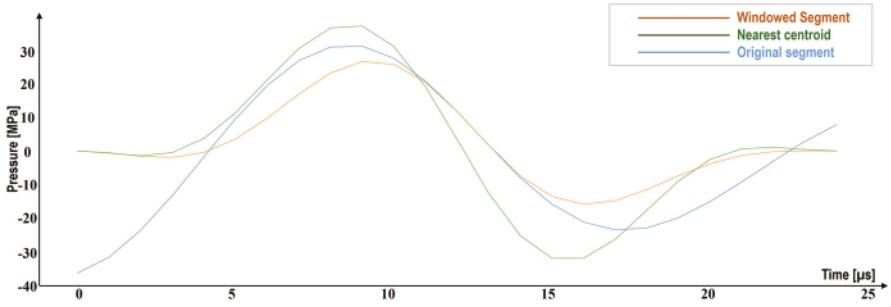

Figure 6.10: Original segment, windowed segment and estimated nearest centroid for the windowed segment.

6.3.7 Signal reconstruction and comparison

It is assumed that the obtained library of centroid shapes is accurate to depict the shape of initial acoustic survey (see step seven in Figure 6.4). If this self-reconstruction is not accurate enough, one can increase the number K – the number of clusters. In this example K=150 was used. Given that, one can rebuild or reconstruct an acoustic signal from the obtained centroids. To reconstruct the entire shape of the acoustic survey, centroids need to be combined together. Reconstruction on clusters is conducted with the built in Python module - `sklearn.cluster`. More information can be found in [178].

For a given segment, the sklearn module finds the nearest centroid from a library of centroids based on Eucledian distance. The corresponding code is given below.

```
nearest_centroid_index = clusterer.predict(segment.reshape(1,-1))[0]
centroids = clusterer.cluster_centers
nearest_centroid = np.copy(centroids[nearest_centroid_index])
```

To reconstruct the segments with the half overlap (e.g. with the defined slide length as was shown in Figure 6.6) the centroids are combined together:

```
position = segment_number * slide_length
reconstruction[int(pos):int(pos+segment_length)] += nearest_centroid
```

With acoustic survey reconstruction on clusters we can reproduce the shape of the acoustic survey. With this reconstruction method we can compare two acoustic signals. If signal #2 contains new features that are not present in signal #1, then the reconstruction error will be higher, since the library of centroids was obtained for signal #1 and it does not contain the shapes to accurately reconstruct signal #2.

To estimate the reconstruction error a percentile score was used. In statistics it is a value below which a given percentage of data in a group of observations fall [179]. To estimate the reconstruction error, I use 98^{th} percentile or the value (score) below which 98% of the data (reconstructed signal) fall. The code listing for the calculation of reconstruction error is:

```
error = reconstruction[0:n_samples] - data[0:n_samples]
error_98 = np.percentile(error, 98)
```

If signal #2 consists only of features present in signal #1 (and thus captured in the library of centroids), then the calculated difference will be relatively low. In the examples below these normal and anomaly reconstruction errors are considered.

Normal reconstruction error

An example of a normal acoustic survey reconstruction on centroids obtained from a normal acoustic survey is shown in Figure 6.11. The estimation of the 98^{th} percentile of the data along the specified time axis gives the reconstruction error of 111352.6.

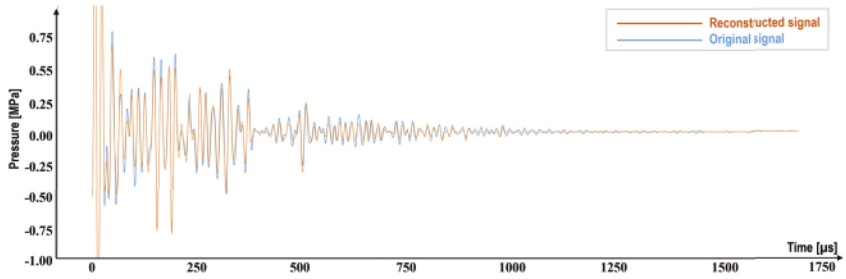

Figure 6.11: Original acoustic survey and reconstructed acoustic survey

Anomaly reconstruction error

If the library of clusters obtained from a normal acoustic survey will be used to reconstruct an anomaly (e.g. karst-related) acoustic survey, the error of reconstruction will be larger. A large reconstruction error occurs when the input is different from normal acoustic surveys, not related to karsts or any other changes of the formation properties ahead of the drill bit. In this example, estimation of the 98^{th} percentile gives the reconstruction error of 247311.0, which is more than 2 times larger than the error of 111352.6 estimated for the reconstruction of normal signal, discussed in previous example. Figure 6.12 depicts the reconstruction of an anomaly acoustic survey (signal reflected from a karst) from the library of clusters obtained from normal acoustic survey.

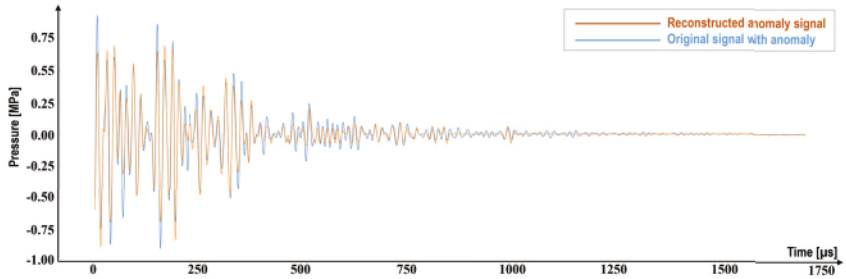

Figure 6.12: Anomaly acoustic signal and its reconstruction from the library of clusters obtained from a non-anomaly acoustic survey

6.3.8 Summary

This section has considered the method of acoustic signal processing. This method can be used to compare acoustic signals and estimate the difference between acoustic surveys. In this method first, the acoustic impulse is generated and reflections are received (e.g. acoustic surveying is taken as was discussed in Section 6.2). Then, the signal is shrunk to eliminate the first direct arrivals in the obtained survey (Section 6.3.3). Once the signal is pre-processed it is divided into equal half overlapping segments (Section 6.3.4. To eliminate discontinuities in the ML method, the windowing function is applied for each segment (Section 6.3.5). The windowed segments are then clustered with the K-means method (Section 6.3.6). The result of clustering is the library of the main shapes that comprises the acoustic survey (library of centroids). This library is then used to reconstruct the next acoustic survey. Depending on whether or not a new acoustic survey contains anomaly reflections, the estimated reconstruction error can be different. The estimated reconstruction error will be *low* if the two signals have similar features, e.g. both correspond to formations without *anomalies* and high for the case when two signals contain different features, e.g. when one of the signals correspond to a formation without an anomaly, while the other one is with an anomaly. The reconstruction error can thus be utilized as a measure of formation changes that occur between the two surveying stations, e.g. due to approaching a karst.

6.4 Numerical modeling

For concept validation and validation of the acoustic surveying technique extensive numerical simulations are conducted in an industrial simulator COMSOL Multiphysics® [180]. This section describes the main parameters of the developed numerical models and simulation results.

6.4.1 Model geometry

Two basic geometries were modeled in this study 16 m and 50 m of vertical section. All the parameters that will be discussed further are identical for both models, except for the length of the section. Below parameters of the model used to study pressure waves propagation in a 16 m well section are considered.

A 2D model geometry is shown in Figure 6.13a. A source of sound is a surface of 0.01 m width located 4 meters below the top of the model. The detector of acoustic waves is located 0.01 m below the top boundary of the model (3.99 m up the transmitter).

To study the influence of different karstification objects on the detection of formation changes and dangerous for drilling karsts ahead of the drill bit, a set of randomly distributed objects was created in the model. Depending on the simulation scenarios four types of randomly distributed objects were considered. For all cases the number of randomly distributed features was set to 100. In the example discussed in this section, random features are vugs with minimum radius 0.01 m and maximum 0.1 m.

6.4.2 Materials

The speed of sound waves propagation and rock density in the model are set according to the real carbonates formation properties in the Loppa High region and given in Table 6.1. The fluid filling the karsts is given by water, to model the physics of sound waves propagation at the interface between two media.

Table 6.1: Material Properties

Material	Density $[kg/m^3]$	Young's modulus $[GPa]$	Poisson's ratio	P-velocity $[km/s]$	S-velocity $[km/s]$
Carbonate	2600	60	0.25	6.94	3.82
Fluid	1000	n/a	0.5	1.48	n/a

6.4.3 Boundary Conditions

The low-reflecting boundary condition is used in the model to ensure that all types of waves pass out of the model domain without unwanted reflections. This condition is applied on the outer surfaces of the model as shown in Figure 6.13b. The condition uses material

properties from the domain to create an impedance match for both pressure waves and shear waves propagating in the domain [181]. Internal boundary conditions at the interface of the two materials are computed automatically by the COMSOL Multiphysics® software.

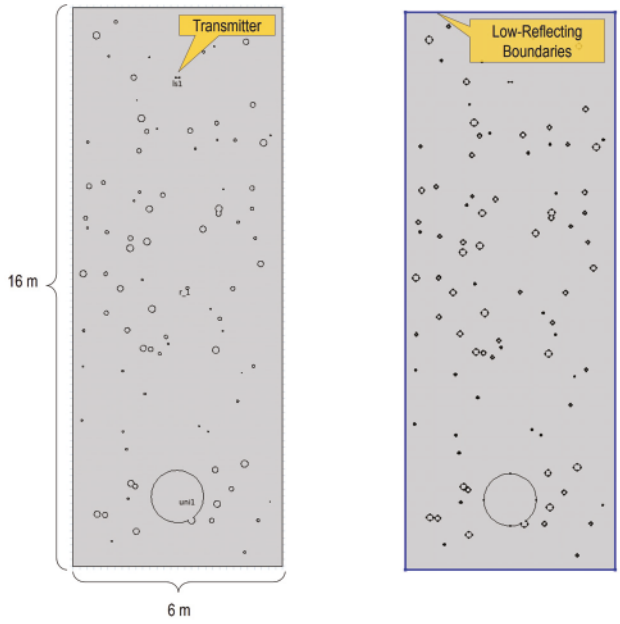

(a) Geometry of the model

(b) Boundary conditions of the model

Figure 6.13: Configuration of the numerical model for acoustic surveying

6.4.4 Acoustic source signal

The model of acoustic wave propagation in a rock medium is developed in Finite Element Method (FEM) Pressure Acoustic Transient interface of the COMSOL Multiphysics® software.

The source signal is defined by Body Load. The velocity of the transducer surface (drill bit surface) is given by:

$$V_n(t) = exp\left(-\frac{(t-2T_0)^2}{T_0/2} sin(2\pi f_0 t)\right) \tag{6.2}$$

with the delay $2T_0$ and the standard deviation $\sigma = T_0/2\sqrt{2}$. Values for the period parameter T_0 and frequency parameter f_0 are provided in Table 6.2.

Taking the partial derivative of Equation 6.2, the source signal is then defined as a Total Force (Body Load) acting on the surface. The profile of acceleration curve, applied to the surface of the transducer to generate acoustic impulse is shown in Figure 6.14.

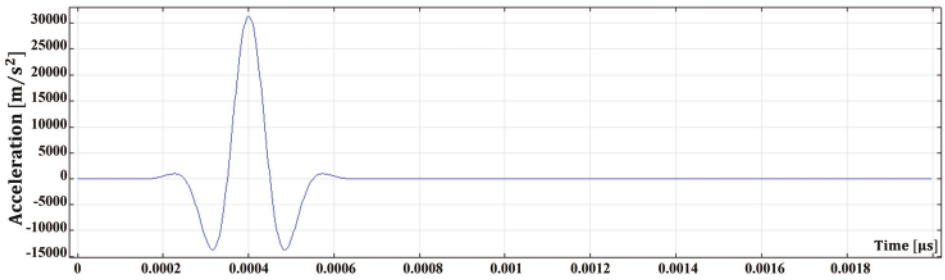

Figure 6.14: Acceleration, applied to the surface of transducer to generate acoustic impulse

Table 6.2: Acoustic signal properties

Transmitter width $[m]$	Signal frequency $[kHz]$	Signal Period $[\mu s]$
0.1	5	0.2

6.4.5 Meshing

The entire geometry of the model is meshed with triangle shaped elements. According to the Comsol Multiphysics acoustic manual, to model acoustic wave propagation in a medium, 5 to 6 mesh elements per wavelength are required. Maximum element mesh size can be calculated by Equation 6.3.

$$h_{max} = \frac{\lambda_{min}}{N} = \frac{c_{min}}{f_{max} N} \tag{6.3}$$

where h_{max} - maximum mesh element size, λ_{min} - minimum wavelength, f_{max} - maximum frequency, c_{min} - minimum sound speed, N - given number of elements per wavelength. In the current model configuration, for the frequency of 5 kHz, maximum mesh element size for solid medium is 0.06 m, for liquid - 0.03 m. The mesh consists of 162651 elements and has 630454 degrees of freedom. An overview of the mesh is shown in Figure 6.15.

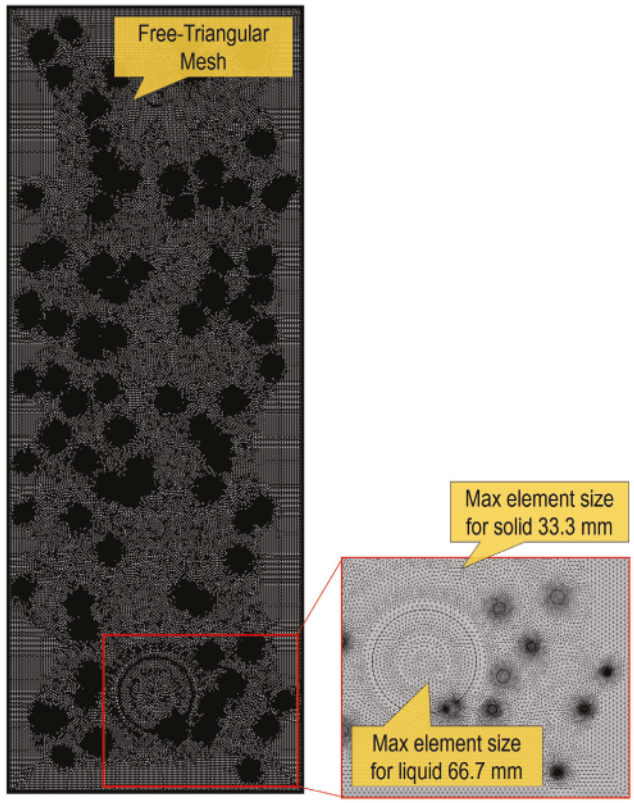

Figure 6.15: Meshing of the model

6.4.6 Solver

To compute the time-varying propagation of pressure waves, a Time-dependent solver with Multifrontal Massively Parallel Sparse (MUMPS) [180] was used. This type of solver is commonly used for computing the solution over time. The model is computed with 4400 μs time steps. When solving transient models, mesh imposed limitations on the time-step size δt are taken by the solver. In [182], a relationship between mesh size and time step was introduced. It is given by given by Courant-Friedrichs-Lewy (CFL):

$$CFL = \frac{c\delta t}{h} \tag{6.4}$$

where c - is the speed of sound and h - is the mesh size. This number is interpreted as a part of an element over which the pressure wave travels in each time step. The value of the CFL number should be less than or equal to 0.5 to minimize computational errors and

ensure that each of the computational errors will fall within the same distribution range. A minimum value of the time step is given by [182]:

$$\triangle t = \frac{h_{max(rock)} CFL}{P - velocity(rock)} \tag{6.5}$$

Based on Equation (6.5), for $h_{max(rock)} = 0.06$ m, $CFL = 0.5$ and $P - velocity(rock) = 6.94$ km/s, a time step of 0.0048 μs was selected to resolve wave propagation in the model.

The model was run on the workstation Dell Precision 7920 with the configuration described in Section 6.3.2. The average time to calculate a solution of the model with the given parameters was ~2 hours.

6.4.7 Pressure distribution

Acoustic pressure waves propagate with a spherical wavefront. Its propagation in the model at different time steps is shown in Figure 6.16. When the acoustic wavefront reaches vugs and the cave at the bottom of the model, reflections occur due to a change in acoustic impedance from rock to water-filled objects. The P-wave [3] reaches the cave at approximately $2.8[\mu s]$. The wave reflected back from the cave reaches the sensor at approximately $6[\mu s]$. Inside the cavity, (Figure 6.16), we can see a pressure wave focusing effect [183]. Inside the cave one part of the wave is transmitted back into the formation, and another part of the wave is transmitted towards the Low-Reflecting bottom boundary of the model.

Reflections from the roof and the bottom of the cave are repeated until the signal is completely attenuated. These repeated reflections from the cave can then be detected by the receiver. The same repeated reflections appear also in smaller vugs. They contribute to generating a smaller amplitude ambient noise in the model as shown in Figure 6.16. All these reflections make classical signal processing challenging and require novel processing methods, e.g. the one described in Section 6.3. The application of this method is demonstrated and validated in the next sections.

[3] A P-wave is a type of elastic body waves, also called seismic waves. The fastest traveling acoustic wave.

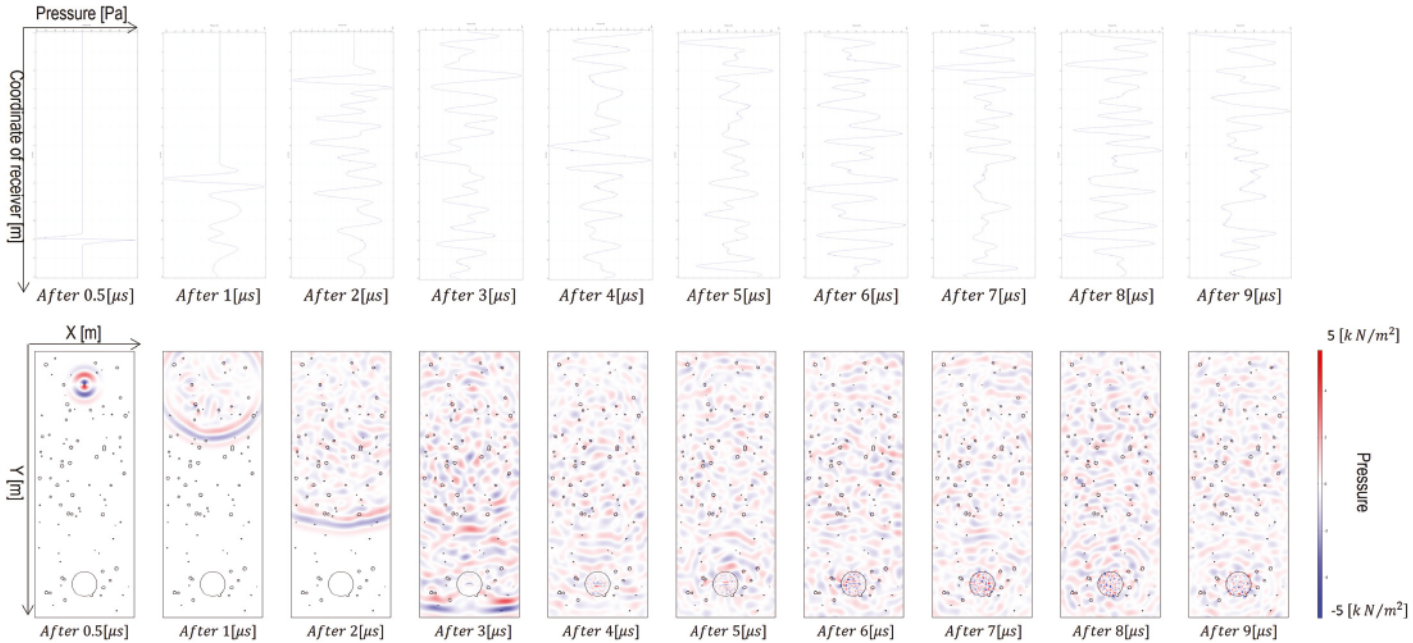

Figure 6.16: Snapshots of the acoustic wave propagation

6.4.8 Numerical model for simulating acoustic surveying in a karstified carbonates formation.

To investigate how dangerous for drilling karst forms can be detected with a novel acoustic surveying concept, a numerical representation of karstified carbonates formation was developed as shown in Figure 6.17. The modeled well section represents a 16 m carbonate rock consisting of vugs karst features, which form heterogeneous isotropy. Vuggy zones are common within the studied Loppa High region. This formation model can serve as a representative model for testing the acoustic surveying method described in this chapter.

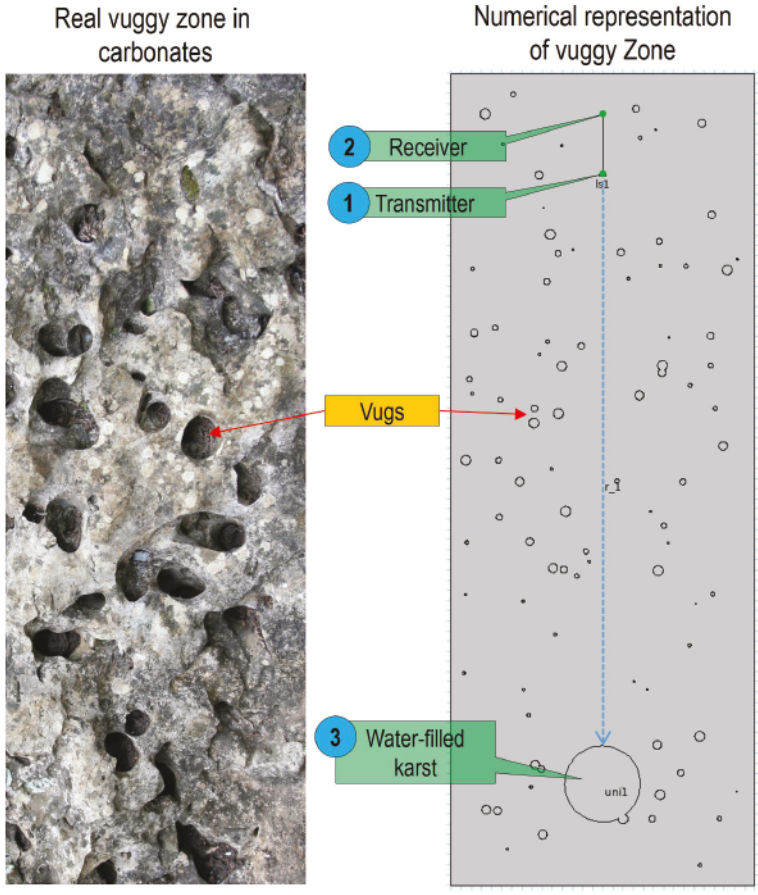

Figure 6.17: Numerical model of a karstified carbonates formation presented by vugs and its instrumentation for testing acoustic surveying. Well section of a 16 m carbonate rock. Photo creator [184]

Instrumentation part of the numerical experiment consists of a transmitter (pointer # 1) and a receiver (pointer # 2) shown in Figure 6.17. The transmitter generates a pulse with the same properties as in Section 6.4.4. It represents a drill bit with a pulse generator.

The receiver of acoustic signals is located at a 4 m offset from the transmitter. This replicates a possible position of a borehole acoustic logging tool within a drilling BHA. In this numerical simulation, instrumentation is simplified and does not represent a real configuration of a drilling BHA, which typically includes such components as the drill bit, mud motor, BHA stabilizers and other LWD tools. However, it is expected that the main principles of acoustic measurements can be captured and tested in simulations with this instrumentation setup.

Each survey starts with an acoustic pulse generated by the transmitter. Waves generated by the transmitter propagate in different directions, including the region ahead of the transmitter (e.g. ahead of the drill bit). Reflected acoustic waves are detected by the receiver (pointer # 2) as shown in Figure 6.17. Once the signal is detected, the transmitter-receiver system moves one meter deeper and a new survey is taken. This process replicates conducting an acoustic survey at a given depth, drilling to a new depth, and conducting the next acoustic survey. In the simulations, this process is repeated for the entire well section up to the water-filled karst (pointer #3).

6.5 Acoustic surveying concept verification - Early detection of karsts

Numerical simulations of consecutive acoustic surveying of a 16 m carbonate rock containing vugs and a larger karst as shown in Figure 6.17 and described in the previous section were conducted to to test the novel acoustic surveying concept described in Section 6.2. The workflow used in this numerical experiment is the following:

- generate an impulse by the transmitter and simulate wave propagation using the model described in Section 6.4.8
- record reflections by the receiver (e.g. record the acoustic survey)
- compare this acoustic survey with the previous acoustic survey to calculate the *difference* between them, as described in Section 6.3
- plot the estimated value of the difference for every new survey

The result of this simulation workflow (e.g. acoustic surveys) for four different scenarios is shown in Figure 6.18. In the scenarios discussed below all karsts are spherical objects of different diameters. Karst diameters vary from 0.5 m (Scenario #1 in Figure 6.18) up to 2.0 m (Scenario #4 in Figure 6.18).

Scenario #1 in Figure 6.18 illustrates the results of acoustic surveying of a well section that contains a cave sized 0.5 m in diameter. The X-axis shows the estimated difference between a new and the previous acoustic surveys. The distance between the sound source and the upper boundary of the karst is marked along the Y-axis. In scenario # 1, starting at a distance less than 6 m, a trend towards an increase in the difference between acoustic surveys can be observed. This indicates that in the acoustic surveys, that are taken closer than 6 m to the cave, there are new signal components (reflections from the cave). This can explain an increase in the difference between acoustic surveys (see Scenario # 1 in Figure 6.18). This simulation also demonstrates the functionality of the tested concept: the increasing difference between consecutive acoustic surveys serves as an indicator of approaching a karst.

With an increase in the cave size, the distance when the cave can be detected also increases (see Scenario # 2 in Figure 6.18). A cave sized 1.0 m can be detected at a distance of approximately 7.0 m. The depth when a cave can be detected, is estimated from the point where the deviation of the difference between acoustic surveys starts.

A similar increase in the distance at which a cave can be detected is observed in Scenario # 3 and Scenario # 4 with cave sizes of 1.5 m and 2.0 m respectively. A 1.5 m cave can be detected at 8.0 m distance from the transmitter (Scenario # 3 in Figure 6.18), 2.0 m cave - at 9.0 m (Scenario # 4 in Figure 6.18). It can be concluded that a consecutive trend in the difference between acoustic surveys can be an indicator of approaching an interface between two media as will be discussed in the next section. In this example, the interface is the boundaries of the karst cave sized from 0.5 m to 2.0 m. Also one can notice that larger

caves can be detected earlier than smaller caves.

Based on this sensitivity analysis the possibility of the detection of karsts with the developed novel acoustic surveying concept was investigated. More than 40 different cases were simulated and it was confirmed that 1) the presence of a consecutive trend of the *difference* between acoustic surveys is an indicator of approaching an interface between two media (as transmitter-receiver instrumentation is approaching the karst in the considered examples) 2) larger caves can be detected earlier than small caves.

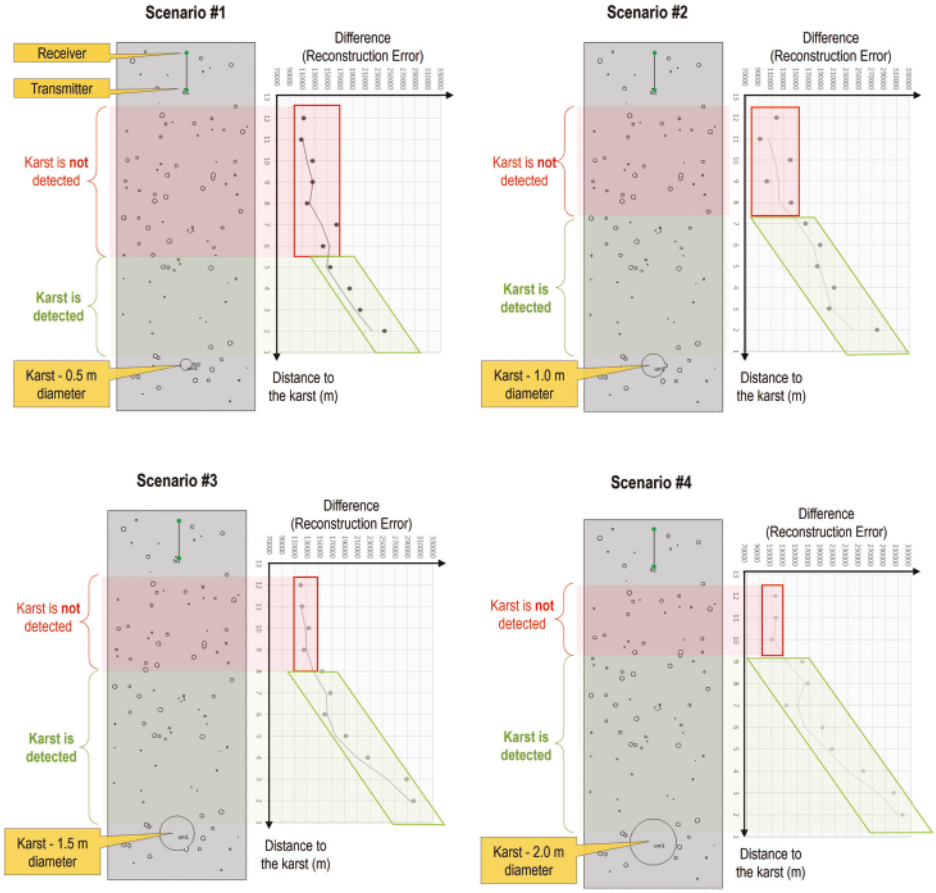

Figure 6.18: Numerical simulation of acoustic surveying of a 16 m carbonate rock section

6.6 Acoustic surveying concept verification - Early detection of formation properties changes

Numerical simulations of consecutive acoustic surveying of a 50 m of carbonate rock consisting of four different formations and a larger karst as shown in Figure 6.20 were conducted to test the novel acoustic surveying concept for early detection of formation property changes.

The modelled well section represents a 50 m carbonate rock consisting of four different formations, marked as Formations # 1, # 2, # 3 and # 4 (see Figure 6.19). The vugs are included in Formation # 4, were discussed in the previous section (Section 6.5). The karst in this numerical experiment is a spherical object of a 1 m diameter. Each formation consists of unique, randomly distributed geological features:

1. Formation # 1 - randomly aligned micro fractures form orthorhombic anisotropy
2. Formation # 2 - vertically aligned micro fractures form horizontal transverse isotropy
3. Formation #3 - horizontally aligned micro fractures form vertical transverse isotropy
4. Formation # 4 - vugs karst features form heterogeneous isotropy

The reasons for introducing such features are: 1) "most elastic media are weakly anisotropic" [185] 2) micro faults, fractures and vugs are the most common features presented within the studied region in the Barents Sea. Therefore, this formation model can serve as a representative model for testing the acoustic surveying method described in this chapter.

Model configuration and the workflow used in this numerical experiment are identical to the ones used in the previous example (Section 6.5). An example of a comparative visual comparison of reconstruction errors is discussed in this section, however more advanced techniqus of fully or semi-automatic trend analysis can be used in future work.

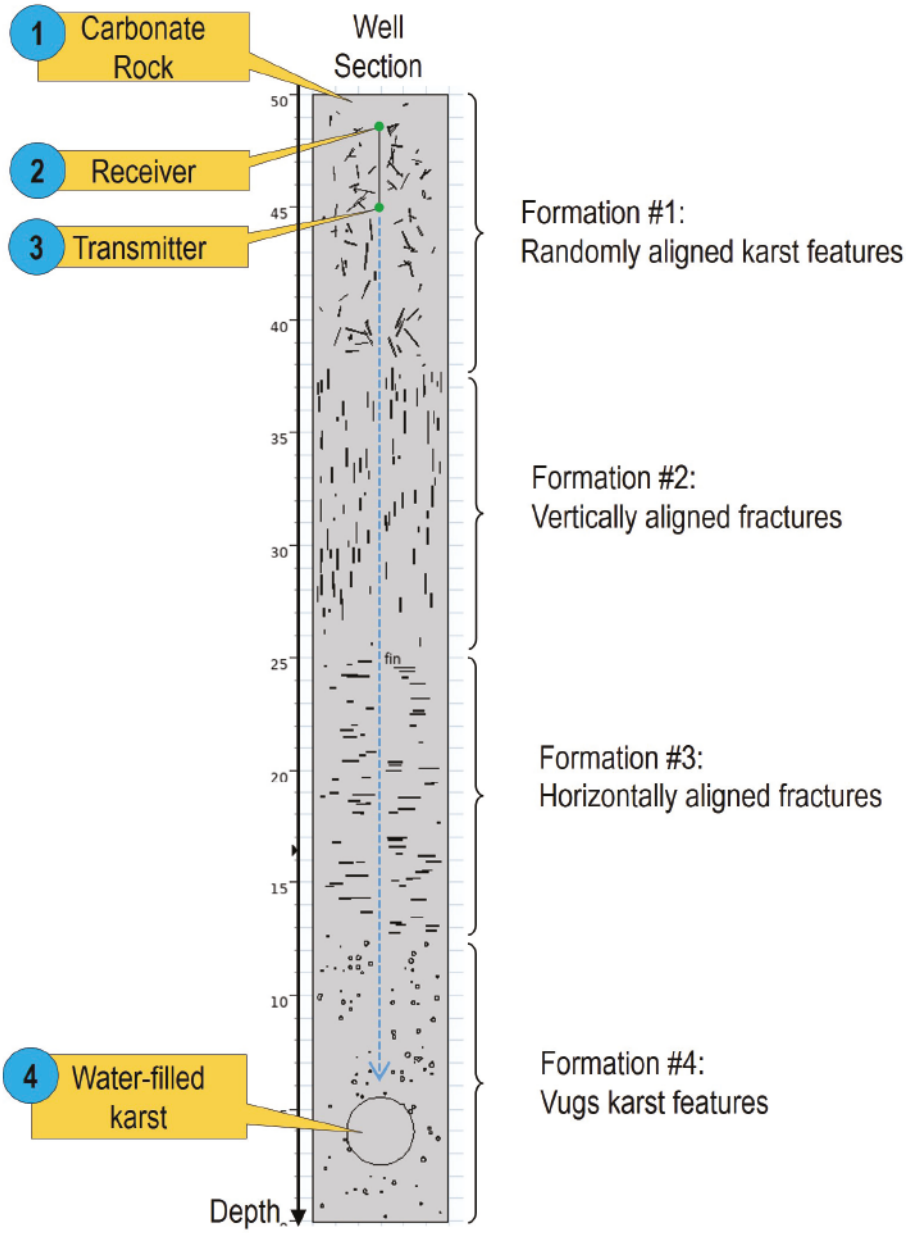

Figure 6.19: Numerical model of a karstified carbonates formation and its instrumentation for testing acoustic surveying. Consecutive acoustic surveys are conducted as we drill through the formations towards a large karst

The result of the simulations with the applied workflow is shown in Figure 6.20. The reflected acoustic signals (e.g. acoustic surveys) obtained in Formation #1 are significantly different from each other. As illustrated in Figure 6.20, this gives the greatest scatter of values in the estimated difference between each survey, compared to other formations (interval #1). This significant difference between surveys taken within Formation #1 can be attributed to the lack of uniformity and variety of angles and positions of fractures. Each new survey taken within Formation #1 consists of unique components reflected from randomly aligned discontinuities and therefore each new survey will be significantly different from previous surveys. However a linear trend in the values of difference can be observed when we reach Formation #2 and start recording reflections from a formation with uniformly aligned geological features (interval #2 in Figure 6.20).

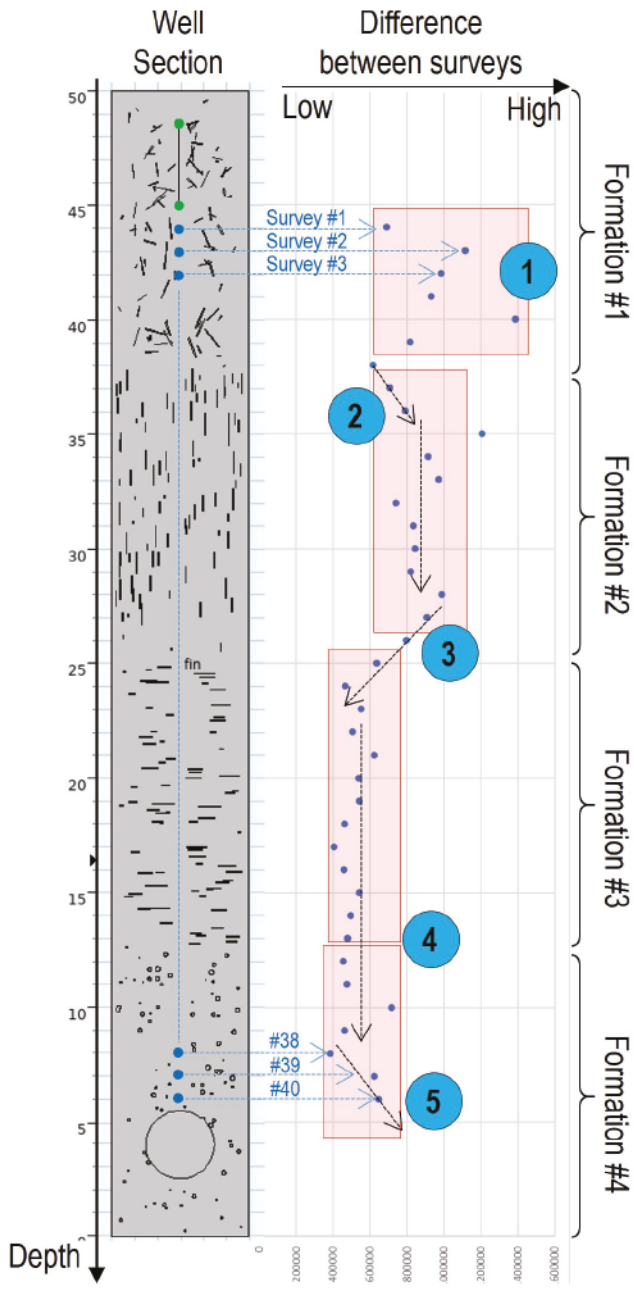

Figure 6.20: Numerical simulation of acoustic surveying of a 50 m carbonate rock section

Compared with Formation #1, it is clear that further acoustic surveying in Formation #2 is characterized by a smaller scattering of values in the acoustic surveys difference. The smaller difference can be explained by a unidirectional fractures distribution within Formation #2, even though the geometrical properties of fractures and their positions are random. In other words, due to a unidirectional spatial distribution of fractures, each new acoustic survey will contain less unique (more similar) reflections. This leads to a decrease in the range of acoustic survey scattering (see Figure 6.20, Formation #2).

A similar to the interval #2 linear decrease of the magnitudes of the *difference* between acoustic surveys, can be observed in interval #3 in Figure 6.20. There is a steady linear trend when new Formation #3 is detected by the receiver. Comparison of acoustic surveys in Formation #3 shows significantly less scattering of the difference values than the previous two formations (Formations #1 and #2). Acoustic surveys, which were taken within Formation #3, are similar and have comparable characteristics in the reflections. Accordingly, the distribution of acoustic survey differences is minimal.

In the transition interval between Formations #3 and #4, there is no visible trend in the magnitudes of *difference* (Figure 6.20, interval #4). Taking into account the small geometrical sizes and low reflection surfaces of the vugs included in Formation #4, these objects do not make significant contributions to the acoustic surveys. Thus the range of acoustic difference distribution in Formation #4 is narrow and similar to Formation #3. The trend observed in interval #5 is an indicator of approaching a water-filled karst located in Formation #4 as shown in Figure 6.20. The trend of the *difference* values in this case is similar to the trends observed in transition intervals #2 and #3. The presence of a trend is an indicator of acquiring new reflected components from geological interfaces located ahead of the bit and can be an indicator of both formation changes ahead of the bit or karst-like object detection. In this particular interval, the difference between acoustic surveys is an indicator of approaching a karst.

In this section a conceptual framework of acoustic surveying when drilling a well section was introduced. Consecutive acoustic surveys taken with 1 m intervals replicated the process of taking acoustic surveys during drilling. It is assumed that drilling is stopped for each acoustic survey. The method of acoustic comparison is utilized to estimate the difference between surveys demonstrates good results for both the detection of formation properties changes and karst detection ahead of the transmitter (e.g. drill bit).

6.7 Conclusions

This chapter has presented a novel geophysical method of surveying formation properties ahead and around the drill bit. In this method consecutive acoustic surveys are conducted at increasing depths as we drill. They are compared with each other using an unsupervised machine learning algorithm. The results of these comparisons are then interpreted to evaluate formation properties ahead and around the drill bit. The method consists of Bottom Hole Assembly (BHA) instrumentation to conduct acoustic surveying, a signal processing algorithm, and a workflow to interpret and utilize the processed acoustic surveying data. Together these three parts (instrumentation, signal processing and interpretation) form the basis of the developed Method of Acoustic Comparisons (MAC) (see Figure 6.21) presented in this chapter.

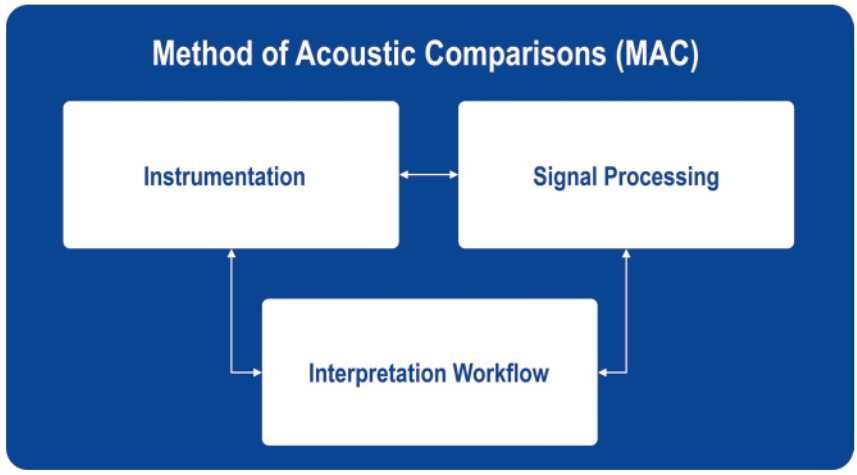

Figure 6.21: Method of Acoustic Comparisons (MAC)

The developed MAC method was tested with more than 80 numerical models for simulating acoustic surveying in karstified carbonates formation. These models represent various karstified carbonates with properties similar to the formation properties in the Loppa High region. The tests validated the applicability of the proposed method to the problem of karst detection ahead of the bit. They also studied its sensitivity with respect to the distance to and the size of karsts to be detected. Finally, through simulations of the drilling/surveying process in a 50 m section with 4 different formations, the tests demonstrated applicability of the method for detecting not only karsts, but also formation changes.

The instrumentation consists of a pulse generator and acoustic sensors. The pulse generator has to be installed at the drill bit. This is a minor modification of the BHA. For acoustic sensors, one can utilize standard Logging While Drilling (LWD) acoustic tools, like SonicScope™ (Schlumberger) or XBAT™ Azimuthal sonic (Halliburton).

The K-means clustering is presented in this chapter is a suitable approach to quantifying similarities between acoustic survey signals. There are, however, other methods that can be used as an alternative to K-means. Studying applicability of these methods, listed below, is considered as future work.

- Autoencoders [186–188] consist of an encoder and decoder. Similarly to the discussed K-Means approach, requires pre-processing of the acoustic signals (segmenting, windowing, and scaling) to form an input array. The encoder is a neural network that is trained to compress the input signal or convert the input array into a reduced dimensionality array. The decoder, another neural network, that is trained to decompress the low-dimensional output of the encoder into the same dimensionality as the input array. The neural networks of the encoder and decoder are trained jointly to minimize the reconstruction error between the input signal and the reconstructed output of the decoder. These trained neural networks capture key features of the acoustic signals used for training. When later on the same encoder-decoder pair is applied to another acoustic survey taken at another location, the resulting reconstruction error can indicate how similar (or different) that new signal is from the ones used in the training of the autoencoder. Then the reconstruction error can be used in the same way as in the K-means approach.
- Density-based algorithms for discovering clusters in large spatial databases with noise such as Self-Organizing Maps (SOM) [189], Expectation Maximization(EM) [190] and DBSCAN [191].
- Algorithms for categorical attributes clustering such as ROCK [192]
- A shared nearest neighbour approaches such as Wave Clustering [193, 194], Find-CBLOF or Cluster-based Local Outlier Factor (CBLOF) [195]
- Algorithms for clustering based on a "similarity measure" such as Euclidean distance or more complex distance measures [196], distance to k-th Nearest Neighbour techniques [197, 198], peer group analysis [199], hyper-graph based techniques such as HOT [200], partition based techniques such as taking a k-th nearest neighbour for instances in each partition [201] and density based methods such as methods that use a local outlier factor for other outlier detection [202].

Future work can also focus on employing multiple acoustic signals in establishing the library of centroids in the K-means method. For example, one can use multiple surveys corresponding to different angular positions of the drilling bit. The method of angular acoustic surveying can be tested and incorporated not only with the discussed in this chapter K-Means clustering method but also with other machine learning techniques listed above.

In the future work one could also study whether it is possible to dynamically change the number of clusters during drilling. It is assumed that for different types of rocks, a different number of clusters is needed to reconstruct the signal. This can contribute to the improvement of the robustness of karsts or other features detection ahead of the drill bit.

The scope of this chapter was limited to presenting the method of acoustic comparisons and validating it through simulations. Further work may include selecting optimal parameters for the method, testing other machine learning techniques for anomalies detection, validation in a lab scale setup and, after further development, in field tests.

Chapter 7

Concluding remarks

7.1 Conclusions and Discussion

This thesis has systematically addressed the research questions formulated in Chapter 1 with the overall goal to find better strategies, methods and technologies for safer drilling in karstified carbonates. This is a multidisciplinary problem. To tackle it different approaches were investigated including geophysical methods, drilling mechanics data, acoustics and signal processing and machine learning. The results obtained in this thesis enabled the following concluding remarks to be made:

Q1 - Conclusions: Based on the analysis of the drilling data (mud logs, drilling reports, site survey reports), drilling mechanics data (surface and downhole measurements), geology (lithology, stratigraphy, biostratigraphy), rock and core (conventional core analysis and core photos), petrophysical reports (Computer Processed Interpretation (CPI), Composite), well logs (wireline, LWD), it is demonstrated that karstification objects tend to appear in groups. These groups of karsts occur in zones with geological conditions favorable for karstification. Such zones can include both dangerous and not dangerous for drilling karstification objects. Encountering either of them can serve as an indicator of drilling through a karstification zone. The overall result of this analysis indicate that encountering dangerous for drilling karsts is not always unpredictable during drilling and that zones with high risk of karsts can be detected.

Q2 - Conclusions: Based on the overview of methods and technologies over the last 40 years, it is concluded that small, dangerous for drilling karsts are the most challenging objects to detect with pre-drill and real-time karst detection methods. Any relevant resistivity, acoustics or seismic-based methods can hardly be used for avoiding drilling into karsts or even for real-time detection of encountering karsts. Moreover, at the moment there is no technology or geophysical method that can consecutively investigate the region in front of the bit and therefore be used for prediction of dangerous for drilling smaller karsts. The identified limitations of existing technologies and methods indicate a gap for further research and development to find methods for safer drilling in karstified

carbonates.

Q3 - Conclusions: Based on the analysis of intervals of karstification it is concluded that there are sequences of drilling events, which preceded hitting dangerous for drilling karst forms. Karsts can be predicted during drilling and zones with high risk of karsts can be detected from real-time drilling measurements. It is confirmed that combination of drilling dynamics and flow-based sets of measurements can be implemented for karst detection while drilling. The identified patterns of real-time measurements in the karst intervals can be utilized for karst detection.

Q4 - Conclusions: An automated algorithm for karst patterns recognition in real-time drilling measurements was implemented to simplify the analysis of drilling data for engineers. The proposed ADF algorithm demonstrates good results for automated event detection and can efficiently locate change points in measurements corresponding to dangerous for drilling karst patterns with high precision. The main value of the discussed approach is that it simplifies the process of the detection of suspicious changes in drilling data. It was shown that the ADF outputs such as WR and calculated signal derivatives can simply indicate that there are changes in drilling data that might be linked either with regular drilling instances or with drilling through karsts. Validation of event detection hypothesis on the field data showed the potential of the ADF algorithm for real-time karst patterns detection from the drilling dynamics and flow-based sets of measurements.

Q5 - Conclusions: A novel acoustic surveying concept for early karsts detection has been introduced. Karsts, undetectable with the state-of-the-art geophysical, seismic or resistivity methods can be detected with the developed concept. The results of more than 80 simulated scenarios indicate that even smaller karsts sized 0.5 m are possible to detect ahead of the drill bit. The utilized signal comparison technique which was used instead of conventional acoustic processing is a promising and a computationally effective technique, that can potentially be used for acoustic surveys comparison in a real drilling environment. It is demonstrated that the developed acoustic surveying concept is not limited to the area of karst detection ahead of the drill bit, but can also be used for advance detection of formation changes. This significantly expands the area of possible applications of the concept.

7.2 Future work

The following further work is proposed:

1 : The method of karst patterns detection based on real-time drilling measurements described in Chapter 4 is limited in terms of the number of wells available for the analysis. Even in closely-studied fields, the percentage of wells, which encountered karsts and at the same time contained a full set of necessary well-log data is rather small.

Being limited to the area of research, the study did not include other geographical regions of karstification. Future work on this subject should go towards additional analysis of well data from other fields with different geology. This will allow one to make a complete picture of unique real-time indicators of karsts, regardless of the geography of the research region.

2 : Future work on the algorithm for automated analysis of real-time drilling data, proposed in Chapter 5, can include extension to multiple inputs (compared to the scalar time series application presented in Chapter 4). This will increase reliability and confidence in the detection of karst patterns and other drilling events. This extension will contribute to a higher degree of automation of event detection to a higher degree and help with subsequent consistent classification of complex real-time drilling data.

3 : It is believed that the method of acoustic comparisons proposed in Chapter 6 has potential for further research and development in the following directions.

First, one can further investigate the application of various methods of signal filtering and preprocessing applied to the measured acoustic signals. They can be used for initial filtering and *cleaning* the measured data of acoustic surveys before they are compared using the method of acoustic comparisons presented in Section 6.3. It is expected that signal filtering (although it is implicitly included in the method itself) can improve the accuracy of signal comparison by the unsupervised machine learning approach implemented in this concept.

Second, based on the generic concept of acoustic comparisons, one can test more methods of signal comparison other than the K-means method studied in this thesis. This can lead to selection of an algorithm that is better suited for this application or to confirmation that the K-means method is indeed the best method for this application.

Third, the performed simulations used an impulse source to excite acoustic waves (Section 6.4.4). Further research can be undertaken to study reflections of the waves continuously generated while drilling by the drill bit due to rock-bit interaction. With more frequent acoustic surveying, e.g. while drilling, comparison of acoustic surveys is expected to be sensitive to both small and large changes in formation properties ahead of the drill bit. Taking into account high computational efficiency of the suggested K-means method to compare acoustic surveys, a novel acoustic concept introduced in this thesis can be tested with the acoustic signal generated by the drill bit while drilling.

Fourth, to investigate the feasibility of both discrete impulse-based and continuous acoustic surveying suggested above, laboratory experiments are required. Numerical models, discussed in this thesis can be used to develop instrumentation and plan experiments.

Bibliography

[1] R. Joshi and K. H. Singh, 'Carbonate Reservoirs: Recent Large to Giant Carbonate Discoveries Around the World and How They Are Shaping the Carbonate Reservoir Landscape,' in Springer Singapore, Jan. 2020, pp. 3–14. DOI: 10.1007/978-981-13-1211-3_1.

[2] L. Gawor and I. Jonczy, 'Surface Karst Landforms of the Notranjska region (southwestern Slovenia),' *Geotourism/Geoturystyka*, vol. 37, pp. 55–60, Feb. 2014. DOI: 10.7494/geotour.2014.37.55.

[3] *Well Control in Carbonate Zone – Total Loss and Kick in Gas Reservoir*, vol. Day 2 Tue, May 03, 2016, OTC Offshore Technology Conference, May 2016. DOI: 10.4043/26930-MS.

[4] *Mud Cap Drilling (MCD) with Continuous Annular Injection - Offshore Malaysia*, vol. All Days, IADC/SPE Asia Pacific Drilling Technology Conference and Exhibition, Aug. 2014. DOI: 10.2118/170544-MS.

[5] *Implementation of PMCD to Explore Carbonate Reservoirs from SemiSubmersible Rigs in Malaysia results in Safe and Economical Drilling Operations*, vol. All Days, SPE/IADC Drilling Conference and Exhibition, Mar. 2013, pp. 1–15. DOI: 10.2118/163479-MS.

[6] *Managing Drilling Losses in the Permian Using Airborne Gravity Full Tensor Gradiometry*, vol. Day 1 Tue, March 05, 2019, SPE/IADC Drilling Conference and Exhibition, Mar. 2019. DOI: 10.2118/194164-MS.

[7] *Experience Using Managed Pressure Cementing Techniques with Riserless Mud Recovery and Controlled Mud Level in the Barents Sea*, vol. Day 1 Wed, April 18, 2018, SPE Norway Subsurface Conference, Apr. 2018, pp. 1–18. DOI: 10.2118/191344-MS.

[8] *Geomechanical Evaluation of Mud Losses and Wellbore Instability in Mumbai High North Field – Implications to Infill Drilling and Reservoir Development*, vol. All Days, SPE Oil and Gas India Conference and Exhibition, Mar. 2012. DOI: 10.2118/155193-MS.

[9] R. R. Giniatullin, V. V. Kireev, D. D. Krepostnov, K. A. Chernokalov, F. A. Zagrivniy, P. Y. Dobrokhleb, D. N. Voitenko and A. M. Polyarush, 'Effective solution for wells drilling in conditions of catastrophic mud losses in fractured reservoirs of the

Yurubcheno-Tokhomskoye field (Russian),' *Neftyanoe khozyaystvo - Oil Industry*, vol. 2017, no. 11, pp. 40–43, Nov. 2017, ISSN: 0028-2448. DOI: 10.24887/0028-2448-2017-11-40-43.

[10] W. Murchison and M. D. Schools, *Lost Circulation for the Man on the Rig*. Murchison Drilling Schools, 2006, ISBN: 9780991637102.

[11] *How can we best manage lost circulation*. Vol. All Days, AADE National Technology Conference "Practical Solutions for Drilling Challenges", Mar. 2003.

[12] *High Resolution 3D Seismic for Mapping Of Subsurface Karsting of Carbonate*, vol. All Days, World Petroleum Congress (WPC), Sep. 2002, pp. 90–99.

[13] *Seismic Reflection Characteristics of Deeply-Buried, Layered, Karstic Carbonate Reservoir Strata*, vol. All Days, SEG International Exposition and Annual Meeting, Sep. 2013, pp. 1–6. DOI: 10.1190/segam2013-0065.1.

[14] R. Sheriff, 'Factors affecting seismic amplitude,' *Geophysical Prospecting*, vol. 23, pp. 125–138, Apr. 1975. DOI: 10.1111/j.1365-2478.1975.tb00685.x.

[15] N. Wang, X.-B. Xie, M.-C. Duan, D. Li and R.-S. Wu, 'Improving seismic image resolution in a carbonate fracture cave region: A case study,' in *SEG Technical Program Expanded Abstracts 2019*. 2019, ch. 1, pp. 32–36. DOI: 10.1190/segam2019-3215909.1.

[16] W. Maia, R. Rubio, F. Junior, J. Haldorsen, R. Guerra and C. Dominguez, 'First Borehole Acoustic Reflection Survey mapping a deepwater turbidite sand,' *Seg Technical Program Expanded Abstracts*, vol. 25, pp. 87–92, Jan. 2006. DOI: 10.1190/1.2369864.

[17] J.-H. Kim, J. Schon, G. Towle and W. W. Whitman, 'An Automatic Inversion Of Normal Resistivity Logs,' *The Log Analyst*, vol. 31, no. 01, pp. 1–10, Jan. 1990, ISSN: 0024-581X.

[18] *Dielectric-Independent 2-MHz Propagation Resistivities*, vol. All Days, SPE Annual Technical Conference and Exhibition, Oct. 1999. DOI: 10.2118/56448-MS.

[19] *Reduce Drilling Risk in HPHT Gas Field Using Innovative Look-Ahead Technology - A Case Study from South China Sea*, vol. Day 2 Tue, January 14, 2020, IPTC International Petroleum Technology Conference, Jan. 2020. DOI: 10.2523/IPTC-19636-ABSTRACT.

[20] *Curing Losses in Vuggy Carbonate Formations*, vol. Day 2 Tue, January 30, 2018, SPE/IADC Middle East Drilling Technology Conference and Exhibition, Jan. 2018. DOI: 10.2118/189327-MS.

[21] *Managing Lost Circulation in Highly Fractured, Vugular Formations: Engineering the LCM Design and Application*, vol. Day 1 Mon, November 11, 2019, Abu Dhabi International Petroleum Exhibition and Conference, Nov. 2019. DOI: 10.2118/197186-MS.

[22] K. Muir, 'MPD techniques address problems in drilling Southeast Asia's fractured carbonate structures.,' in *International Association of Drilling Contractors*, Galveston, Texas: Drilling Contractor, 2006, pp. 34–36.

[23] *MudCap Drilling: New Variations, Drivers, Limitations, and Lessons Learned – Case Histories*, vol. All Days, SPE/IADC Managed Pressure Drilling and Underbalanced Operations Conference and Exhibition, Apr. 2014, pp. 1–7. DOI: 10.2118/168956-MS.

[24] *PMCD Technique Enables Coring & Wireline Logging Operations in Total Lost Circulation*, vol. Day 3 Thu, March 03, 2016, SPE/IADC Drilling Conference and Exhibition, Mar. 2016, pp. 1–13. DOI: 10.2118/178805-MS.

[25] *Maximising Logging While Drilling Value in Carbonate Wells Drilled in Pressurised Mud Cap Drilling Conditions: Challenges, Solutions, and Advances*, vol. All Days, SPE Asia Pacific Oil and Gas Conference and Exhibition, Oct. 2015, pp. 1–12. DOI: 10.2118/176356-MS.

[26] *Successful Implementation of PMCD Technology in Kazakhstan*, vol. Day 3 Wed, October 17, 2018, SPE Russian Petroleum Technology Conference, Oct. 2018, pp. 1–10. DOI: 10.2118/191513-18RPTC-MS.

[27] *ECD Management Toolbox for Floating Drilling Units*, vol. Day 1 Mon, May 05, 2014, OTC Offshore Technology Conference, May 2014, pp. 1–23. DOI: 10.4043/25292-MS.

[28] *Underground Rock Dissolution and Geomechanical Issues*, vol. All Days, U.S. Rock Mechanics/Geomechanics Symposium, Jun. 2019, pp. 1–12.

[29] A. Waltham and P. Fookes, 'Engineering classification of karst ground conditions,' *Quarterly Journal of Engineering Geology and Hydrogeology*, vol. 36, no. 2, pp. 101–118, May 2003. DOI: 0.1144/1470-9236/2002-33.

[30] J. Nicod, 'A Little Contribution to the Karst Terminology: Special or Aberrant Cases of Poljes?' *Acta Carsologica*, vol. 32, no. 2, pp. 29–39, Jan. 2003. DOI: 10.3986/ac.v32i2.334.

[31] E. Prohic, Z. Peh and S. Miko, 'Geochemical characterization of a karst polje, an example from Sinjsko polje, Croatia,' *Environmental Geology*, vol. 33, no. 4, pp. 263–273, 1998. DOI: 10.1007/s002540050245.

[32] P. Bella, 'Genetic Types of Caves in Slovakia,' *Acta Carsologica*, vol. 27, no. 2, pp. 15–23, Jul. 1998. DOI: 10.3986/ac.v27i2.499.

[33] A. Palmer, 'Origin and morphology of limestone caves,' *Geol. Soc. Am. Bull.*, vol. 103, pp. 1–21, Jan. 1991. DOI: 10.1130/0016-7606(1991).

[34] D. Ford and P. W. Williams, 'Hydrogeology and Geomorphology 6th Edition,' in Chichester: John Wiley & Sons, 2009, ch. 7.

[35] V. Andreychouk, Y. Dublyansky, E. Y. and L. G., 'Karst in the earth's crust: Its distribution and principal types,' in Jan. 2009, pp. 53–62, ISBN: 978-83-87431-93-8.

[36] P. E. Dhelie, V. Danielsen, J. E. Lie, A. K. Evensen, A. Wright, N. Salaun, J.-L. Rivault, R. Siliqi, C. Grubb, V. Vinje and A. Camerer, 'Improving seismic imaging in the Barents Sea by source-over-cable acquisition,' in *SEG Technical Program Expanded Abstracts 2018*. 2018, ch. 2, pp. 71–75. DOI: 10.1190/segam2018-2998198.1.

[37] *Techlog Wellbore Software Platform - Integration of all wellbore-centric data types into multidiscipline workflows*, https://www.software.slb.com/products/techlog, Accessed: 2021-09-27.

[38] *Petrel E&P Software Platform*, https://www.software.slb.com/products/petrel, Accessed: 2021-09-27.

[39] A. Bahar and M. Kelkar, 'Journey From Well Logs/Cores to Integrated Geological and Petrophysical Properties Simulation: A Methodology and Application,' *SPE Reservoir Evaluation & Engineering*, vol. 3, pp. 444–456, Oct. 2000. DOI: 10.2118/66284-PA.

[40] *Techniques and Experiences Using Exploration 3D Seismic Data to Map Drilling Hazards*, vol. All Days, OTC Offshore Technology Conference, May 1996. DOI: 10.4043/7968-MS.

[41] *Evaluation of LCMs in Cement to Seal Wide Natural Fractures*, vol. Day 2 Wed, October 18, 2017, SPE Asia Pacific Oil and Gas Conference and Exhibition, Oct. 2017, pp. 1–8. DOI: 10.2118/187026-MS.

[42] *Managing Lost Circulation in Highly Fractured, Vugular Formations: Engineered Usage of High Fluid Loss Squeeze and Reticulated Foam Lost Circulation Materials*, vol. Day 3 Thu, March 05, 2020, SPE/IADC Drilling Conference and Exhibition, Mar. 2020, pp. 1–11. DOI: 10.2118/199635-MS.

[43] *Successful PMCD Application Significantly Improved Drilling Efficiency on Carbonate Drilling*, vol. Day 1 Mon, August 22, 2016, IADC/SPE Asia Pacific Drilling Technology Conference and Exhibition, Aug. 2016. DOI: 10.2118/180658-MS.

[44] A. Swan, 'Geostatistical Software Library and User's Guide, 2nd ed.,' *Geological Magazine*, vol. 136, no. 1, pp. 83–108, 1999. DOI: 10.1017/S0016756899531774.

[45] *Analysis of Factors Affecting Carbonate Fracture-Cave Imaging*, vol. All Days, SEG International Exposition and Annual Meeting, Sep. 2013. DOI: 10.1190/segam2013-0318.1.

[46] X. Feng, Y. Wang, X. Wang, N. Wang, G. Gao and X. Zhu, 'The application of high-resolution 3D seismic acquisition techniques for carbonate reservoir characterization in China,' *The Leading Edge*, vol. 31, no. 2, pp. 168–179, 2012. DOI: 10.1190/1.3686914.

[47] P. Lin, S. Peng, J. Zhao and X. Cui, 'Diffraction separation and imaging using multichannel singular-spectrum analysis,' *GEOPHYSICS*, vol. 85, no. 1, pp. 1–88, Oct. 2020. DOI: 10.1190/geo2019-0201.1.

[48] B. Piwakowski, J. Watelet, D. Moreaux and K. Sbai, 'High resolution seismic prospection of old gypsum mines - evaluation of detection possibilities,' ser. Meeting Environmental & Engineering Geophysic, Sep. 1996, pp. 149–152.

[49] M. V. Constable, F. Antonsen, S. O. Stalheim, P. A. Olsen, O. Z. Fjell, N. Dray, S. Eikenes, H. Aarflot, K. Haldorsen, G. Digranes, J. Seydoux, D. Omeragic, M. Thiel, A. Davydychev, J.-M. Denichou, D. Salim, M. Frey, D. Homan and S. Tan, 'Looking Ahead of the Bit While Drilling: From Vision to Reality,' *Petrophysics - The SPWLA Journal of Formation Evaluation and Reservoir Description*, vol. 57, no. 05, pp. 426–446, Oct. 2016.

[50] *Shear Slowness Determination From Dipole Measurements*, vol. All Days, SPWLA Annual Logging Symposium, Jun. 1997, pp. 1–14. DOI: 0.30632/SPWLA-2021-0001.

[51] D. W. Hilchie, *Wireline : a history of the well logging and perforating business in the oil fields*. Boulder, Colorado: D.W. Hilchie, 1990, p. 200.

[52] *Is There Any Uniqueness And/or Resolution In Resistivity Inversion?* Vol. All Days, SEG International Exposition and Annual Meeting, Oct. 1989.

[53] T. Asch, J. Abraham and T. Irons, 'A discussion on depth of investigation in geophysics and aem inversion results,' Aug. 2015, pp. 2072–2076. DOI: 10.1190/segam2015-5915199.1.

[54] Brian C, Stephen DB, Jacques J, Martin L, inventors; Schlumberger Technology Corp, assignee. Well logging apparatus having toroidal induction antenna for measuring, while drilling, resistivity of earth formations. US Patent 5,235,285A. 1993 August 10.

[55] *Near-Bit Propagation Resistivity for Reservoir Navigation*, vol. All Days, SPE Annual Technical Conference and Exhibition, Sep. 1994, pp. 1–13. DOI: 10.2118/28318-MS.

[56] *An analysis of the at-bit resistivity decision making process*, vol. All Days, IPTC International Petroleum Technology Conference, Dec. 2008, pp. 1–8. DOI: 10.2523/IPTC-12513-MS.

[57] *Formation Evaluation and Geological Interpretation from the Resistivity-at-the-Bit Tool*, vol. All Days, SPE Annual Technical Conference and Exhibition, Oct. 1995, pp. 1–13. DOI: 10.2118/30550-MS.

[58] M. Biot, 'Theory of Propagation of Elastic Waves in a Fluid Saturated Porous Solid. II. Higher Frequency Range,' *Journal of the Acoustical Society of America*, vol. 28, pp. 179–191, 1956. DOI: 10.1121/1.1908241.

[59] *Measurement Of Formation Permeability Using Stoneley Waves From An Lwd Acoustic Tool*, vol. All Days, SPWLA Annual Logging Symposium, Jun. 2009.

[60] C. Sayers, Z. Nagy, J. Adachi, V. Singh, K. Tagbor and P. Hooyman, 'Determination of in-situ stress and rock strength using borehole acoustic data,' *SEG Technical Program Expanded Abstracts*, vol. 28, pp. 3505–3509, Jan. 2009. DOI: 10.1190/1.3255591.

[61] *A New Sonic Array Tool for Full Waveform Logging*, vol. All Days, SPE Annual Technical Conference and Exhibition, Sep. 1984, pp. 1–7. DOI: 10.2118/13285-MS.

[62] *Case Studies of Borehole Acoustic Reflection Survey (BARS)*, vol. All Days, SPWLA Formation Evaluation Symposium of Japan, Sep. 2016.

[63] Brett JF, Goetz JF, Roberts AP, inventors; OIL and GAS CONSULTANTS INTĹ Inc Seismic Recovery LLC, assignee. Methods of employing vibrational energy in a borehole. US Patent 5,309,405A. 1994 May 03.

[64] Bjorn N, Paulsson P, inventors; Chevron Research and Technology Co, assignee. Nondestructive downhole seismic vibrator source and processes of utilizing the vibrator to obtain information about geologic formations. US Patent 4,702,343A. 1986 March 18.

[65] Dedole P, Grolet P, Laurent J, inventors; IFP Energies Nouvelles IFPEN, assignee. Device for generating sound pulses inside a well, by percussion. US Patent 4,648,478A. 1984 Januar 23.

[66] H. C. Hardee, 'Downhole pereodic seismic sources,' *Geophysical Prospecting*, vol. 31, no. 1, pp. 57–71, Feb. 1983, ISSN: 0016-8025. DOI: 10.1111/j.1365-2478.1983.tb01041.x.

[67] Hardee HC, Hills RG, Striker RP, inventors; US Department of Energy, assignee. Down hole periodic seismic generator. US Patent 4,805,727A. 1982 October 28.

[68] Hardee HC, inventor; US Department of Energy, assignee. Fluid driven torsional dipole seismic source. US Patent 4,982,811A. 1989 August 08.

[69] *Three-component Downhole Seismic Vibrator*, vol. All Days, SEG International Exposition and Annual Meeting, Oct. 1988, pp. 1–4.

[70] *Experimental Studio of Downhole Seismic Sources*, vol. All Days, SEG International Exposition and Annual Meeting, Oct. 1989.

[71] D. L. Howlett, 'Comparison of borehole seismic sources under consistent field conditions,' in *SEG Technical Program Expanded Abstracts 1991*. 2005, ch. 2, pp. 18–21. DOI: 10.1190/1.1888977.

[72] Farr JB, Ward RW, inventors; BP America Production Co, assignee. Seismic velocity determination. US Patent 3,881,168A. 1973 December 11.

[73] Klaveness A, inventor; Alf Klaveness, assignee. Seismic well logging system and method. US Patent 4,207,619A. 1975 February 24.

[74] Beresford JM, Crowther PA, inventors; Thales Underwater Systems Ltd, assignee. Acoustic sensor. US Patent 5,798,488A. 1994 March 30.

[75] Leggett JV, inventor; Baker Hughes Inc, assignee. Measurement-while-drilling acoustic system employing multiple, segmented transmitters and receivers. US Patent 6,084,826A. 1995 January 12.

[76] Mathiszik H, Oppelt J, inventors; Baker Hughes Inc, assignee. Apparatus and method for acoustic position logging ahead-of-the-bit. US Patent 2005/003,491,7A1. 2003 August 14.

[77] Wajid R, inventor; Wajid Rasheed, assignee. Look ahead advance formation evaluation tool. International Publication Patent Number WO2011/080,640,A3. 2011 July 07.

[78] R. Meehan, D. Miller, J. Haldorsen, M. Kamata and B. Underhill, 'Rekindling interest in seismic while drilling,' *Oilfield Review*, vol. 5, pp. 3–13, Jan. 1993.

[79] Staron P, Gros P, Arens G, inventors; Societe National Elf Aquitaine, assignee. Instantaneous acoustic logging in a borehole. Canada Patent 1,255,783A. 1984 May 25.

[80] Ollivier Yves RM, inventor; CGG SA, assignee. Apparatus for the acquisition of a seismic signal transmitted by a rotating drill bit. US Patent 5,248,857A. 1990 April 27.

[81] Airhart TP, Montgomery MG, Kingman John EE, Livesay RB, inventors; Atlantic Richfield Company, assignee. System for real-time look-ahead exploration of hydrocarbon wells. WIPO (PCT) Patent WO1993/007,514,A1. 1992 October 02.

[82] J. Haldorsen, D. Miller and J. Walsh, 'Multichannel approach to signature estimation and deconvolution for drill bit imaging,' in *SEG Technical Program Expanded Abstracts 1992*. 2005, ch. 1, pp. 181–184. DOI: 10.1190/1.1822033.

[83] I. James W. Rector and B. A. Hardage, 'Radiation pattern and seismic waves generated by a working roller-cone drill bit,' *GEOPHYSICS*, vol. 57, no. 10, pp. 1319–1333, 1992. DOI: 10.1190/1.1443199.

[84] J. W. Rector and B. P. Marion, 'The use of drillbit energy as a downhole seismic source,' *GEOPHYSICS*, vol. 56, no. 5, pp. 628–634, May 1991, ISSN: 0016-8033. DOI: 10.1190/1.1443079.

[85] C. Naville, P. Layotte, G. Pignard and J. Guesnon, 'Well seismic - Application of the TRAFOR MWD system to drill-bit seismic profiling,' *EAEG*, Jun. 1994. DOI: 10.3997/2214-4609.201409887.

[86] L. Petronio, F. Miranda, F. Poletto and R. Miandro, 'Seisbit Seismic-while-Drilling Technique Summary of Results Obtained in Onshore Surveys,' *EAGE*, vol. -, pp. 18–26, Oct. 2003, ISSN: 2214-4609. DOI: 10.3997/2214-4609-pdb.8.T023.

[87] A. Azbek, 'Adaptive beamforming with generalized linear constraints,' in *SEG Technical Program Expanded Abstracts 2000*. 2005, ch. 5, pp. 2081–2084. DOI: 10.1190/1.1815855.

[88] L. Chabot, D. C. Henley, R. J. Brown and J. C. Bancroft, 'Single-well seismic imaging using full waveform sonic data: An update,' in *SEG Technical Program Expanded Abstracts 2002*. 2005, ch. 7, pp. 368–371. DOI: 10.1190/1.1817255.

[89] P. Comelli, A. Craglietto, G. Dordolo, A. Schleifer, G. Vascotto and F. Zgauc, 'SEISBIT 3D: The new seismic while drilling data acquisition system,' *bgta*, vol. 43, pp. 109–118, Mar. 2002. DOI: 10.1190/geo2019-0449.1.

[90] *Drill Bit As a Seismic Source For Near-well Imaging*, vol. All Days, SEG International Exposition and Annual Meeting, Nov. 2008. DOI: 10.1190/1.3054815.

[91] E. Raknes, T. Moser, B. Arntsen, S. E. Johansen and S. Sangesland, 'Surface Seismic While Drilling - Imaging of Well Bores in Seismic Context,' vol. 2017, pp. 1–5, Jun. 2017. DOI: 10.3997/2214-4609.201701456.

[92] Robbins CA, Linyaev EJ, Malloy RL, Young DJ, Birchak JR, Minear J, Shah V, inventors; Halliburton Energy Services Inc, assignee. Vertical seismic profiling in a drilling tool. Canada Patent 2,342,765A1. 1999 September 02.

[93] *Seismic Measurement While Drilling: Conventional Borehole Seismics On Lwd*, vol. All Days, SPWLA Annual Logging Symposium, Jun. 2001, pp. 1–10.

[94] *Seismic While Drilling and Geophysical Monitoring in the Southern Apennine Range*, European Association of Geoscientists and Engineers, 1998. DOI: 10.3997/2214-4609.201408297.

[95] *Demonstrations of Real-Time Borehole Seismic From an LWD Tool*, vol. All Days, SPE Annual Technical Conference and Exhibition, Sep. 2001. DOI: 10.2118/71365-MS.

[96] J. Haldorsen, M. Krasovec, S. Raikes, T. Harrold, D. Day and J. Clippard, 'Comparison of full waveform seismicmwd and conventional vsp data from the south caspian sea,' Jan. 2002. DOI: 10.3997/2214-4609-pdb.5.B026.

[97] S. B. O. Adrian, M. Alfonso, A. Leonardo and G. Rito, 'Minimizing drilling risks for exploration well in deep water using seismic while drilling technology,' in *Rio Oil and Gas Expo and Conference*, vol. 8, Rio de Janeiro, Brazil, Sep. 2010, pp. 115–125.

[98] *Seismic Guided Drilling: Near Real Time 3D Updating of Subsurface Images and Pore Pressure Model*, vol. All Days, IPTC International Petroleum Technology Conference, Mar. 2013, pp. 1–6. DOI: 10.2523/IPTC-16575-MS.

[99] *Cave Geomorphology and its Effects on Oil Recovery Factors in Tarim Karst Reservoirs, West China*, vol. All Days, IPTC International Petroleum Technology Conference, Dec. 2014. DOI: 10.2523/IPTC-17722-MS.

[100] *Seismic Description of Karst Topography And Caves of Ordovician Carbonate Reservoirs, Lungu Area, Tarim Basin, West China*, vol. All Days, SEG International Exposition and Annual Meeting, Oct. 2010.

[101] *Cave System Analysis - An Effective Approach to Predict Hydrocarbons in Cavernous Carbonate Reservoir*, vol. All Days, IPTC International Petroleum Technology Conference, Mar. 2013. DOI: 10.2523/IPTC-16783-MS.

[102] *Surface Measurement and Analysis of Drillstring Vibrations While Drilling*, vol. All Days, SPE/IADC Drilling Conference and Exhibition, Feb. 1993. DOI: 10.2118/25777-MS.

[103] *Use of Surface Measurement of Drillstring Vibrations to Improve Drilling Performance*, vol. All Days, World Petroleum Congress (WPC), May 1994.

[104] R. Wylie, I. Soukup, H. Mata, S. Cuff and A. Ho, 'The Drilling Optimization Benefits of Direct Drillstring Surface Measurements – Case Studies from Field Operations,' in *SPE/IADC Drilling Conference and Exhibition*, London, England, UK: Society of Petroleum Engineers, 2015, pp. 1–28. DOI: 10.2118/173112-MS.

[105] *Applications Of Measurements While Drilling*, vol. All Days, SPE Annual Technical Conference and Exhibition, Oct. 1981, pp. 1–16. DOI: 10.2118/10324-MS.

[106] D. S. Grosso, J. C. Raynal and D. Rader, 'Report on MWD Experimental Downhole Sensors,' *Journal of Petroleum Technology*, vol. 35, no. 05, pp. 899–904, May 1983. DOI: 10.2118/10058-PA.

[107] *Applications of Measurements While Drilling (MWD): Development of the East Breaks Field, Offshore Texas*, vol. All Days, SPE/IADC Drilling Conference and Exhibition, Mar. 1985, pp. 1–9. DOI: 10.2118/13487-MS.

[108] *Shock Sub Performance Tests*, vol. All Days, SPE/IADC Drilling Conference and Exhibition, Mar. 1998, pp. 1–13. DOI: 10.2118/39323-MS.

[109] R. Teale, 'The concept of specific energy in rock drilling,' *International Journal of Rock Mechanics and Mining Sciences & Geomechanics Abstracts*, vol. 2, no. 1, pp. 57–73, 1965. DOI: 10.1016/0148-9062(65)90022-7.

[110] *Relationships Between Formation Strength, Drilling Strength, and Electric Log Properties*, vol. All Days, SPE Annual Technical Conference and Exhibition, Oct. 1988, pp. 1–14. DOI: 10.2118/18166-MS.

[111] *Real Time Advanced Surface Flow Analysis for Detection of Open Fractures*, vol. All Days, SPE Europec featured at EAGE Conference and Exhibition, Jun. 2012. DOI: 10.2118/154927-MS.

[112] *Real-Time Advanced Mud Returns Flow Analysis Combined with Advanced Mud Gas and Elemental Analysis on Drill Cuttings Aids Fracture Detection and Interpretation in Unconventional Reservoirs: A Case Study*, vol. All Days, AAPG, Apr. 2018.

[113] *Planning of an MPD and Controlled Mud Cap Drilling CMCD Operation in the Barents Sea Using the CML Technology*, vol. Day 1 Tue, March 28, 2017, SPE/IADC Managed Pressure Drilling and Underbalanced Operations Conference and Exhibition, Mar. 2017. DOI: 10.2118/185286-MS.

[114] *Guaranteed Active Failure Detection and Isolation for Linear Dynamical Systems*, vol. 34, 11, 1998, pp. 1345–1358. DOI: https://doi.org/10.1016/S0005-1098(98)00079-X.

[115] *Auxiliary signal design for failure detection in differential-algebraic equations*, vol. 4, 2, 2014, pp. 151–179.

[116] *A hybrid stochastic-deterministic input design method for active fault diagnosis*, Dec. 2013, pp. 5656–5661, ISBN: 978-1-4673-5717-3. DOI: 10.1109/CDC.2013.6760780.

[117] 'Auxiliary signals for improving fault detection,' in *Auxiliary Signal Design in Fault Detection and Diagnosis*, X. J. Zhang, Ed. Berlin, Heidelberg: Springer Berlin Heidelberg, 1989, pp. 45–91, ISBN: 978-3-540-46643-7. DOI: 10.1007/BFb0009316.

[118] *Active incipient fault detection in continuous time systems with multiple simultaneous faults*, vol. 1, 2, 2011, pp. 211–224.

[119] *A Survey of Fault Detection, Isolation, and Reconfiguration Methods*, vol. 18, 2010, pp. 636–653.

[120] *Passive robust fault detection approaches using interval models*, vol. 35, 1, 15th IFAC World Congress, 2002, pp. 443–448. DOI: https://doi.org/10.3182/20020721-6-ES-1901.00407.

[121] H. Wang, H. Wang, G. Jiang, J. Li and Y. Wang, 'Early fault detection of wind turbines based on operational condition clustering and optimized deep belief network modeling,' *Energies*, vol. 12, no. 6, 2019, ISSN: 1996-1073. DOI: 10.3390/en12060984.

[122] Z. Mao, X.-G. Yan, B. Jiang and M. Chen, 'Adaptive fault-tolerant sliding-mode control for high-speed trains with actuator faults and uncertainties,' *IEEE Transactions on Intelligent Transportation Systems*, vol. 21, no. 6, pp. 2449–2460, 2020. DOI: 10.1109/TITS.2019.2918543.

[123] T. Xue, M. Zhong, L. Li and S. X. Ding, 'An optimal data-driven approach to distribution independent fault detection,' *IEEE Transactions on Industrial Informatics*, vol. 16, no. 11, pp. 6826–6836, 2020. DOI: 10.1109/TII.2020.2976043.

[124] *Qualitative Representation of Trends (QRT): Extended method for identification of consecutive inflection points*, vol. 48, Jan. 2013, pp. 187–199. DOI: 10.1016/j.compchemeng.2012.08.010.

[125] *A novel interval-halving framework for automated identification of process trends*, vol. 50, 1, 2004, pp. 149–162. DOI: https://doi.org/10.1002/aic.10014.

[126] *Challenges in the industrial applications of fault diagnostic systems*, vol. 24, 2, 2000, pp. 785–791. DOI: https://doi.org/10.1016/S0098-1354(00)00374-4.

[127] *Representation of process trends—III. Multiscale extraction of trends from process data*, vol. 18, 4, An International Journal of Computer Applications in Chemical Engineering, 1994, pp. 267–302. DOI: https://doi.org/10.1016/0098-1354(94)85028-3.

[128] *A generative approach to qualitative trend analysis for batch process fault diagnosis*, Jul. 2013, pp. 1958–1963. DOI: 10.23919/ECC.2013.6669494.

[129] *A new qualitative trend analysis algorithm based on global polynomial fit*, vol. 63, 2017, pp. 3374–3383.

[130] *Piecewise Polynomial Expression of Beach Profiles*, vol. 26, Sep. 2010, pp. 851–859. DOI: 10.2112/08-1122.1.

[131] *A study of polynomial fit-based methods for qualitative trend analysis*, vol. 37, 2016, pp. 21–33. DOI: https://doi.org/10.1016/j.jprocont.2015.11.003.

[132] *Smooth representation of trends by a wavelet-based technique*, vol. 24, Sep. 2000, pp. 1913–1943. DOI: 10.1016/S0098-1354(00)00594-9.

[133] *Identification of trends in process measurements using the wavelet transform*, vol. 22, 1998, pp. 491–496. DOI: https://doi.org/10.1016/S0098-1354(98)00092-1.

[134] *Using discrete wavelet transforms to analyze trends in streamflow and precipitation in Quebec and Ontario (1954-2008)*, vol. 475, Dec. 2012, pp. 204–228. DOI: 10.1016/j.jhydrol.2012.09.049.

[135] *A Syntactic Pattern-Recognition Approach for Process Monitoring and Fault Diagnosis*, vol. 8, 1, USA: Pergamon Press, Inc., Feb. 1995, pp. 35–51. DOI: 10.1016/0952-1976(94)00058-U.

[136] *Demand Forecasting Using Artificial Neural Network Based on Quantitative and Qualitative Data*, Sep. 2020, pp. 1–6. DOI: 10.1109/IBDAP50342.2020.9245614.

[137] *Kernel Partial Least Squares Regression in Reproducing Kernel Hilbert Space*, vol. 2, JMLR.org, Mar. 2002, pp. 97–123.

[138] *Nonparametric Estimation of Regression Functions with Both Categorical and Continuous Data*, vol. 119, Mar. 2004, pp. 99–130. DOI: 10.1016/S0304-4076(03)00157-X.

[139] L. Ralaivola and F. d'Alche-Buc, 'Time series filtering, smoothing and learning using the kernel Kalman filter,' in *Proceedings. 2005 IEEE International Joint Conference on Neural Networks*, vol. 3, 2005, pp. 1449–1454. DOI: 10.1109/IJCNN.2005.1556088.

[140] C. N. Babu and B. E. Reddy, 'A moving-average filter based hybrid ARIMA–ANN model for forecasting time series data,' *Applied Soft Computing*, vol. 23, pp. 27–38, 2014, ISSN: 1568–4946. DOI: 10.1016/j.asoc.2014.05.028.

[141] M.-W. Gui, 'The Basics of Noise Detection and Filtering for Borehole Drilling Data,' *The Open Civil Engineering Journal*, vol. 2, pp. 1–10, Sep. 2008. DOI: 10.2174/1874149500802010113.

[142] E. Voigtman and J. D. Winefordner, 'Low-pass filters for signal averaging,' *Review of Scientific Instruments*, vol. 57, pp. 957–966, 1986.

[143] X. J. Jiang and P. J. Scott, 'Chapter 9 - free-form surface filtering using wavelets and multiscale decomposition,' in *Advanced Metrology*, X. J. Jiang and P. J. Scott, Eds., Academic Press, 2020, pp. 195–246, ISBN: 978-0-12-821815-0. DOI: 10.1016/B978-0-12-821815-0.00009-5.

[144] A. Al-Odienat and A. Al-Mbaideen, 'Optimal length determination of the moving average filter for power system applications,' *International Journal of Innovative Computing, Information and Control*, vol. 11, pp. 691–705, Jan. 2015.

[145] D. Acharya, A. Rani, S. Agarwal and V. Singh, 'Application of adaptive savitzky-golay filter for eeg signal processing,' *Perspectives in Science*, vol. 8, Jul. 2016. DOI: 10.1016/j.pisc.2016.06.056.

[146] H. Zhang, Y. Yuan and W. Piao, 'The spline filter: A regularization approach for the gaussian filter,' *Precision Engineering*, vol. 36, no. 4, pp. 586–592, 2012, ISSN: 0141-6359. DOI: 10.1016/j.precisioneng.2012.04.008.

[147] W. R. Fawcett and J. E. Kent, 'Methods of numerical differentiation in the analysis of thermodynamic data for the mercury–solution interface,' *Canadian Journal of Chemistry*, vol. 48, no. 1, pp. 47–53, 1970. DOI: 10.1139/v70-007.

[148] F. Hickernell and S. Yang, 'Simplified analytical expressions for numerical differentiation via cycle index,' *Journal of Computational and Applied Mathematics - J COMPUT APPL MATH*, vol. 224, pp. 433–443, Feb. 2009. DOI: 10.1016/j.cam.2008.05.024.

[149] P. Holoborodko, 'Smooth noise robust differentiators,' Sep. 2008.

[150] 'A new method for numerical differentiation based on direct and inverse problems of partial differential equations,' *Applied Mathematics Letters*, vol. 43, pp. 61–67, 2015, ISSN: 0893-9659. DOI: 10.1016/j.aml.2014.11.016.

[151] F. Sharifi, V. Hayward and C.-S. Chen, 'Discrete-Time Adaptive Windowing for Velocity Estimation,' *Control Systems Technology, IEEE Transactions on*, vol. 8, pp. 1003–1009, Dec. 2000. DOI: 10.1109/87.880606.

[152] *Matlab*, https://www.mathworks.com/products/matlab.html, Accessed: 2021-10-07.

[153] M. Basseville and I. Nikiforov, *Detection of Abrupt Change Theory and Application*. Apr. 1993, vol. 15, pp. 67–120, ISBN: 0-13-126780-9.

[154] *Changes of Variance in First-Order Autoregressive Time Series Models-With an Application*, vol. 25, 3, [Wiley, Royal Statistical Society], 1976, pp. 248–256.

[155] *A Fully Automated Periodicity Detection in Time Series*, Jan. 2020, pp. 43–54, ISBN: 978-3-030-39097-6. DOI: 10.1007/978-3-030-39098-3_4.

[156] *Unsupervised non-parametric change point detection in quasi-periodic signals*, Feb. 2020, pp. 1–9.

[157] S. Lloyd, 'Least squares quantization in pcm,' *IEEE Transactions on Information Theory*, vol. 28, no. 2, pp. 129–137, 1982. DOI: 10.1109/TIT.1982.1056489.

[158] T. Dunning and E. Friedman, *Practical Machine Learning: A New Look at Anomaly Detection*. O'Reilly Media, 2014, ISBN: 9781491914182.

[159] *SonicScope*, https://www.slb.com/drilling/surface-and-downhole-logging/logging-while-drilling-services/sonicscope-multipole-sonic-while-drilling-service, Accessed: 2021-08-31.

[160] *Ecg*, https://github.com/tdunning/anomaly-detection, Accessed: 2021-10-07.

[161] *Keras*, https://keras.io, Accessed: 2021-09-30.

[162] *TensorFlow: Large-Scale Machine Learning on Heterogeneous Systems*, https://www.tensorflow.org/, Accessed: 2021-09-30.

[163] *Anaconda documentation vers. 2-2.4.0*, https://docs.anaconda.com/, Accessed: 2021-09-30.

[164] *Cuda, release: 10.2.89*, https://developer.nvidia.com/cuda-toolkit, Accessed: 2021-09-30.

[165] S. Chetlur, C. Woolley, P. Vandermersch, J. Cohen, J. Tran, B. Catanzaro and E. Shelhamer, *Cudnn: Efficient primitives for deep learning*, 2014. arXiv: 1410.0759 [cs.NE].

[166] C. R. Harris, K. J. Millman, S. J. van der Walt, R. Gommers, P. Virtanen, D. Cournapeau, E. Wieser, J. Taylor, S. Berg, N. J. Smith, R. Kern, M. Picus, S. Hoyer, M. H. van Kerkwijk, M. Brett, A. Haldane, J. F. del Río, M. Wiebe, P. Peterson, P. Gérard-Marchant, K. Sheppard, T. Reddy, W. Weckesser, H. Abbasi, C. Gohlke and T. E. Oliphant, 'Array programming with NumPy,' *Nature*, vol. 585, no. 7825, pp. 357–362, 2020. DOI: 10.1038/s41586-020-2649-2.

[167] T. Kluyver, B. Ragan-Kelley, F. Pérez, B. Granger, M. Bussonnier, J. Frederic, K. Kelley, J. Hamrick, J. Grout, S. Corlay, P. Ivanov, D. Avila, S. Abdalla and C. Willing, 'Jupyter notebooks – a publishing format for reproducible computational workflows,' in *Positioning and Power in Academic Publishing: Players, Agents and Agendas*, F. Loizides and B. Schmidt, Eds., IOS Press, 2016, pp. 87–90.

[168] D. Feibiao, J. Yanqiao, Y. Yingchun, Y. Qin, X. Limei and X. Xiaomei, 'Direction-of-arrival tracking using a co-prime microphone array: A particle filter perspective,' *Applied Acoustics*, vol. 170, 2020, ISSN: 0003-682X. DOI: 10.1016/j.apacoust.2020.107499.

[169] J. Vergeynst, T. Vanwyck, R. Baeyens, T. De Mulder, I. Nopens, A. Mouton and I. Pauwels, 'Acoustic positioning in a reflective environment: going beyond point-by-point algorithms,' *Animal Biotelemetry*, vol. 8, 2020. DOI: 10.1186/s40317-020-00203-1.

[170] X. Zhong and A. Premkumar, 'Particle Filtering Approaches for Multiple Acoustic Source Detection and 2-D Direction of Arrival Estimation Using a Single Acoustic Vector Sensor,' *IEEE Transactions on Signal Processing*, vol. 60, pp. 4719–4733, Sep. 2012. DOI: 10.1109/TSP.2012.2199987.

[171] M. Landisman, A. Dziewonski and Y. Sato, 'Recent Improvements in the Analysis of Surface Wave Observations,' *Geophysical Journal International*, vol. 17, no. 4, pp. 369–403, May 1969, ISSN: 0956-540X. DOI: 10.1111/j.1365-246X.1969.tb00246.x.

[172] X. Jin and J. Han, 'K-means clustering,' in *Encyclopedia of Machine Learning*, C. Sammut and G. I. Webb, Eds. Boston, MA: Springer US, 2010, pp. 563–564, ISBN: 978-0-387-30164-8. DOI: 10.1007/978-0-387-30164-8_425.

[173] *An efficient k-means clustering algorithm: analysis and implementation*, vol. 24, 7, 2002, pp. 881–892. DOI: 10.1109/TPAMI.2002.1017616.

[174] *The global k-means clustering algorithm*, vol. 36, 2003, pp. 451–461.

[175] T. Hastie, R. Tibshirani and J. Friedman, *The Elements of Statistical Learning: Data Mining, Inference, and Prediction*, ser. Springer series in statistics. Springer, 2009, ISBN: 9780387848846.

[176] L. Kaufman and P. Rousseeuw, *Finding Groups in Data: An Introduction To Cluster Analysis*. Jan. 1990, pp. 123–150, ISBN: 0-471-87876-6. DOI: 10.2307/2532178.

[177] *Estimating the Number of Clusters in a Data Set Via the Gap Statistic*, vol. 63, Feb. 2001, pp. 411–423. DOI: 10.1111/1467-9868.00293.

[178] F. Pedregosa, G. Varoquaux, A. Gramfort, V. Michel, B. Thirion, O. Grisel, M. Blondel, P. Prettenhofer, R. Weiss, V. Dubourg, J. Vanderplas, A. Passos, D. Cournapeau, M. Brucher, M. Perrot and E. Duchesnay, 'Scikit-learn: Machine learning in Python,' *Journal of Machine Learning Research*, vol. 12, pp. 2825–2830, 2011.

[179] L. Bornmann, L. Leydesdorff and R. Mutz, *The use of percentiles and percentile rank classes in the analysis of bibliometric data: Opportunities and limits*, 2012. arXiv: 1211.0381 [cs.DL].

[180] *Comsol multiphysics v. 5.6.* url=https://comsol.com, Accessed: 2021-09-30.

[181] R. Holland, *Design of resonant piezoelectric devices*. M.I.T. Press, 1969, ISBN: 9780262080330.

[182] R. Courant, K. Friedrichs and H. Lewy, 'On the Partial Difference Equations of Mathematical Physics,' *IBM Journal of Research and Development*, vol. 11, no. 2, pp. 215–234, 1967. DOI: 10.1147/rd.112.0215.

[183] D. L. C. Y. Qun, 'Numerical simulation of seismic wave propagation in cave carbonate reservoir,' *Geophysical Prospecting for Petroleum*, vol. 49, no. 2, pp. 121–126, 2010.

[184] E. Howat, S. Mishra, J. Schuetter, B. Grove and A. Haagsma, *Identification of vuggy zones in carbonate reservoirs from wireline logs using machine learning techniques*, Apr. 2016. DOI: 10.13140/RG.2.2.30165.73443.

[185] L. Thomsen, 'Weak Elastic Anisotropy,' *Geophysics*, vol. 51, pp. 1954–1966, Oct. 1986. DOI: 10.1190/1.1442051.

[186] *A deep learning framework for financial time series using stacked autoencoders and long-short term memory*, vol. 12, 7, Public Library of Science, Jul. 2017, pp. 1–24. DOI: 10.1371/journal.pone.0180944. [Online]. Available: https://doi.org/10.1371/journal.pone.0180944.

[187] *Anomaly Detection Based on Convolutional Recurrent Autoencoder for IoT Time Series*, vol. 52, 1, 2022, pp. 112–122. DOI: 10.1109/TSMC.2020.2968516.

[188] *Analysis of different RNN autoencoder variants for time series classification and machine prognostics*, vol. 149, 2021, pp. 107–322. DOI: https://doi.org/10.1016/j.ymssp.2020.107322.

[189] *Clustering approaches for anomaly based intrusion detection*, Jan. 2002, pp. 579–584.

[190] *The expectation-maximization algorithm*, vol. 13, 6, 1996, pp. 47–60. DOI: 10.1109/79.543975.

[191] *A Density-Based Algorithm for Discovering Clusters in Large Spatial Databases with Noise*, KDD'96, Portland, Oregon: AAAI Press, 1996, pp. 226–231.

[192] *Rock: A robust clustering algorithm for categorical attributes*, vol. 25, 5, 2000, pp. 345–366. DOI: https://doi.org/10.1016/S0306-4379(00)00022-3.

[193] *WaveCluster: A Multi-Resolution Clustering Approach for Very Large Spatial Databases*, 1998.

[194] *Data Mining of Time Series Based on Wave Cluster*, vol. 1, May 2009, pp. 1–14. DOI: 10.1109/IFITA.2009.132.

[195] *Discovering cluster-based local outliers*, vol. 24, 2003, pp. 1641–1650.

[196] *Similarity Measures for Categorical Data: A Comparative Evaluation*, vol. 30, Apr. 2008, pp. 243–254. DOI: 10.1137/1.9781611972788.22.

[197] *Nearest-Neighbor Clutter Removal for Estimating Features in Spatial Point Processes*, vol. 93, 442, Taylor and Francis, 1998, pp. 577–584. DOI: 10.1080/01621459.1998.10473711.

[198] *k-Nearest neighbour classifiers*, vol. 54, Apr. 2007. DOI: 10.1145/3459665.

[199] *Unsupervised Profiling Methods for Fraud Detection*, 2002, pp. 1–16.

[200] *HOT: Hypergraph-Based Outlier Test for Categorical Data*, Jan. 2003, pp. 399–410. DOI: 10.1007/3-540-36175-8_40.

[201] *Efficient algorithms for mining outliers from large data sets*, 2000.

[202] M. M. Breunig, H.-P. Kriegel, R. T. Ng and J. Sander, 'Optics-of: Identifying local outliers,' in *Principles of Data Mining and Knowledge Discovery*, J. M. Żytkow and J. Rauch, Eds., Berlin, Heidelberg: Springer Berlin Heidelberg, 1999, pp. 262–270, ISBN: 978-3-540-48247-5.

[203] S. N. Ahmed, 'Chapter 8 - Signal processing,' in *Physics and Engineering of Radiation Detection (Second Edition)*, S. N. Ahmed, Ed., Second Edition, Elsevier, 2015, pp. 477–540, ISBN: 978-0-12-801363-2. DOI: 10.1016/B978-0-12-801363-2.00008-5.

[204] M. Feldman, 'Hilbert transforms,' in *Encyclopedia of Vibration*, S. Braun, Ed., Oxford: Elsevier, 2001, pp. 642–648, ISBN: 978-0-12-227085-7. DOI: 10.1006/rwvb.2001.0057.

[205] H. Austerlitz, 'Chapter 10 - Data Processing and Analysis,' in *Data Acquisition Techniques Using PCs (Second Edition)*, H. Austerlitz, Ed., Second Edition, San Diego: Academic Press, 2003, pp. 222–250, ISBN: 978-0-12-068377-2. DOI: 10.1016/B978-012068377-2/50010-3.

[206] T. L. Szabo, 'Chapter 8 - WAVE SCATTERING AND IMAGING,' in *Diagnostic Ultrasound Imaging*, ser. Biomedical Engineering, T. L. Szabo, Ed., Burlington: Academic Press, 2004, pp. 213–242, ISBN: 978-0-12-680145-3. DOI: 10.1016/B978-012680145-3/50009-8.

Appendix A

Visualization of acoustic reflections

Different techniques for sound waves visualization and wave characterization can be used when rough estimation of sound reflections and absorption is needed. However these techniques are effective only to some extent. Typically it is challenging to deal with such complicated phenomena as sound reflection, diffraction and scattering, especially when certain components of acoustic reflections need to be identified (e.g. karst reflections). Moreover the application of conventional acoustic signal processing methods, such as pulse-echo reflections, is often limited by 1) simplified geometries of the instrumentation part 2) region of study which is typically close to the transmitter [203]. This appendix demonstrates the results of sound waves visualization. It was conducted in an attempt to identify karst-related reflections by visual analysis of time-spatial distribution plots.

Sound wave propagation simulations are based on the FEM discussed in Chapter 6. The instrumentation setup is shown in Figure A.1.

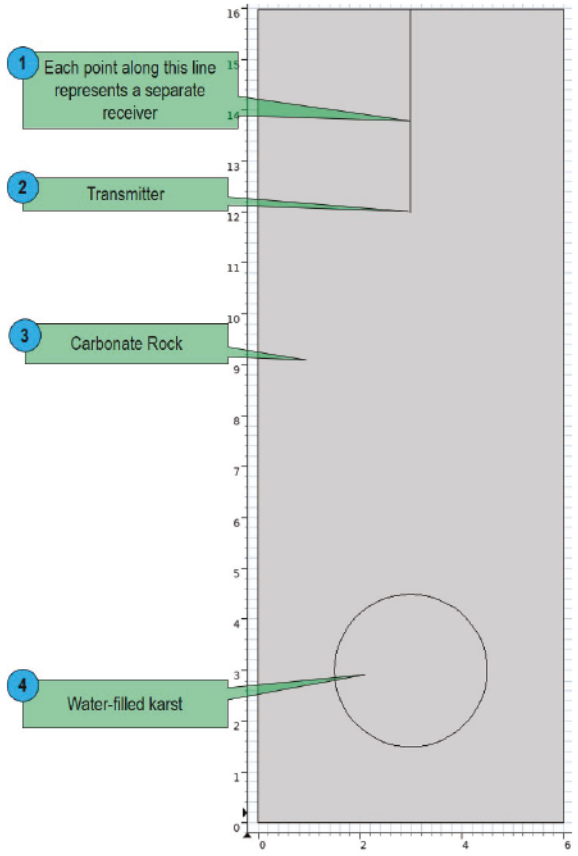

Figure A.1: Numerical simulation of karst detection with a line of receivers

To visualize acoustic reflections, instead of a single receiver, which was used to detect reflected signals described in Chapter 6 (see Figure 6.20), I implement a line of receivers. This allows reflections to be obtained at each point on the *receiver line*. Such configuration of instrumentation can be considered as a virtual representation of a borehole sonic tool consisting of many receivers located closely to each other. This instrumentation setup benefits from obtaining sound signals at each point along the receiver line and helps in the identification of visual components of karsts reflections.

In total, four different scenarios with fixed distances to the cave (7 m, 5 m, 3 m and 1 m) were simulated in the COMSOL Multiphysics®. Parameters of the developed numerical model are similar to that described in Chapter 6, Section 6.4.

Figure A.2 shows the time spatial distribution plots. The X-axis represents the coordinate of each of the receiver located onto receiver line. The Y-axis is the time axis. For convenience of visual analysis additional amplification of the reflections were applied. However, as can be seen in Figure A.2, it is challenging to find the difference between simulated scenarios visually. For example, the time-spatial distribution plot obtained for the case with the maximal distance to the cave (Figure A.2a) is visually similar to the case with the minimal distance to the cave (Figure A.2d).

In the next attempt to find a visual difference between the different scenarios discussed above, one of the quadrature filters was applied. These filters are typically used in systems with continuous signals and helped to extract a base signal from wave forms [204]. The results of the Hilbert transform of a signal are shown in Figure A.3. For more information on the subject of the Hilbert transform I refer the reader to [205, 206]. As can be seen in Figure A.3, it is still challenging to visually compare different scenarios and find the difference between them when the virtual BHA is approaching the cave.

Comparison of these figures reveals that the propagation of the wave front is very complex. Multiple unwanted reflections are not optimal from the seismic point of view and the positioning of the transmitter and receivers makes detection of karst-related reflections challenging. This motivates the development of an unsupervised ML technique presented in Section 6.3.

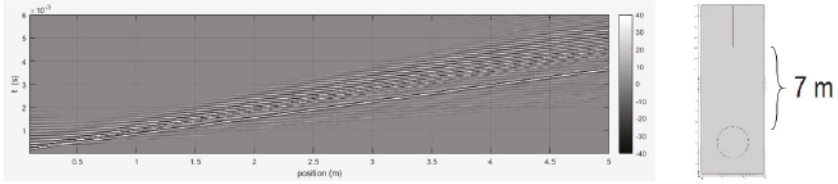

(a) Distance to the karst 7 m

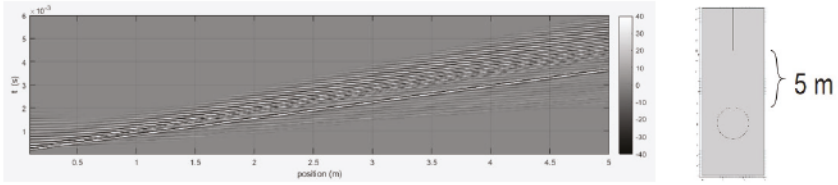

(b) Distance to the karst 5 m

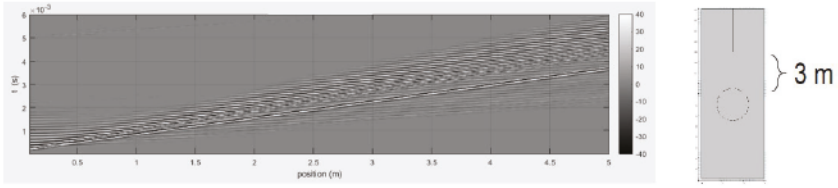

(c) Distance to the karst 3 m

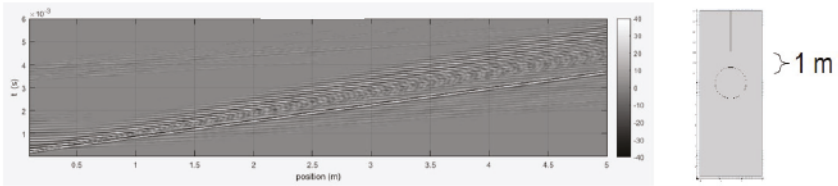

(d) Distance to the karst 1 m

Figure A.2: Comparison of time-spatial distribution plots for scenarios with different distances to the karst

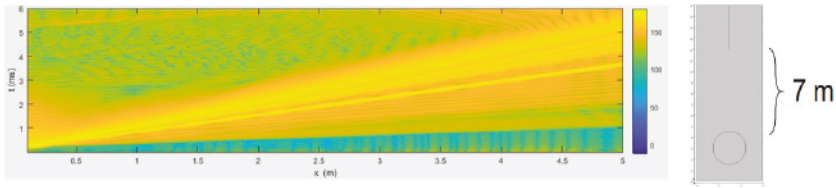

(a) Distance to the karst 7 m

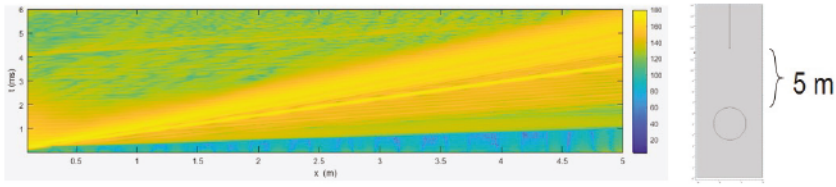

(b) Distance to the karst 5 m

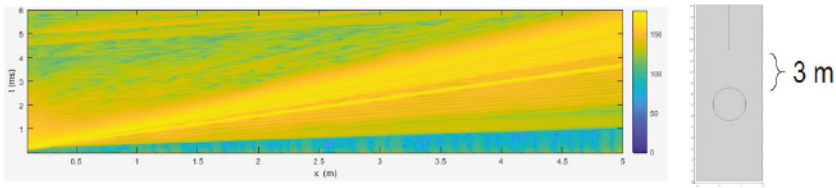

(c) Distance to the karst 3 m

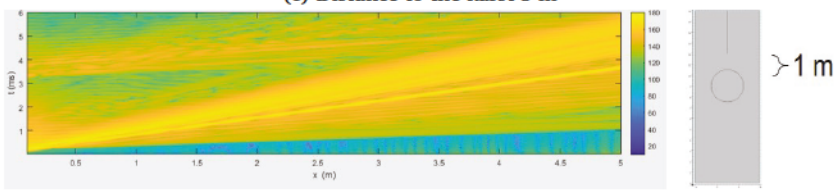

(d) Distance to the karst 1 m

Figure A.3: Comparison of Hilbert magnitudes of signals for scenarios with different distances to the karst